SYNTHESIS AND CHARACTERIZATION OF CU/ZNO/AL2O3 CATALYST BY DIFFERENT METHODS AND INVESTIGATION OF PERFORMANCE IN METHANOL STEAM REFORMING FOR HYDROGEN GENERATION

Ayşe Ece BEDİR SEZGİN

Master's Thesis

Department of Chemical Engineering

Programme in Process and Reactor Design

Supervisor: Assoc. Prof. Dr. Elif AKBAY

Eskişehir

Eskişehir Technical University

Institute of Graduate Programs

January 2022

ABSTRACT

SYNTHESIS AND CHARACTERIZATION OF CU/ZNO/AL2O3 CATALYST BY DIFFERENT METHODS AND INVESTIGATION OF PERFORMANCE IN METHANOL STEAM REFORMING FOR HYDROGEN GENERATION

Ayşe Ece BEDİR SEZGİN

Department of Chemical Engineering

Programme in Process and Reactor Design

Eskişehir Technical University, Institute of Graduate Programs, January 2022

Supervisor: Assoc. Prof. Dr. Elif AKBAY

Today's world has environmental issues such as climate change and greenhouse gas emission due to the fossil fuels usage. These environmental concerns and fast depletion of fossil fuel resources increased the research for the production of hydrogen from alternative and renewable sources. Proton exchange membrane fuel cell system is a promising power generation technology fed by hydrogen as an environmentally friendly and sustainable solution. In this regard, hydrogen production through methanol steam reforming (MSR) reaction has the potential to be an appropriate method with the advantages of having low amount of carbon monoxide, no sulphur production so that there is no requirement for desulfurization, having good energy density, relatively high H/C ratio and low reforming temperature. However, endothermic nature of the reaction and not having comprehensive distribution infrastructure are drawbacks of this process. MSR is based on reaction of methanol and steam with the help of catalyst and releases hydrogen and carbon dioxide. The catalyst activity and selectivity are the properties, which can be enhanced by the structure of the catalyst. In this study, in order to obtain a catalyst having better structure and catalytic behavior, which exhibits high specific surface area, high metal dispersion and higher activity for H_2 production, the effect of preparation methods on the structure and catalytic behavior of $Cu/ZnO/Al_2O_3$ were investigated. Conventional coprecipitation, sequentially coprecipitation and ball milling methods were studied. The results show that the catalysts obtained by sequentially coprecipitation has a high specific surface area and dispersion giving a higher activity which promotes the superior catalytic performance depending on formation of active

copper material with higher copper specific surface and a stronger $Cu - ZnO$ synergy thanks to proper incorporation of zinc oxide species into precursors.

Keywords: Methanol steam reforming, Hydrogen production, Cu/ZnO/Al2O3 catalyst.

ÖZET

FARKLI YÖNTEMLERLE HAZIRLANAN CU/ZNO/AL2O3 KATALİZÖRÜNÜN SENTEZİ VE KARAKTERİZASYONU VE METANOL BUHAR REFORMİNG İLE HİDROJEN ÜRETİMİ İÇİN ETKİNLİĞİNİN İNCELENMESİ

Ayşe Ece BEDİR SEZGİN

Kimya Mühendisliği Anabilim Dalı

Proses ve Reaktör Tasarımı Bilim Dalı

Eskişehir Teknik Üniversitesi, Lisansüstü Eğitim Enstitüsü, Ocak 2022

Danışman: Doç. Dr. Elif AKBAY

Günümüz dünyası, fosil yakıtların kullanımına bağlı olarak iklim değişikliği ve sera gazı salınımı gibi çevresel sorunlarla karşı karşıyadır. Bu çevresel kaygılar ve fosil yakıt kaynaklarının hızla tükenmesi, alternatif ve yenilenebilir kaynaklardan hidrojen üretimine yönelik araştırmaları arttırdı. Proton değişim membranlı yakıt hücresi sistemi, çevre dostu ve sürdürülebilir bir çözüm olarak umut vaad eden bir enerji üretim teknolojisidir. Bu bağlamda metanol buhar reforming (MSR) reaksiyonu ile hidrojen üretimi, düşük miktarda karbon monoksit, kükürt üretiminin olmaması bu nedenle de kükürt giderimine gerek olmaması, iyi enerji yoğunluğuna sahip olması, nispeten yüksek H/C oranı ve düşük reform sıcaklığı gibi avantajları ile uygun bir yöntem olma potansiyeline sahiptir. Ancak reaksiyonun endotermik doğası ve methanolun kapsamlı dağıtım altyapısına sahip olmaması bu prosesin dezavantajlarıdır. MSR, katalizör yardımıyla metanol ve buharın reaksiyonuna dayanır ve hidrojen ve karbondioksit açığa çıkar. Katalizör aktivitesi ve seçicilik, katalizörün yapısı tarafından geliştirilebilir özelliklerdir. Bu çalışmada, hidrojen üretimi için yüksek yüzey alanı, yüksek metal dağılımı ve daha yüksek aktivite sergileyen daha iyi yapıya ve katalitik davranışa sahip bir katalizör elde etmek için hazırlama yöntemlerinin katalizörün yapısı ve katalitik davranışı üzerindeki etkisi araştırılmıştır. Konvansiyonel birlikte çöktürme, sıralı birlikte çöktürme ve bilyeli öğütme yöntemleri incelenmiştir. Sonuçlar, sıralı birlikte çöktürme yöntemiyle elde edilen katalizörlerin yüksek yüzeyli aktif bakır oluşumu ve çinko oksitin prekursör içine düzgün bir şekilde yerleşmesi sayesinde oluşan daha güçlü $Cu - ZnO$ sinerjisine bağlı olarak üstün katalitik performansını destekleyen daha iyi aktivite veren yüksek yüzey alanına ve metal dağılımına sahip olduğunu göstermektedir.

Anahtar Sözcükler: Methanolün buharla reformlanması, Hidrojen üretimi, Cu/ZnO/Al2O3 katalizörü.

CONTENTS

Page

LIST OF TABLES

Page

LIST OF FIGURES

Page

1. INTRODUCTION

Today, society becomes more energy dependent. Therefore, scientists seek for new portable and more efficient energy sources. Fuel cells are one of the promising solutions for this pursuit. Although, currently battery technologies such as li-ion batteries have an increasing trend, fuel cells have serious advantages over conventional engines and batteries. According to (Ryan O'Hayre, Suk-Won Cha, Whitney Colella, 2016) these advantages can be listed as follows:

• Their energy production efficiencies are far higher than conventional combustion engines.

• They don't have any moving parts, and this increases their reliability and lifetime.

• They have nearly zero toxic emissions.

• Unlike batteries, they can be easily scaled to other power and energy levels.

• They have higher energy densities compared to the batteries.

• They can be quickly recharged by means of fueling, on the other hand, batteries must be plugged in for a certain time period.

Polymer electrolyte membrane fuel cells (PEM fuel cells / PEMFCs) have number of technological advantages over its alternatives such as lower operating temperatures, high power density, longer storage durability, and higher number of life-cycles. Hence, PEMFC and its feedstock hydrogen as an energy carrier, gain attraction in recent years.

Improvement of PEM fuel cell systems including fuel reformer stands out worldwide due to their higher productivity, ecological benefits, and possible market. (Tellez-cruz et al., 2021). There are various types of hydrogen generation technologies for PEMFCs, and the most common types of them are given in detail (Holladay et al., 2009). However high purity hydrogen as a feeding fuel is essential for PEMFCs. This restriction also brings some limitations regarding storage and transportation of fuel. Therefore, hydrogen generation from both alcohols and hydrocarbons steam reforming reaction is preferred (Kalamaras & Efstathiou, 2013). Most research (Azizan et al., 2020) (Shen & Song, 2002) on hydrogen production for fuel cells depend on two sorts of carbon compounds:

- Oxygen-containing compound, like (methanol, etc.) and ether (dimethyl ether, etc.),
- Hydrocarbons like natural gas, diesel fuel etc.

Although hydrocarbons steam reforming is researched mostly and having high energy density, they are suffering from difficulties in technical processes i.e., conversion efficiency of fuel, desulfurization step, high pressure, and temperature requirement (Lakeman, 2003). Furthermore, gas purification is more complex compared to the use of oxygen-containing compound. Another promising option for hydrogen production for PEMFCs is the methanol steam reforming (Zhang et al., 2005). The production of hydrogen from methanol steam reforming has essential advantages over hydrocarbons reforming processes including good gravimetric and volumetric energy density, no sulfur production which means that there are no requirements for desulfurization, relatively high H/C ratio and low reforming temperature ($200 - 300$ ℃) since reaction conditions are mild because of low ΔH (Shen & Song, 2002) (Kalamaras & Efstathiou, 2013). On the other hand, although hydrocarbon fuels have extensive distribution infrastructure, methanol has not such an infrastructure, which is the main drawback of the use of methanol.

In this process the most studied catalyst are copper containing ones, especially CuO/ZnO and $Cu/ZnO/Al_2O_3$ due to their high selectivity and activity (Zhang et al., 2005). Dispersion, metal surface area and particle size are important parameters for catalyst and conversion rely upon status of copper. It is also stated that catalyst with high copper dispersion shows better performance in methanol steam reforming. Since all these parameters are directly affected by the structure of catalyst, the effect of the preparation method on the structure and catalytic behavior of the $Cu/ZnO/Al_2O_3$ catalysts with respect to methanol conversion, H_2 production and CO concentration are significant points to work on. There are several methods such as impregnation, co-precipitation, and oxalate gel–coprecipitation comparatively examined for the preparation of catalysts for the production of hydrogen by methanol steam reforming. Regarding the synthesis of $Cu/ZnO/Al_2O_3$ catalyst with high content of Cu, the preparation method of co-precipitation was chosen. This process has some difficulties, such as multistep processing and the need for sensitive pH and temperature control, alkaline metal contamination (Zhang et al., 2005). Co-precipitation procedure comprises the mixing of metal nitrates

and sodium carbonate solutions at a controlled pH and temperature. Initially formed precipitate structure is amorphous. While it is aged, the formation of crystalline precursors is obtained. This ageing step is considered as necessary to generate the optimum crystalline hydroxycarbonate precursors from an amorphous phase resulting desired highly active catalyst characteristics (Zhang et al., 2005) (Paul J. Smith et al., 2017). In this study, both amorphous georgeite and crystalline malachite hydroxycarbonate precursors were synthesized. In preparation steps of malachite, initially georgeite is formed as a transient phase and then rapidly transforms into malachite. Zn is incorporated into georgeite to form zincian georgeite and zincian malachite. While zincian malachite was obtained by both conventional co-precipitation and sequentially co-precipitation method, zincian georgeite was prepared by procedure modified sequentially co-precipitation to inhibit crystalline malachite phase formation. Additionally, ball milling method was studied in catalyst synthesis. Mechanical mixing of copper oxide and zinc oxide powder at ambient conditions directly without any thermal treatment was investigated. All synthesized catalysts' activity were assessed in MSR reaction experimentally.

2. HYDROGEN GENERATION TECHNOLOGIES

2.1. HYDROGEN: A Fuel of Future as a Sustainable Pathway

Hydrogen is an energy carrier but not a primary energy source. It is used as a fuel source for fuel cell electric vehicles (FCEVs). However, portable storage at vehicle scale is a barrier for now. Furthermore, hydrogen is combined with carbon dioxide for the production of methanol or dimethyl ether (DME), which are important transportation fuels. It could possibly be used as a large-scale replacement for coke in steelmaking and other metallurgical processes in the future. According to the International Energy Agency (IEA) (IEA, 2019), pure hydrogen demand was around 74 million tonnes (Mt) in 2018, with 38.2 Mt used in oil refining and 31.5 Mt utilized in ammonia synthesis. It is stated that there was also a need for further 42 Mt of hydrogen combined with other gases, such as carbon monoxide. 12 Mt was used in methanol production, while 4 Mt was used to make steel from direct-reduced iron (DRI). It is demonstrated in **Figure *2.1***. In addition, hydrogen production from main sources is given in **Figure *2.2***. Most of today's hydrogen is produced by steam reforming or coal gasification of natural gas. Both methods lead CO_2 emission, therefore, these hydrogen production methods cannot be classified as carbon-free processes. In fact, future demand will mainly be zero-carbon hydrogen (World Nuclear Association, 2021). Therefore, plans for hydrogen production are primarily based on electrolysis using electricity from renewable sources. Although the renewable sources have intermittent generation characteristic, their usage is a viable and sustainable alternative to using grid electricity to produce hydrogen. This interest is growing with the declining costs for renewable electricity, in particular for solar PV and wind. Data belongs to 2018 year for hydrogen production costs according to sources was shown in **Figure *2.3***. If hydrogen can be produced without emitting carbon dioxide, it is becoming a more important component of future energy systems.

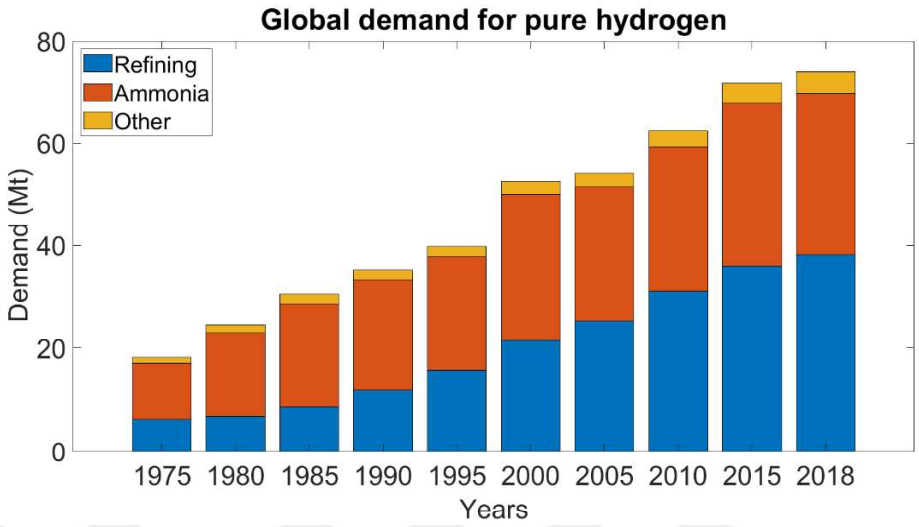

Figure 2.1. *Global demand for hydrogen (IEA, 2019)*

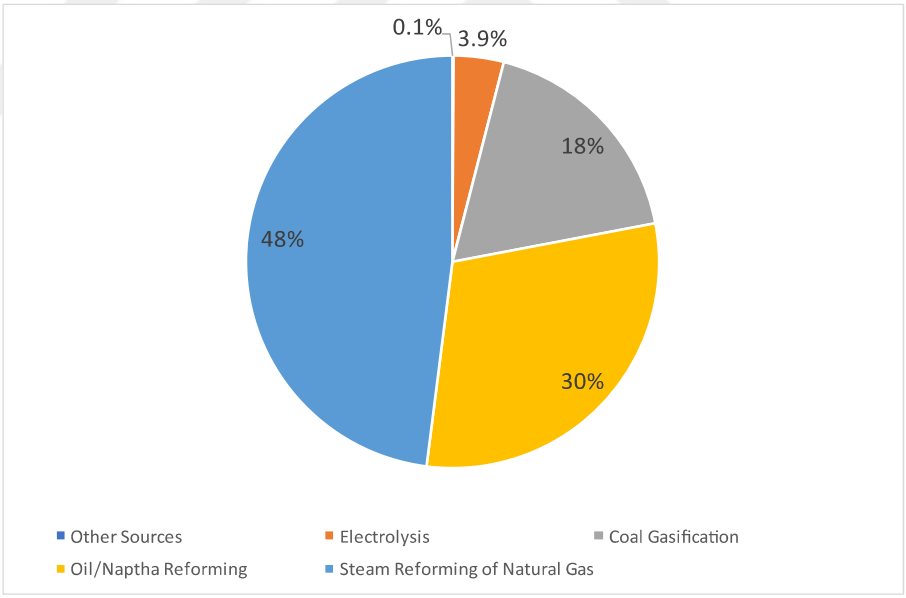

Figure 2.2. *Global hydrogen production from main sources (Ewan & Allen, 2005)*

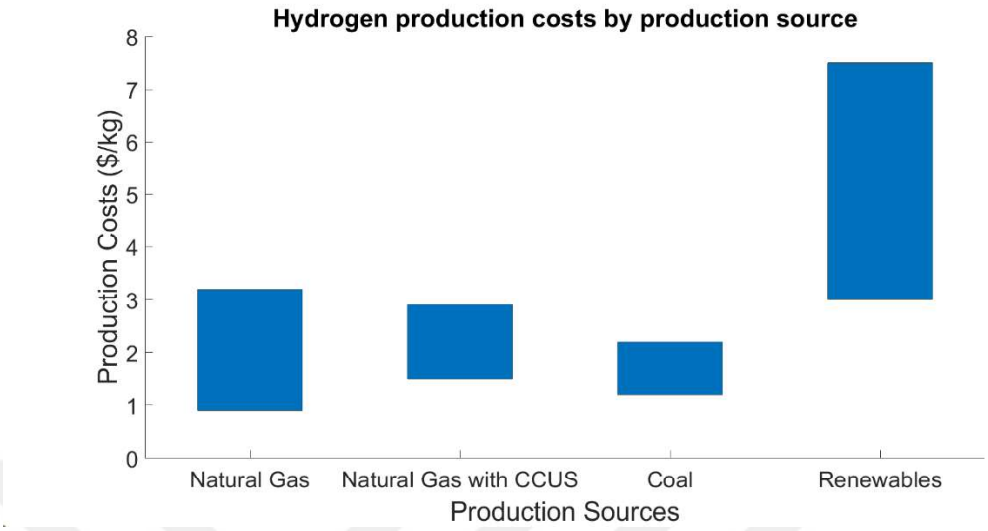

Figure 2.3. *Hydrogen production costs by production source (IEA, 2019)*

Table 2.1. *Properties of elemental hydrogen (P.N.N. Laboratory, 2021; Royal society of Chemistry (RSC), 2017)*

Property	Value
Atomic number	1
Relative atomic mass	1.008
Molecular weight (g/mol)	2.02
State at 20℃	Gas
Thermal conductivity* ($W/m.K$)	0.182
Cp* ($J/g.K$)	14.29
Cv* ($J/g.K$)	10.16
Enthalpy* (kJ/kg)	3858.1
Entropy* (kJ/kg)	53.14
Internal energy* (kJ/kg)	2648.3
Melting point (℃)	-259.16
Boiling point (℃)	-252.879
Density* (kg/m^3)	0.08375
Specific volume* (m^3/kg)	11.94
Viscosity* ($g/cm.s$)	8.813×10^{-5}
Flame temperature (℃)	2045

* measured at normal temperature and pressure; 20 ℃ and 1 atm

2.2. Hydrogen from Fossil Fuel Reforming

There are three main fossil fuel reforming technologies for hydrogen production, which are namely steam reforming (SR), partial oxidation (POX), and autothermal reforming (ATR). The benefits and drawbacks of each of these processes are outlined in

Table 2.2 below.

Steam reforming generally requires energy to drive the process. It does not demand oxygen. It has a higher H_2/CO ratio as well as having a low operating temperature compared to partial oxidation and autothermal reforming. In POX process, to produce hydrogen, hydrocarbons are partially oxidized with oxygen. The energy to initiate this process is provided by the partial oxidation (combustion) reaction. It is more sulfur tolerant than steam and autothermal reforming. Autothermal reforming is a hybrid of steam reforming and partial oxidation. It covers the intensive energy requirements of reforming with a combination of exothermic oxidation and endothermic steam reforming. Therefore, ATR reactor has a compact form consisting of a combustion zone and a catalyst bed. It operates between temperatures ranging from 900 ℃ to 1000 ℃ (Lamb et al., 2020).

While autothermal reforming and partial oxidation do not need an external heat source as a cost advantage both processes primarily desire pure oxygen supply results in additional cost as it requires oxygen separation unit. Compared to other fossil fuel reforming technologies, steam reforming is more cost effective and more commonly used method of hydrogen production.

Table 2.2. *Comparison of SR, POX and ATR technologies (Holladay et al., 2009)*

Technology	Advantages	Disadvantages
Steam Reforming	Widely used industrial process	Highest air emissions
	Lowest operating temperature	External igniter to start up
	No O_2 requirement	
	Best H_2/CO ratio	
Partial Oxidation	Reduced desulfurization requirement	Low H_2/CO ratio
	Short start-up period	High operating temperatures
	Higher Sulphur tolerance	Expensive reactor material
Autothermal Reforming	Both exothermic and endothermic reaction	Limited commercial experience
		Air/oxygen requirement

The most used fuels in the world are obtained from crude oil. The main fuels are made by the fractional distillation of crude oil. The volumetric and gravimetric energy densities of diesel fuel are very high in comparison, having more than twice the energy density of methanol. However, diesel reforming has disadvantages and there are some technical difficulties in its process. Some of these issues are; compared to methanol, diesel reform requires much higher temperatures and reduces conversion efficiency. In addition, diesel contains significant amounts of sulfur compounds that are toxic to conventional reformer and fuel cell catalysts. Moreover, gas purification is more complex compared to methanol as it involves the removal of hydrogen sulfide and carbon monoxide.

The main advantages of diesel fuel are (Lakeman, 2003):

- High energy density
- A large distribution network advancement
- Existing military logistics fuel

The main disadvantages are:

- Desulfurization requirement
- High pressure and temperature requirement
- Complex purification process
- Management of exhaust gas byproduct management (storage/discharge)

2.3. Hydrogen from Renewable Sources

Hydrogen could be also produced by renewable sources of the biomass-based approaches, electrolysis, and thermochemical water splitting. In the following sub-sections these methods are explained.

2.3.1. Biomass gasification

Within the close term, it is possible to that biomass become a renewable organic substitute to petroleum. Biomass can be obtained from a wide range of sources, such as animal wastes, agricultural wastes, municipal solid wastes, olive waste, crop residues, sawdust, aquatic plants, herbaceous species (Demirbas, 2006). Gasification technology commonly used with biomass and coal as fuel feedstock in many processes. It requires large scale reactors and continuously feeding of massive volume of materials. The process is based on partial oxidation and through gasification reactions product gas of a mixture of hydrogen, methane, higher hydrocarbons, carbon monoxide, carbon dioxide, nitrogen

and residue carbon particles (Demirbas, 2006) (Asadullah et al., 2002). Efficiencies are in the range of $35-50\%$ based on the lower heating value (Holladay et al., 2009). Syngas with a H_2/CO of the gasification process can be fed to a Fischer-Tropsch reactor to convert this syngas to higher hydrocarbons like gasoline and diesel (Choudhury et al., 2015). However, gasification process has some disadvantages (Jin et al., 2017). Those can be listed as follows:

- This technology needs a large variety of resources to gather the high amount of biomass to the processing plants.
- The moisture in the biomass and it is needed to be vaporized because it decreases thermal efficiency of gasification process.
- This technology gives a complex mixture of higher aromatic hydrocarbons called as "tars" in the product gas. In this manner, gas cleaning is one of the challenging points for the application.

Calcined dolomites and steam reforming nickel-based catalysts used in a secondary reactor are preferred as a most common solution for gas clean up and upgrade processes (Asadullah et al., 2002). Furthermore, to increase hydrogen concentration in product gas, WGS reactor can be used in the systems for hydrogen production. The usage of oxygen in gasification plants is cost prohibitive thus it limits the gasifiers to the use of air. It causes dilution of the product gas and NO_x formation. Therefore, cost effective developments are needed for hydrogen production and commercialization.

2.3.2. Electrolysis

In (Dincer & Acar, 2015), electrolysis is represented as the most basic industrial process in order to produce almost pure hydrogen. According to (Bermudez & Hannula, 2021), current ratio of electrolysis in all hydrogen production methods is around 0.03%. However, it is expected to rise $\sim 38\%$ by 2030 (Bermudez & Hannula, 2021).

In this process a DC voltage is applied to the water with the use of electrodes, and water decomposes into H_2 and O_2 gases. The source of the electrical energy determines the overall cost and environmental effects of electrolysis. If renewables are used, then the electricity cost increases. Nevertheless, the hydrogen is produced without any CO_2 emission. On the other hand, while coal fired power plants decreases the cost of electrical energy, they cause significant carbon footprint.

In (Bhandari et al., 2014) authors divide the electrolysis technologies into three, namely alkaline, polymer membrane and solid oxide electrolyzers. While alkaline electrolyzers are commercially used and a mature technology, PEM electrolyzers are gaining attention in the literature.

While in alkaline electrolyzer method a diaphragm is used to separate the product gases, other methods utilize membrane technology.

In practice to increase the rate of electrolysis reactions and current density, some catalysts are used. Platinum is one of the most used heterogeneous catalysts, and it is applied to the electrode surfaces.

In (Dincer & Acar, 2015), authors emphasize the importance of the desalination and demineralization processes to purify the used water, because the performance of electrolyzers is directly affected by the purity of the water. For example, in case of brine usage, it will cause chlorine production instead of oxygen.

2.3.3. Thermochemical water splitting

Although electrolysis is a relatively naive method, it has some efficiency issues. Thermochemical water splitting method can solve this problem and can provide higher efficiencies. Average efficiency of electrolysis method is around 24%, on the other hand, efficiency of thermochemical water splitting method can rise to 50% (Rosen, 2010). Compared to the electrolysis method this process does not require catalysis to drive reactions. This is the major advantage of thermochemical water splitting. Other advantages of thermochemical water splitting cycles can be listed as:

- No need for $O_2 - H_2$ separation membranes (Safari & Dincer, 2020)
- Generate large amount of hydrogen at lower temperature range of $\sim 1200\ K$ compared to one-step process (Rosen, 2010)
- No input electrical energy requirement (Safari & Dincer, 2020)
- All chemicals used in the thermochemical cycle can be recycled except water, which is the material source of hydrogen production (Dincer & Acar, 2015)

Although different methods exist in the literature for thermochemical water splitting, national laboratories from U.S. and France developing sulphur-iodine ($S - I$) cycle-based plants to produce hydrogen (Dincer & Acar, 2015). In (Safari & Dincer,

2020) authors describe multiple-step cycles. To illustrate the $S-I$ cycle process a four-step cycle is used in this work. The first reaction of $S-I$ cycle sulphuric acid is decomposed as follows:

$$H_2SO_{4(aq)} \xrightarrow{heat\ (300-500℃)} H_2O_{(g)} + SO_{3(g)}$$

In the second step the product gases (H_2O and SO_3) are heated to $800-900℃$. Then SO_3 gas decomposes as follows:

$$SO_{3(g)} \xrightarrow{heat\ (800-900℃)} \frac{1}{2}O_{2\ (g)} + SO_{2(g)}$$

Spontaneously the resultant SO_2 gas reacts with iodine and water at low temperatures, exothermically:

$$SO_{2(g)} + I_{2(g)} + H_2O_{(l)} \rightarrow 2\mathrm{HI}_{(g)} + H_2SO_{4(aq)}$$

As final step, HI decomposes into H_2 at temperatures around $425-450℃$, with an endothermic reaction, according to:

$$2\mathrm{HI}_{(g)} \xrightarrow{heat\ (425-450℃)} H_{2(g)} + I_{2(g)}$$

I can be seen from the given $S-I$ cycle steps, there is no side reactions during the cycle. Since the chemicals (H_2SO_4 and I_2) are not dissipated and they can be reused. Unfortunately, due to the high temperature requirement of the given $S-I$ cycle steps, a limited number of thermal energy sources are available. Nuclear power plants can be given as an example for such thermal energy sources. Moreover, concentrated solar and biomass combustion can be given as possible sustainable thermal energy sources to initiate the relevant reactions steps.

3. METHANOL STEAM REFORMING

3.1. The Use of Methanol as a Feedstock

The most favorable liquid hydrocarbons are methanol, ethanol, dimethyl ether (DME), gasoline, diesel etc. to get high yield of hydrogen in hydrogen production.

Methanol or methyl alcohol, the simplest primary alcohol, has the formula of CH_3OH. It is volatile, colorless, flammable, and miscible with water in all proportions. It is poisonous for human consumption. Some of properties of methanol are shown in **Table *3.1***. There are several advantages associated with using methanol in steam reforming process as a hydrogen production feedstock. Methanol Steam Reforming (MSR) temperature is lower $(200 - 300\ ^oC)$ compared to that of the other common hydrocarbons (Sá et al., 2010). Moreover, the reaction can be operated in atmospheric pressure. The risk of coke formation is low. It has low start-up energy. The generated carbon monoxide is low. Since methanol has no strong carbon-carbon bonds in its structure less energy is required in order to break the molecule.

Table 3.1. *Properties of methanol (PubChem Compound Summary for CID 887, Methanol, 2022)*

Property	Value
Molecular weight (g/mol)	32.042
Melting point (°C)	-97.6
Boiling point (°C)	64.7
Density $(kg/m^3\ at\ 25$ °C)	0.7866
Viscosity $(mPa.s\ at\ 25$ °C)	0.544
Heat of combustion (kJ/mol)	726.1
Heat of vaporization (kJ/mol)	37.34
Vapor pressure $(kPa\ at\ 20$ °C)	12.9
Flash point (°C)	15.6
Auto ignition temp. (°C)	464

3.2. Methanol Steam Reforming (MSR) Reaction Network

The MSR process is considered a viable way to provide hydrogen with high yield in addition to having a very low CO selectivity. For this process, the most studied and proposed catalyst groups are copper-based and metal group 8-10. The general operating conditions is at relatively low temperatures, $200–300$ °C. The molar water/methanol ratio of $1.5:1$ is regarded as the best suitable ratio, and it is applied in most of the studies.

Reaction mechanism consists of methanol steam reforming reaction (1), water gas shift reaction (2) and methanol decomposition reaction (3). While water gas shift reaction is exothermic, others are endothermic reactions.

The overall reaction network of can be described as follows:

$$CH_3OH + H_2O \leftrightarrow CO_2 + 3H_2 \qquad \Delta H = 49.7\ \text{kJ/mol} \qquad (1)$$

$$CH_3OH \leftrightarrow CO + 2H_2 \qquad \Delta H = 90.2\ \text{kJ/mol} \qquad (2)$$

$$CO + H_2O \leftrightarrow CO_2 + H_2 \qquad \Delta H = -41.2\ \text{kJ/mol} \qquad (3)$$

In the literature, the product stream of MSR (at 1 bar with the feed molar ratio of 1) consists of 4% CO, 22% CO_2, and 74% H_2 is defined (*Methanol Steam Reforming Over Silica Aerogel Supported*, 2018).

4. CATALYSTS

Catalysts can be classified into two main groups, namely homogeneous and heterogeneous ones. While in homogeneous catalysis, all reaction components are in the same uniform phase of gas or liquid, heterogeneous catalysis can be in several phases. Generally, the heterogeneous catalyst is a solid and the reactants are in gas or liquid state (Chorkendorff & Niemantsverdriet, 2003).

Heterogeneous catalysis has a significant role in petrochemicals and chemical industries as well as clean energy applications.

According to (Rothenberg, 2008), in a typical heterogeneous reaction:

- Gaseous reactants enter the reactor
- The reactant molecules diffuse through the catalyst pores.
- The catalyst surface having active sites adsorbs the reactant molecules.
- The reaction is initialized and the products leave the catalyst surface to the gas phase.

4.1. MSR Catalysts

Methanol steam reforming is a heterogeneously catalyzed reaction. As it is mentioned before, copper-based and group 8-10 catalysts are two common types of catalysts used in this process.

Group 8-10 catalysts shows better thermal and longer stability but they produce less amount of hydrogen due to low activity. In addition, they are considerably expensive. The copper-based catalysts have high activity, high selectivity, as well as low cost. However, they have disadvantage of deactivation due to sintering, and coke formation. At the tempertaures higher than $300\ ^{o}C$ the copper-based catalysts are highly prone to sintering. Dispersion, metal surface area and particle size are important parameters for catalyst performance and conversion rely upon status of copper. It is stated that catalyst with high copper dispersion shows better performance in methanol steam reforming. Therefore, different promoters have been studied in the literature to enhance the copper status as well as the catalyst performance. The addition of alumina (Al_2O_3) increases the catalyst surface area and improves copper dispersion. Furthermore, zinc is also effective in increasing the catalyst stability and methanol conversion also a better copper status (Sá et al., 2010). Therefore, in this process the most studied catalyst are CuO/ZnO and

$Cu/ZnO/Al_2O_3$ due to their high selectivity and activity (Zhang et al., 2005). All these desired properties are determined by the structure of catalyst, which has a direct contact with the catalyst preparation method. There are numerous studies on $Cu/ZnO/Al_2O_3$ bulk catalyst employed in MSR process in the literature, while only a few works have studied related to preparation methods especially regarding co-precipitation result in different precipitating agents and structures, which have effect on catalytic behavior of the $Cu/ZnO/Al_2O_3$. Therefore, it is required to concentrate more on that the effect of the preparation method on the structure in order to give high copper dispersion, surface area etc. and catalytic behavior of the $Cu/ZnO/Al_2O_3$ catalysts with respect to methanol conversion, H_2 production and CO concentration.

4.2. Literature Review

There are different issues studied on to enhance MSR catalyst properties. Some researhers are focused on stability of copper-based MSR catalyst. Catalyst deactivation is explained by sintering, coke deposition, catalyst poisoning. Using the water molar fraction above the stoichiometry is proposed to prevent this problem. Another approach followed to prepare more active copper-based catalysts is using different promotors (Iulianelli et al., 2014) (Jeong et al., 2006) (Li et al., 2004). The most common used promoters for copper-based catalysts are ZnO, ZrO_2, CeO_2, or Al_2O_3. These promoters support well copper dispersion and increase the surface area. Also they provide long term stability to the catalyst. Changing the preparation method are also one of the studied topics for improving the catalytic activity and the most used for cooper-based catalysts (Shishido et al., 2004) (Prasetyaningsih et al., 2016) (Iulianelli et al., 2014) (Huang et al., 1997). Co-precipitation, wet-impregnation, ball milling methods are worked to investigate the role of the preparation methods in supporting surface area, copper dispersion and and the particle size (IGBN Makertihartha & Gunawan, 2009) (Paul J. Smith et al., 2017) (Huang et al., 1997) (Paul John Smith, 2015). In addition to copper-based catalysts, group 8–10 metals are being studied for MSR reaction (Iwasa et al., 1998). Especially Pd catalysts are drawing the attention of many researchers. It is found that $Pd/ZnO/Al_2O_3$ catalyst shows higher stability comparing with $Cu/ZnO/Al_2O_3$ (Conant et al., 2008). The effects of the Pd/ZnO catalyst preparation on the methanol steam reforming, activity and selectivity, interaction between Pd and ZnO, catalyst structure are examined in studies (Chin et al., 2003) (Wang et al., 2006). A large number of articles were recently examined as part of the comprehensive search for more active and selective catalysts for MSR (Sá

et al., 2010). **Table *4.1*** shows examples from a comprehensive literature review on the various types of catalysts used in MSR.

Table 4.1. *Different types of catalysts used in MSR*

Catalyst	**Preparation Method**	**SBET (m^2g^{-1})**	**SCu (m^2g^{-1})**	**(°C)**	**XMeOH (%)**	**yCO**	**Activity ($\mu molH_2\ gram_{cat}^{-1}s^{-1}$)**
Cu/ZnO/Al2O3 (Jeong et al., 2006) (Sengodan et al., 2018)	CP	90.8	23.7	60	79	0.0073	-
Cu/ZnO/Al2O3 (Shishido et al., 2004)	HP	97.5	47	50	97.3	-	109
Cu/ZnO/ZrO2/Al2O3 (Jeong et al., 2006) (Sengodan et al., 2018)	CP	129.7	25.9	60	92	0.0010	-
Cu/ZrO2 (Yao et al., 2006)	IMP	13.1	1	60	10	0	3
Cu/ZrO2 (Yao et al., 2006)	CP	64.2	3.5	60	62	0.009	56
Cu/ZnO (Shishido et al., 2004)	CP	40.7	16	50	46.4	-	105
Cu/ZnO (Shishido et al., 2004)	HP	76.4	41.6	50	94.2	-	109
Cu/ZnO/ZrO2 (Agrell et al., 2003)	CP	81.8	15.5	95	90	0.0005	-
Pd/ZrO2 (Iwasa et al., 1998)	IMP	-	31.1 *Smetal	20	64.3	-	-
Pd/CeO2 (Iwasa et al., 1998)	IMP	-	170.6 *Smetal	20	62.4	-	-
Pd/ZnO (Iwasa et al., 1998)	IMP	-	10.4 *Smetal	20	54.2	-	-

By looking at the results of this literature review, followings can be deduced:

- $Cu/ZnO/Al_2O_3$ is cost effective choice comparing to group 8–10 metals studied in MSR
- Desirable properties of $Cu/ZnO/Al_2O_3$ catalayst can be listed as follows:
    - Large surface area
    - High Cu dispersion
    - $Cu-ZnO$ interface

  Although it has aforementioned benefits, it has also some disadvantages. Those can be listed as follows:
    - Easily deactivated by sintering
    - Low equilibrium conversion
    - Relatively low methanol selectivity
- In $Cu/ZnO/Al_2O_3$catalyst, the components can be summarized as follows:
    - **Copper** is the active part in methanol steam reforming
    - **Zinc oxide** is added to improve the dispersion of copper, to avoid the sintering of copper and for its reducibility
    - **Aluminum oxide** provides thermal protection, long term stability, improves surface area and lower the sintering
- Regarding catalytic activity results and structurel properties which is favor for MSR although Cu based ZnO and Al_2O_3 supported $Cu/ZnO/Al_2O_3$ catalyst have been studied mostly it has still areas to be studied to enhance its properties and achieve better performance.
- Different synthesize methods having changing parameters have a significant influence on catalyst activity and it should be investigated the relationship between synthesis, structure and activity in more detail.

4.3. Catalyst Preparation Methods

There are several methods such as impregnation, co-precipitation, oxalate gel–coprecipitation and ball milling comparatively examined for the preparation of catalysts for the production of hydrogen by methanol steam reforming. Some of the common preparation methods are summarized in **Table *4.2***.

Table 4.2. *Classification of common preparation methods*

Method	Summary
Impregnation	A solution comprising active components is submerged in a carrier. The leftover liquid is removed by heat treatment or at room conditions. After drying, calcining, and reduction, the catalyst is obtained.
Precipitation	A precipitating agent is added to an aqueous solution of a metallic salt in order to create a crystal hydrated oxides and carbonates.
Sol-gel Method	The sol-gel process begins with the formation of a colloidal solution known as sol. It is a solid-particle suspension in a liquid medium and to make it, hydrolysis and partial condensation of metal alcohols or inorganic salts are used to. By further condensation, gel form is created. Since the gel is a diphasic substance which encases the solvent in solids, heat treatments are applied to remove encapsulated liquid and finally the solid catalyst of nano particles is obtained. (Y. Zhang, 2020)
Physically Mixing	This approach is used to make mixed powder catalysts. The catalyst components are physically mixed with or without a binder or surfactant support in a ball mill to make these types of catalysts. After that, the mixture is agglomerated and activated.

The synthesis of $Cu/ZnO/Al_2O_3$ catalyst with regarding desired properties which is discussed previous chapter with high content of Cu, the preparation method of co-precipitation was chosen. However, this process has some difficulties, such as multistep processing and the need for sensitive pH and temperature control, alkaline metal contamination (Zhang et al., 2005). Co-precipitation procedure comprises the mixing of metal nitrates and sodium carbonate solutions at a controlled pH and temperature. Initially formed precipitate structure is amorphous. When it is aged, the formation of crystalline precursors is obtained. This ageing step is considered as necessary to generate optimum crystalline hydroxycarbonate precursors from an amorphous phase resulting desired highly active catalyst characteristics (Zhang et al., 2005) (Paul J. Smith et al., 2017). In this study, both the amorphous georgeite and crystalline malachite hydroxycarbonate precursors were synthesized. In preparation steps of malachite, initially georgeite is formed as a transient phase and then rapidly transforms into malachite. Zn is incorporated into georgeite to form zincian georgeite and zincian malachite. While zincian malachite was obtained by both conventional co-precipitaion and sequentially co-precipitation method, zincian georgeite was prepared by procedure modified sequentially co-

precipitation to inhibit crystalline malachite phase formation. Moreover, one more catalyst sample was prepared from directly oxide forms of CuO, ZnO and Al_2O_3. In co-precipitation method, these oxide forms are obtained from nitrate forms ($Cu(NO_3)_2$, $Zn(NO_3)_2$, $Al(NO_3)_3$) during precipitation. Therefore, one sample was prepared by directly mixing oxides and then it is shaped as a pellet form.

Specifications of the co-precipitation method can be listed as follows:

- High content of copper
- Improves the dispersion of copper oxide
- Decrease the particle size of the copper oxide
- Multistep processing
- The need for sensitive pH and temperature control
- Alkaline metal contamination

Preparation steps of the co-precipitation method can be seen in **Figure *4.1***.

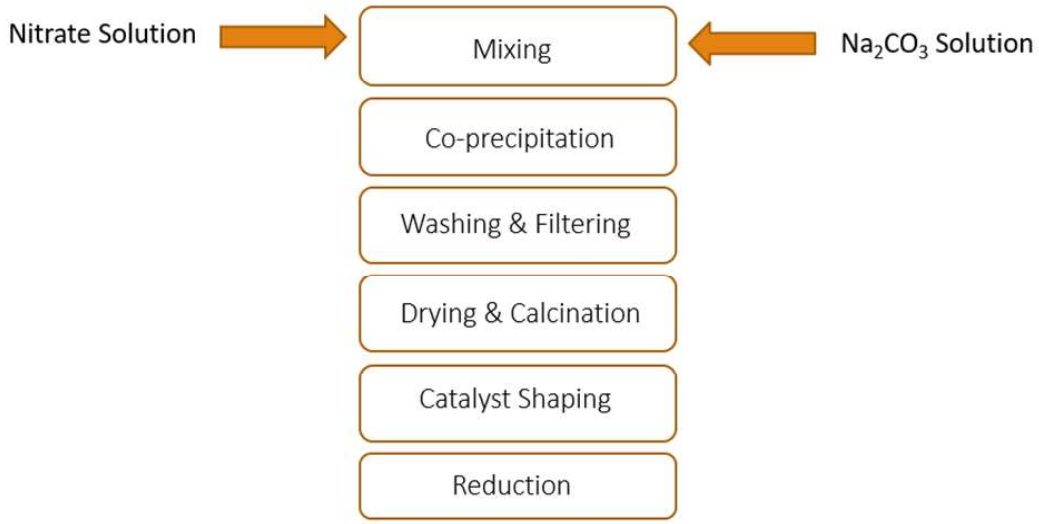

Figure 4.1. *Co-precipitation method procedure*

5. PROPOSED METHODOLOGY

5.1. Problem Definition

Despite the fact that $Cu/ZnO/Al_2O_3$catalyst has been studied in many researches to improve its catalytic activity in MSR, there are still areas that need to be investigated to improve its properties giving higher performance. Since the basis of this performance is Cu/ZnO synergy which provides the active sites for the reaction, it is necessary to create effective precursor structures for this aim.

5.2. Objective of the Study

According to the literature survey done for MSR process, it was concluded that the effect of preparation methods on the structure and catalytic behavior of $Cu/ZnO/Al_2O_3$ was not discussed adequately. The aim of this study is to get better structure and catalytic behavior of catalyst, which exhibits high specific surface area, high dispersion and higher activity for H_2 production. For this purpose, catalysts having a different preparation procedures which show active and stable performance synthesized. The catalyst activity was tested in MSR reaction setups experimentally.

In conclusion, the following issues were covered and followed as a procedure.

- Synthesis of $Cu/ZnO/Al_2O_3$ catalysts
- Catalysts characterization (XRD, N_2 adsorption/desorption (BET method), SEM)
- Testing the catalyst performance in reactor system
- Investigating the activity of synthesized catalyst in short term and long term periods, as well as under stop-start operating conditions.
- Testing for reproducibility and regeneration process effects

5.3. Contributions

The main objective of this study was to investigate the relationships between synthesis, structure and the activity for methanol steam reforming catalysts by different preparation methods. As a contribution, these different preparation techniques and their effects studied in terms of as follows:

- Performance comparison of $Cu/ZnO/Al_2O_3$ catalysts sythesized by conventional co-precipitation and sequentially co-precipitation methods in MSR

- Precursor formation, phase and morphology differences depending on synthesize route and parameters such as pH, ageing time and temperature and its effects on methanol steam reforming. Some precipitate phases seem to favor the superior catalytic behavior with well dispersion of copper, good surface properties and structure.
- Investigation of catalyst shaping techniques with extrusion and pelletizing
- Working with large amounts of catalysts compared to the amounts used in lab-scale studies in the literature. It is a good step for scale ups in MSR studies considering catalyst synthesizing in a large batches and reactor system design.
- The effectiveness of the ball milling method for uniform metal oxide dispersion with crystalline refining to prepare mixed oxide catalyst was studied. It has cost advance and short term preparation period compared to multi-step impregnation and precipitation methods as a promising and alternative method.

6. EXPERIMENTAL

6.1. Catalyst Preparation

6.1.1. Catalyst samples prepared by conventional and sequentially co-precipitation method

Zincian georgeite, an amorphous copper–zinc hydroxycarbonate and zincian malachite a crystalline copper-zinc hydroxycarbonate were prepared by sequentially coprecipitation using nitrate salts. Also two more samples were prepared with conventional co-precipitation procedure. While one of them was shaped with extrusion, the other one was shaped with press machine. Polyvinyl alcohol (PVA) and carboxymethyl cellulose (CMC) were used to easily perform the extrusion process and to add porosity to the catalyst structure as a binder. On the other hand, while shaping the catalyst with press, no binders were used. The calculation of metal loading amount for all synthesized catalysts was given in Appendix A.

The first catalyst sample of copper–zinc hydroxycarbonates was synthesized by the conventional co-precipitation procedure including mixing $Cu(NO_3).xH_2O$, $Zn(NO_3).xH_2O$ and $Al(NO_3)_3.xH_2O$ solution (each of 1 M) with using deionised water to give same $CuO : ZnO : Al_2O_3$ mass ratio of 55/33/12 for comparative purposes . This solution was pre-heated along with a separate aqueous solution of Na_2CO_3 (1 M). The hydroxycarbonates were precipitated by combining these two solutions simultaneously at 65 ℃, keeping the pH constant at $7.0 - 8.0$. The precipitates were aged for 2 hours keeping the temperature constant and the color change was observed. Ageing process was then followed by filtration to collect the precipitates then washed with deionised water (25 ℃) in order to minimise their sodium content. A conductivity meter was used to make sure that there was no further change in sodium content within the solution and then dried at 110 ℃ for 12 h in a muffle furnace. After all, it was calcinated at 350 ℃ to obtain oxide forms. Fianlly, powder catalyst was pelletized and reduced in hydrogen at 300 ℃ in total of 3 hours, with a heating rate of $5\ ℃/min$. The schematic view of synthesis procedure and parameters are shown in **Figure *6.1***.

Second catalyst sample was prepared by following the the same precipitation procedure. After it was dried, PVA and CMC mixture having a mass fraction of 10% with respect to total catalyst amount is solved in water and added and then mixed with a mechanical mixer until it gained a homogeneous consistency. It was shaped with

extrusion and left to dry at ambient conditions overnight. It was then calcinated at 350 ℃ to obtain oxide forms and reduced in hydrogen at 300 ℃ in total of 3 hours, with a heating rate of 5 ℃/min.

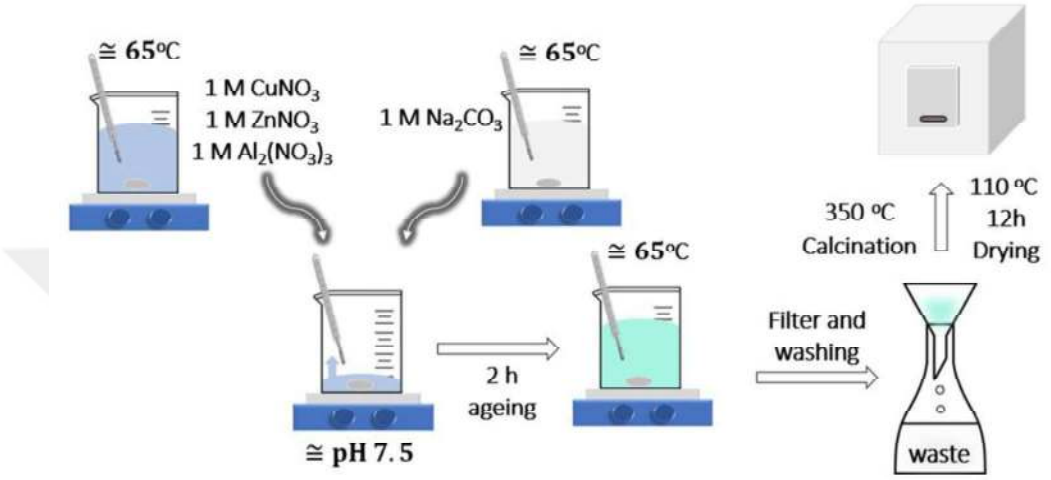

Figure 6.1. *Conventional co-precipitation*

The third catalyst sample of copper–zinc hydroxycarbonates was prepared by sequencially co-precipitation procedure following; $Al(NO_3)_3.xH_2O$ solution (1 M) and Na_2CO_3 (1 M) solution were prepared using deionised water and heated up to 40 ℃. These two solutions were firstly precipitated at constant temperature of 40 ℃ and left the solution stirring for 15 minutes. Meanwhile, a mixed $Cu(NO_3).xH_2O$ and $Zn(NO_3).xH_2O$ solution (each of 1 M) was prepared by using deionised water to give $CuO/ZnO/Al_2O_3$ mass ratio of 55/33/12 . These two solutions were pre-heated along with a separate aqueous solution of Na_2CO_3 (1 M). The hydroxycarbonates were precipitated by combining these two solutions simultaneously at 40 ℃, keeping the pH constant at $6.5 - 7.0$ into the first prepared $Al(NO_3)_3$ content solution. The precipitates were aged for 15 minutes at constant temperature around 40 ℃. During this process the solution retained its blue color. Ageing process was then followed by filtration to collect the precipitates then washed with deionised water (25 ℃) in order to minimise their sodium content. A conductivity meter was also used to control change in sodium content within the solution and then dried at 40 ℃ for 12 h in a muffle furnace. In corporation of zinc into the georgeite phase and mild ageing conditions inhibit crystallisation into zincian malachite or aurichalcite. Sensitive temperature and pH control, ageing time and the exclusion of alkali metals acting as catalyst poisons from the synthesis procedure are the key points

which should be considered for the enhanced catalyst performance. The synthesis procedure and parameters of the third catalysts are schematized in **Figure *6.2***. Finally, the catalyst was pelletized and reduced with hydrogen at 300 ℃ in total of 3 hours, with a heating rate of 5 ℃/min.

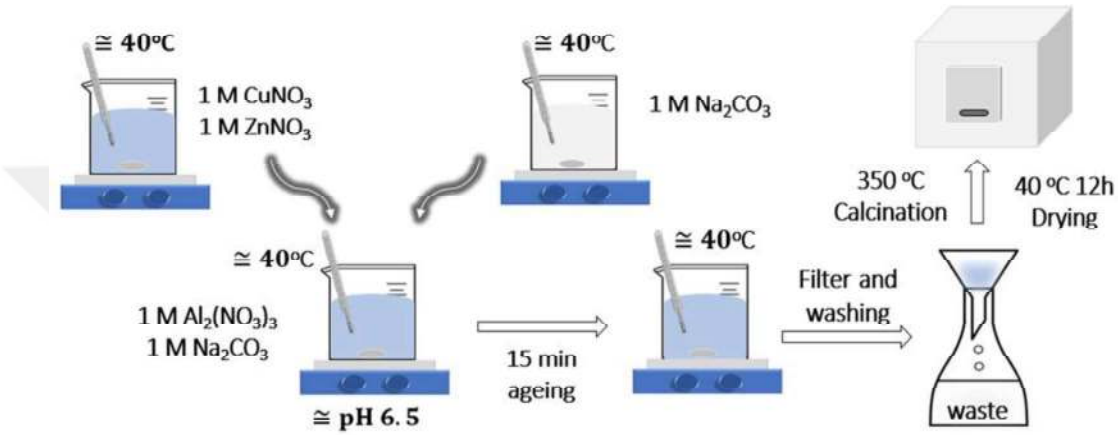

Figure 6.2. *Sequentially co-precipitation*

The fourth copper–zinc hydroxycarbonates sample was prepared in the same precipitation sequence but temperature was kept at 80 ℃ and the ageing duration was chosen as 3 hours. At this time solution color changed from blue to green. In addition, drying of precipitate was performed at 110 ℃ for 12 hours. The synthesis procedure and parameters of fourth catalysts are schematized in **Figure *6.3***. Pictures belong to ageing, filtration and drying are given in **Figure *6.4*** respectively. Afterwards, calcination, shaping with press as a pellet form and reduction were carried out under the same conditions that the first and third catalyst had. Reduction process with hydrogen in quartz glass tube reactor used in all calatalysts is shown in **Figure *6.5***.

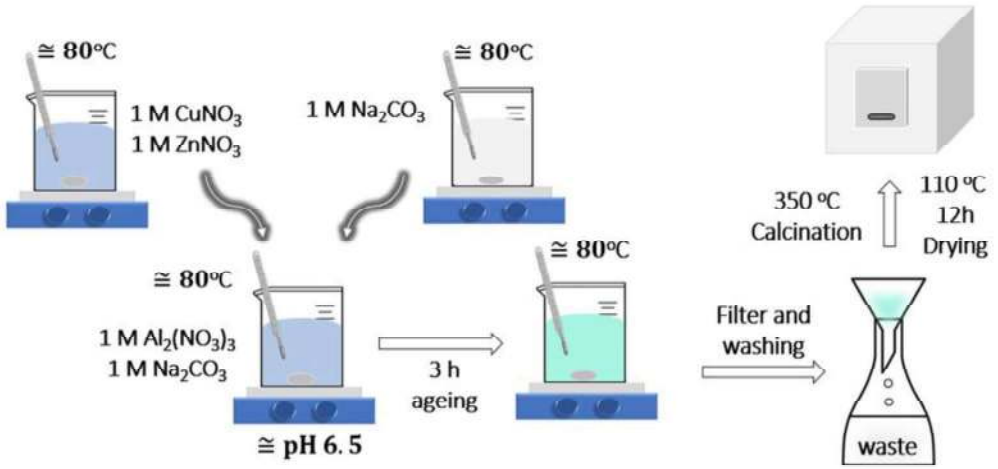

Figure 6.3. *Sequentially co-precipitation*

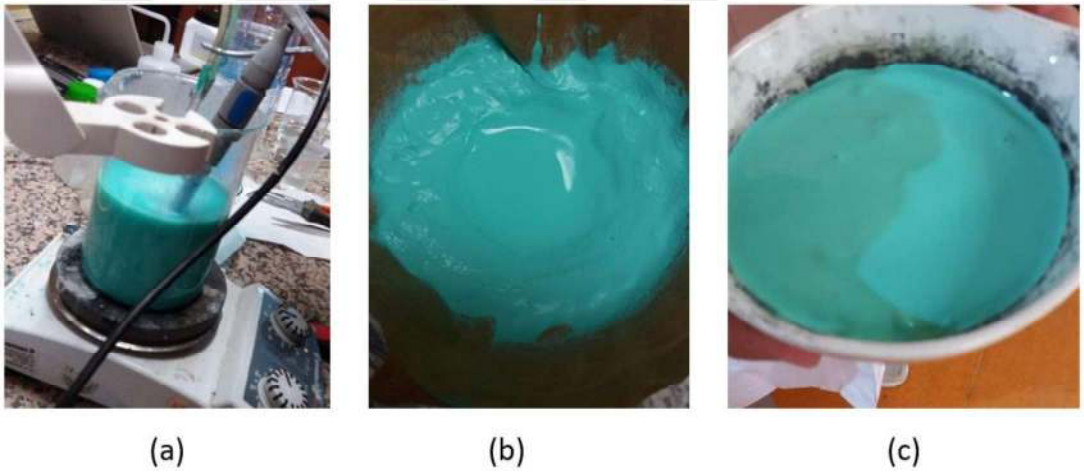

Figure 6.4. *Figures of (a) ageing (b) filtration (c) drying*

Figure 6.5. *Reduction with hydrogen in quartz glass tube reactor*

Catalysts in pellet form were obtained by shaping the catalyst with the help of a press and a press die set made according to the desired dimensions. Pelletizing equipments, images of the final catalysts in pellet form and the commercial catalyst are given in **Figure *6.6***. All the catalyst were synthesized to have a same mass ratio of 55% CuO / 33% ZnO /12% Al_2O_3 which is a similar composition and sizes with commercial Hifuel R120 catalyst so that we had a chance to compare their performance in MSR reaction.

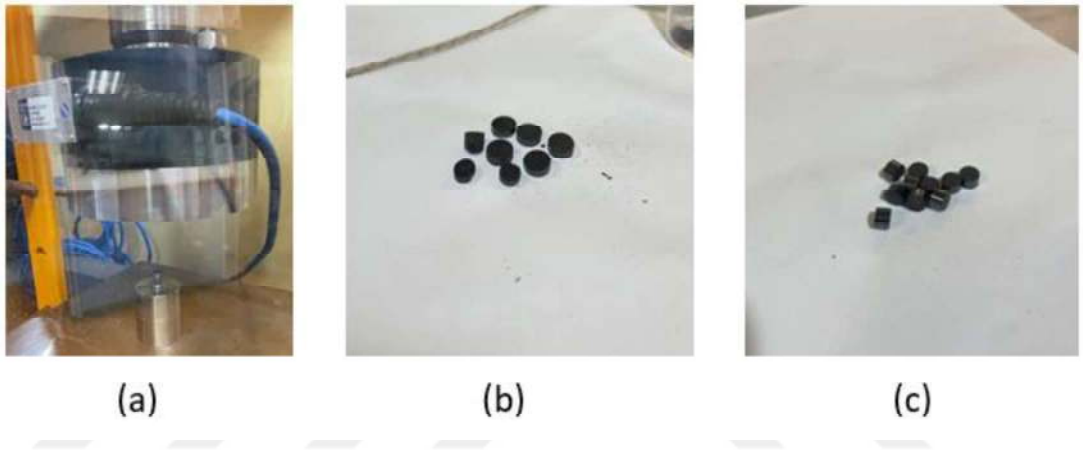

Figure 6.6. *Figures of (a) press machine and press die set (b) synthesized pellet form catalyst (c) commercial Hifuel R-120 catalyst*

The synthesized catalysts by co-precipitation and sequentially co-precipitation procedures are summarized in Table **Table *6.1***

Table 6.1. *Parameters of catalysts synthesis methods*

Catalyst Number	Preparation method	Precipitation reagent	Phases	pH	Temperature	Ageing time
1	Co-Precipitation	Na_2CO_3	Zincian malachite/ aurichalcite	7-8	65 °C	2 hours
2	Co-Precipitation	Na_2CO_3	Zincian malachite/ aurichalcite	7-8	65 °C	2 hours
3	Sequentially co-Precipitation	Na_2CO_3	Zincian georgeite	6.5-7.0	40 °C	15 minutes
4	Sequentially co-Precipitation	Na_2CO_3	Zincian malachite/ aurichalcite	6.5-7.0	80 °C	3 hours

6.1.2. Catalyst samples prepared by ball milling

One more catalyst sample was prepared by ball milling in ambient air. Principle of the process is grinding mixture of copper oxide zinc oxide and alumina oxide powders into very fine particles by metal balls. This helps in size reduction of the catalyst. Laboratory type "Retsch planetary ball mill PM 200" machine shown in **Figure *6.7*** was used for this purpose. The amount of metal oxides of CuO, ZnO and Al_2O_3 having the same mass fraction with the previous catalysts was mixed and placed in container along with balls. After closing container with tight lids, container rotation speed was arranged to 150 rpm for 12 hours. Rotation of the container causes different movements between the balls so that collision occurs between the balls and oxide powders. As a result crushed particles was obtained and its size was reduced. It is shown in **Figure *6.8***. It is important that milling time is critical because undesired phases and agglomarations can be observed if oxide powders are milled for longer time. Also speed of the rotation is very important. If the speed is high, then balls can be attached to the walls during the movement and they impose no force effect on the material. Therefore milling speed and time were determined after a few trials according to desired oxide mixture properties. After milling process calcination was perfomed at a same temperature of 350 ℃ and then shaped. Reduction procedure was applied similarly with previouse preparations.

Figure 6.7. *Retsch planetary ball mill PM 200 machine*

Figure 6.8. *Grinded mixture of copper oxide, zinc oxide and alumina oxide powders*

Temperature programmed reduction (TPR) provides information on the mechanism of the underlying reduction process. According to the literature, in the temperature range of $150 - 300$ ℃ low temperature (LT) peaks can be attributed to the reduction of copper oxide species in close contact with zinc oxide, since a strong interaction with ZnO can facilitate the reduction of CuO. Also, pure CuO is reduced at a higher temperature of 290 ℃. Furthermore, the small high temperature (HT) peaks in the temperature range of $300 - 350$ ℃ may indicate the presence of a small portion of CuO which interacts less strongly with ZnO and/or larger CuO crystallites hence higher temperature is required for reducing. On the other hand, since copper agglomeration is observed at the temperature values above 300 ℃, reduction temperature of was chosen as 300 ℃ regarding the operating temperature in MSR as well as being ensure complete reduction of CuO species.

6.2. Naming of the Catalyst

The synthesized CuO, ZnO and Al_2O_3 catalysts were named in format as "CZA - #". CZA is representing the components and the following number is used to sort catalysts by having different preparation procedure. The synthesized catalysts are given in **Table *6.2***.

Table 6.2. *The synthesized catalysts*

Catalyst Sample ID	Preparation method	Phases	Shaping
CZA-1	Co-Precipitation	Zincian malachite/ aurichalcite	Press
CZA-2	Co-Precipitation	Zincian malachite/ aurichalcite	Extrusion
CZA-3	Sequentially co-Precipitation	Zincian georgeite	Press
CZA-4	Sequentially co-Precipitation	Zincian malachite/ aurichalcite	Press
CZA-5	Ball milling	-	Press

6.3. Catalyst Characterization

The synthesized catalysts were characterized using different techniques of X-Ray Diffraction (XRD), Nitrogen Adsorption/Desorption Analysis (BET), Scanning Electron Microscopy (SEM).

6.3.1. X-Ray Diffraction (XRD)

The crystal structure of the catalyst was analysed using the X-ray diffractometer. Rigaku Miniflax 600 in ESTU Material Science Laboratory was used for the analysis. Bragg angle values were set in the range of 10°-90° with a step size of 1°/min for the high angle XRD pattern while Bragg angle values were choosen in the range of 1°-10° with a step size of 0.5°/min for the low angle XRD pattern.

6.3.2. Nitrogen adsorption/desorption analysis (BET)

In order to determine the multipoint Brunauer, Emmett and Teller (BET) surface area, pore volume, adsorption-desorption isotherms, and pore size distributions, Micromeritics Tristar II 3020 device at ESTU Material Science Laboratory was used. Catalyst samples were degassed at 120 ℃ for 3-hour before the BET analysis.

6.3.3. Scanning Electron Microscopy (SEM)

In order to determine catalyst morphology QUANTA 400F field-emission scanning Electron microscope in the METU Central Laboratory is used.

6.4. Activity Test

6.4.1. Experimental setup

To measure catalytic activity, MSR experiments were carried out in a vertical tubular reactor (I.D. 25 mm and Length 340 mm) at atmospheric pressure. An evaporator (I.D. 25 mm and Length 270 mm) was used before the reformer as a pre heater/evaporator.

Two furnaces were used to supply required heat to reactor and evaporator. The temperature was measured by means of three thermocouples inserted in the bed, one at the centre of the bed axis, another one at the outlet of the bed axis, and, the third one on the inside of the bed wall having a same axis with first one. In addition, two more thermocouples are used at the inlet and the outlet of the evaporator. Reformer outlet gas composition was determined by using a gas chromatograph. Outlet gas flow was measured by a flowmeter while the inlet feed flow is arranged with a peristaltic pump. The schematic diagram of the experimental setup is shown in **Figure *6.9***

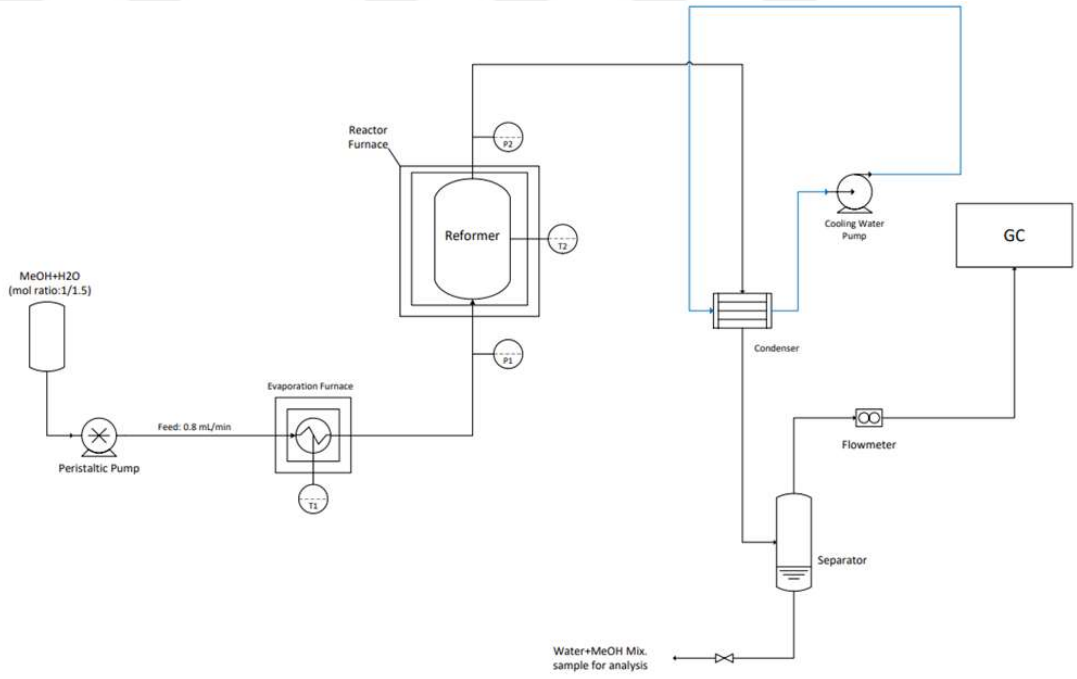

Figure 6.9. *Schematic diagram of experimental set up*

6.4.2. Experimental procedure

Sixteen grams of each catalyst samples were loaded into the reactor. Methanol and distilled water were initially mixed in required proportions. Then the mixture was passed through the evaporator maintained at $513\ K$, by means of a peristaltic pump to evaporate the water and methanol and also ensure that the reactants reach the temperature values close to reaction temperature before feeding to the reactor. Vaporized reactants entered in the reactor for steam reforming of methanol. Experiment set up is shown in **Figure *6.10***. Reactions took place under the atmospheric conditions. The product gas and unreacted reactants are passed through a glass condenser and liquid–gas separator funnel.

For condensation, water maintained at $287\ K$ was circulated. Unconverted products were collected in funnel after condensation, products from the gas sampler were passed through a gas flow meter and then vented. For the optimum temperature, feed composition and GHSV values, a series of experiment were carried out before, by varying these parameters. For the tempertaure determination, an experiment set having a temperature range of $533 - 563\ K$ was studied and MSR performance was evaluated. GHSV value was determined around 6000 h^{-1} and the calculation was given in Appendix C. The steam to methanol ratio was kept constant at 1.5 in order to lower CO concentration. During the experiments no CO was observed in the analysis. Experiments were conducted for six hours. The operating parameters used in the experiments are given in **Table *6.3***.

Figure 6.10. *Experimental set up*

Table 6.3. *Operating parameters*

Parameter	Value
Weight of catalyst loaded (g)	16
Temperature (K)	≅553.15
Pressure (atm)	-
Steam/Methanol ratio (mol/mol)	1.5
Run time (h)	6
Gas hour space velocity (GHSV)(h^{-1})	6000

6.4.3. Product analysis

The MSR products were composed of hydrogen and carbon dioxide with unreacted methanol and water. The unconverted methanol and water, which were condensed and separated from the product gas, were collected and their densities were measured. According to volume and density curve for methanol and water in addition to measured values, conversion data was calculated. Catalyst activity and performance is evaluated based on this methanol conversion. The calculation was given in detail in Appendix B and Appendix C. In addition, gas analyses were carried out using Gas Chromotography (Agilent Technologies 6890N). Products were analyzed in 25 m x 0.320 mmid capillary column. It takes 7 minutes for gas sample analysis. It starts with 80 ℃ and remains at that temperature for 3 minutes. Then the temperature increases to 185 ℃ with a rate of $35\ ℃/_{min}$. Finally it stays at 185 ℃ for 1 minute and program finishes. This temperture program is given in **Table *6.4***. At a certain time intervals (every two hours) samples were taken from the product gas were sent to the Gas Chromotograph to analyze the gaseous composition.

Table 6.4. *Temperature program for gas analysis*

Initial Temperature (℃)	**Final Temperature (℃)**	**Rate of Change of Temperature (℃/min)**	**Time (min)**
80	80	-	3
80	185	35	3
185	185	-	1

7. RESULTS AND DISCUSSIONS

7.1. Catalyst Characterization Results

7.1.1. X-Ray Diffraction (XRD) results

The XRD patterns of the catalyst samples of $CuO/ZnO/Al_2O_3$ before the reduction were examined to check the CuO existance. After calcination, CuO was detected in all catalyst as expected. As an example, XRD pattern of one of the sythesized catalysts (CZA-3) is shown in **Figure *7.1***. As can be seen, diffraction peaks at 32.5°, 35.5°, and 75.2°, corresponding CuO were observed.

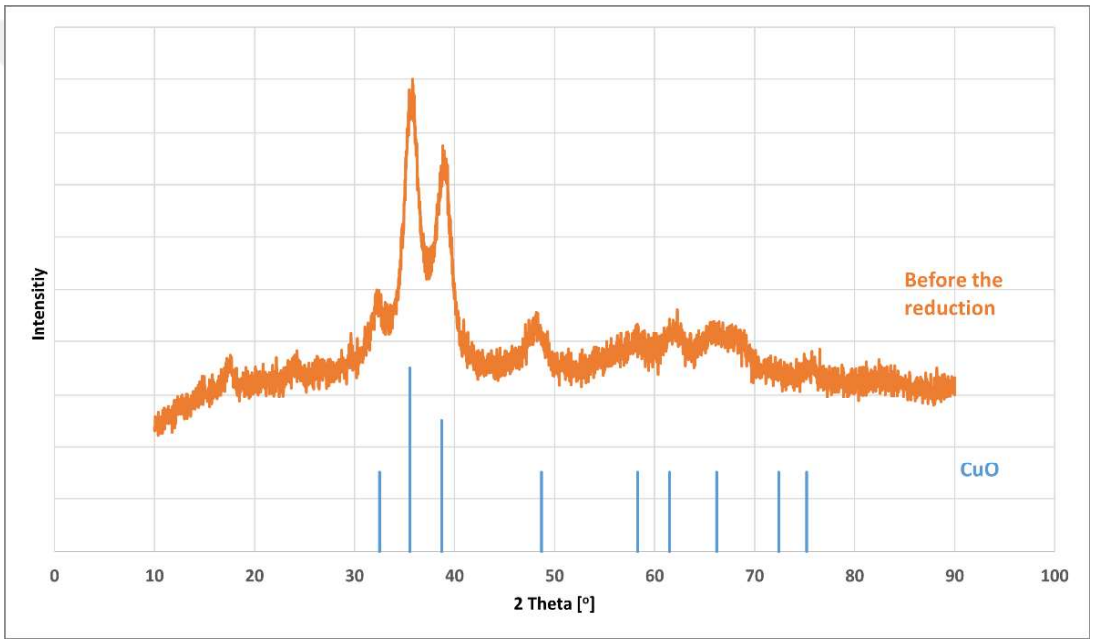

Figure 7.1. *XRD pattern of synthesized catalyst samples before the reduction*

Since copper oxide turned to copper after the reduction, it is expected to observe that there are diffractions peaks corresponding to copper in XRD analysis. XRD patterns of a reduced catalysts are shown in **Figure *7.2***, **Figure *7.3***, **Figure *7.4***, **Figure *7.5***, and **Figure *7.6***. All the synthesized catalysts exhibited a crystalline structure. Diffraction peaks at 43.3°, 50.5°, and 74.1°, corresponding to (111), (200), and (220) planes of copper were observed. In addition, diffraction peaks at 31.9°, 34.6°, 36.4°, 47.7°, 56.8°, 56.8°, 63.1°, and 68.2°, corresponding to (100), (002), (101), (102), (103), (110) and (112) planes of zincite were observed. For all catalyst, reflections for both Cu and ZnO were identified clearly. There were no peaks corresponding to aluminum oxides. Aluminum

oxides either too highly dispersed in a form of very small particles or existed as an amorphous phase in the reduced catalysts. It may also be explained considering the low content of aluminum oxide. Although Al_2O_3 was not detected in the XRD pattern, it could be observed in EDS results. For the comparison, Hifuel R-120 cataltyst XRD pattern was given in **Figure** *7.7*. The results shows similarity with the commercial Hifuel R-120 catalyst and studies related to $Cu/ZnO/Al_2O_3$in literature (Ren et al., 2019).

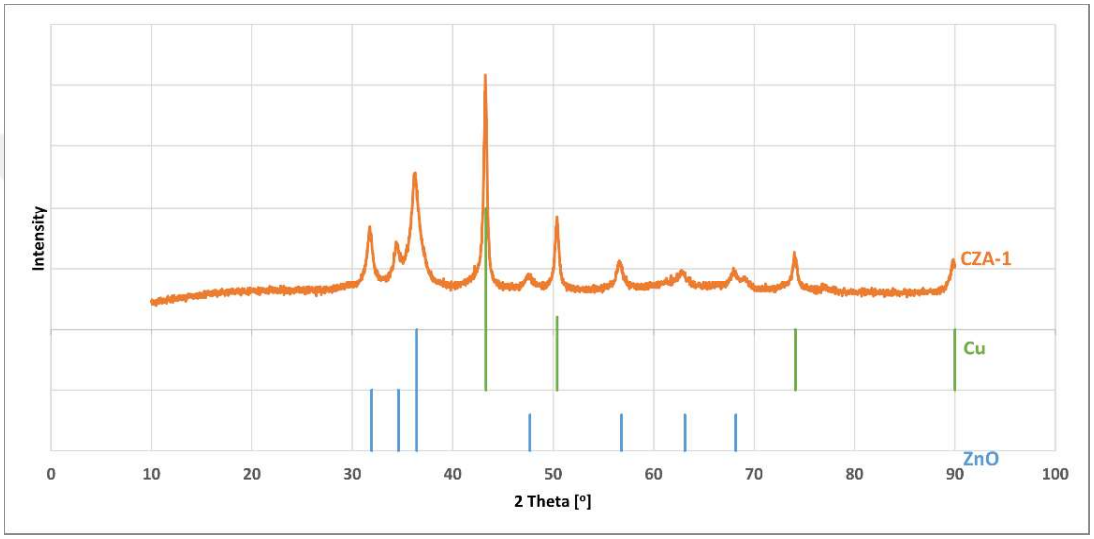

Figure 7.2. *XRD pattern of CZA-1*

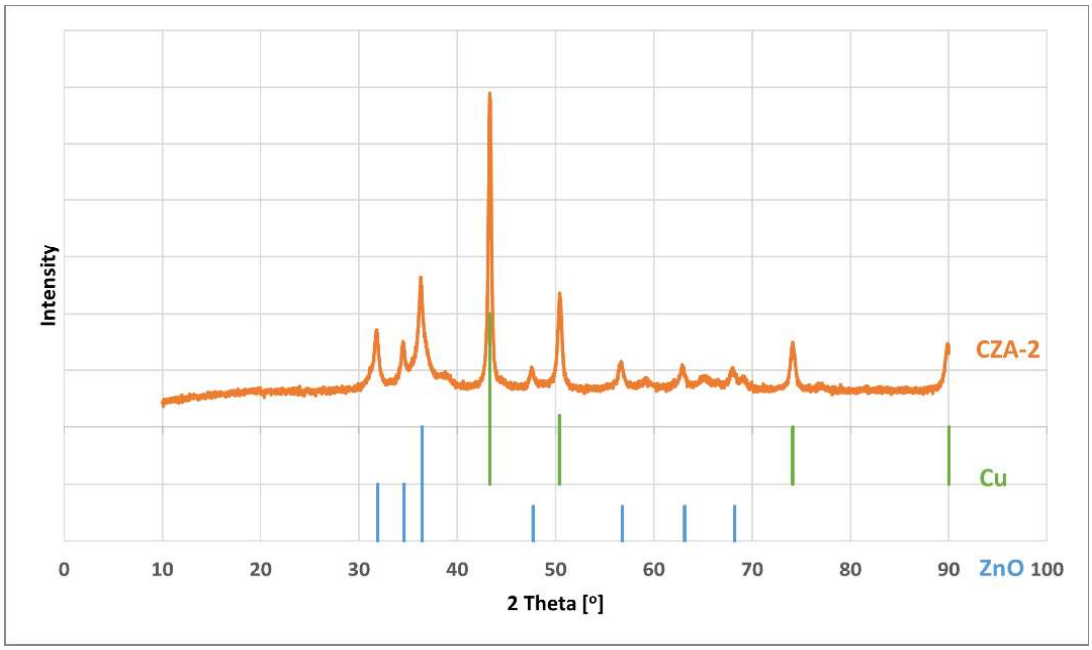

Figure 7.3. *XRD pattern of CZA-2*

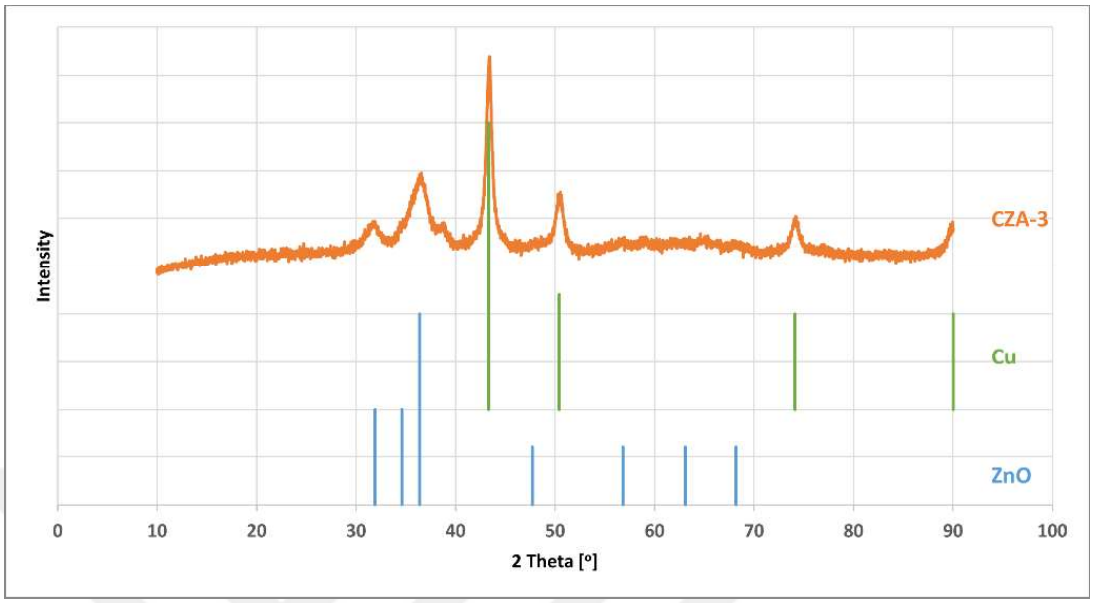

Figure 7.4. *XRD pattern of CZA-3*

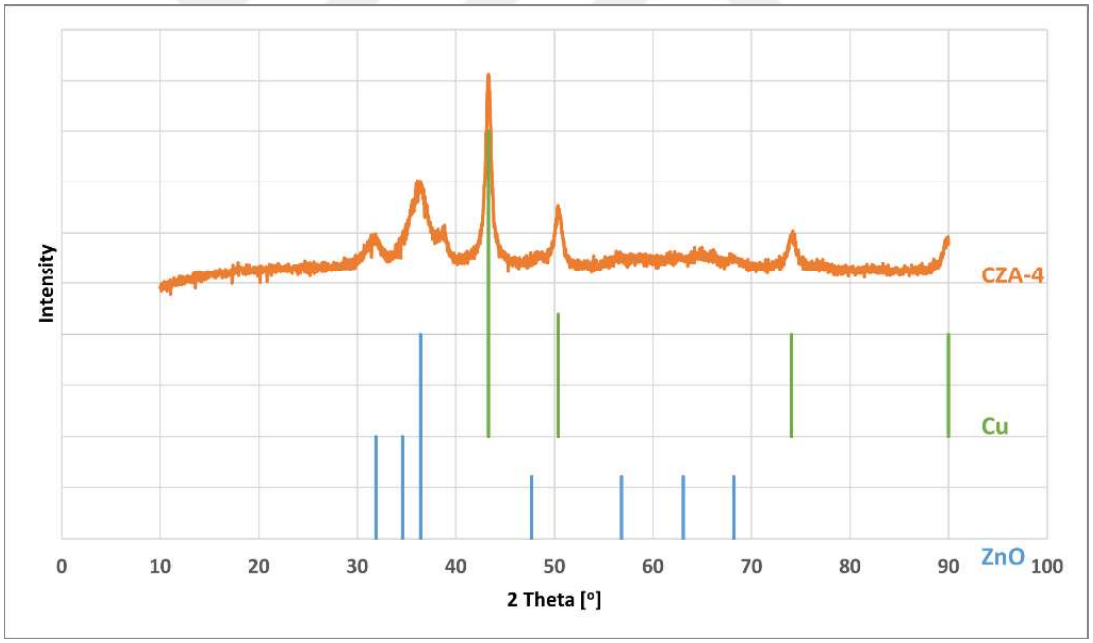

Figure 7.5. *XRD pattern of CZA-4*

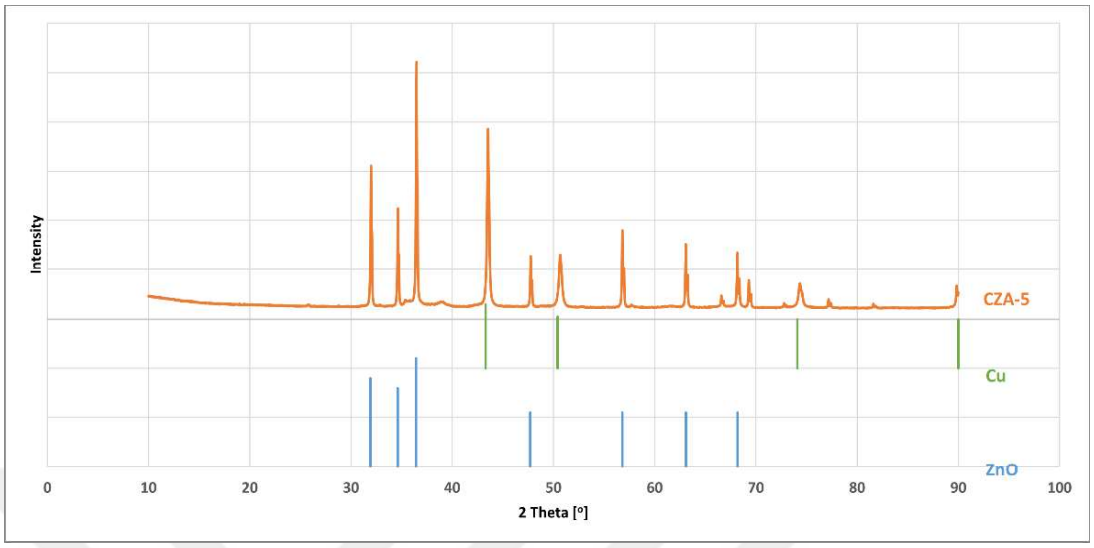

Figure 7.6. *XRD pattern of CZA-5*

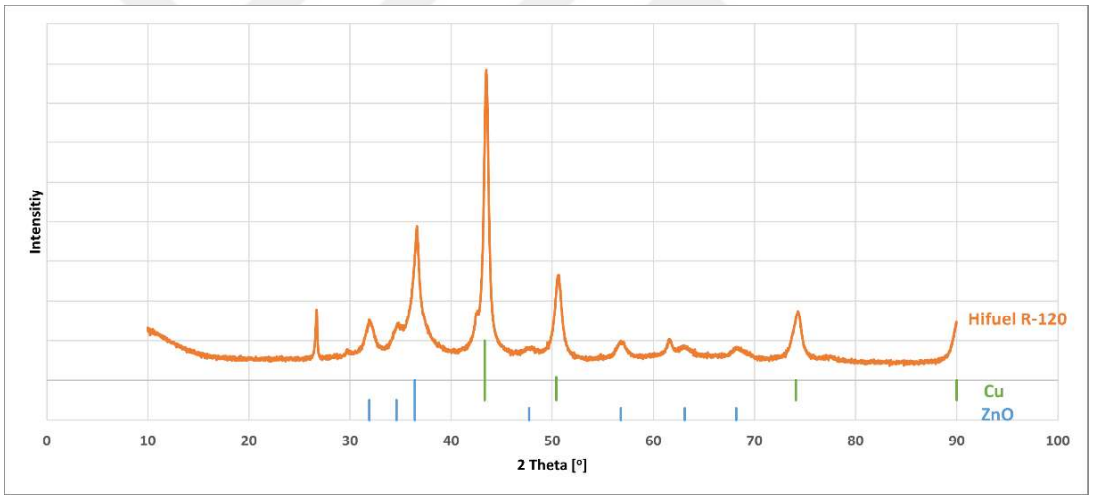

Figure 7.7. *XRD pattern of Hifuel R-120*

According to studies in literature, the catalysts with higher content of copper, the diffraction peaks of Cu show low intensity. Acting as a spacer and stabilizer ZnO paticles prevents direct contact of Cu particles which results in sintering and agglomeration. Furthermore, addition of Al_2O_3 and ZnO to Cu is effective on decreasing the degree of crystallinity, which could be related to the decrease in crystallite size of the catalyst. These were also observed for all synthesized catalyst in this study. Since all synthesized catalyst have almost same amount of metals, the differences in size of Cu crystallites in catalyst may be explained effects of preparation methods. Walter et al. (Walter et al., 2019), indicates that the catalyst preparation method let to the formation of larger particles, and some catalysts show less intense reflections for Cu and ZnO.

CZA-3 (amorphous zincian georgeite) and CZA-4 (crystalline zincian malachite) catalysts exhibited a low degree of crystallinity. They show less intense reflections for Cu and ZnO. The results indicated that the crystallite sizes of Cu in CZA-3 and CZA-4 synthesized by sequentially co-precipitation are 15.67 nm and 15.95 nm respectively while the size increased in the catalyst CZA-1 and CZA-2 prepared by conventional co-precipitation. The XRD results also revealed that the incorporation of ZnO into precursors forming $Cu - ZnO$ synergy has a positive effect on the dispersion of copper crystals. The Cu crystallite size is smaller than the catalysts that obtained in conventional co-precipitation. These results confirmed that the sequentially precipitation has positive influence providing high and uniform dispersion of copper in catalyst and large surface area. Crystallite size in the catalyst CZA-5 has the largest value compared to other ones. Similar results have been reported for co-precipitation method (Walter et al., 2019). CZA-5 prepared by ball milling showed more intense reflections both for Cu and ZnO in comparison to catalysts prepared by co-precipitation. This indicated that the ball milling method led to the formation of large particles. Cu and ZnO seem to exist in two separate phases hence the largest particle size can be also related to the pure copper sample. Similar XRD patterns were examined for the $Cu - ZnO$ based catalysts obtained physically mixing in literature (Huang et al., 1997).

The Sherrer equation was also used to measure the crystal sizes of Cu obtanined from reduced catalysts. The results of particle size of Cu crystallites with the (111) plane in the catalyst is reported in **Table *7.1***.

Table 7.1. *Copper crystallite (111) size obtained from their corresponding diffraction peak by Scherrer equation*

Catalyst	Cu crystal size (nm)
CZA-1	25.52
CZA-2	27.07
CZA-3	15.67
CZA-4	15.95
CZA-5	38.87
Hifuel R-120	17.52

7.1.2. N2 adsorption/desorption results

Surface area, pore volume and diameter of the catalysts were obtained from the N_2 adsorption/desorption analysis. Results are shown in **Table *7.2*** for sythesized catalyst and commercial Hifuel R-120 catalyst.

Table 7.2. *Physical properties of synthesized catalysts and commercial Hifuel R-120 catalyst*

Catalyst Sample ID	BET surface area (m^2/g)	BJH Adsorption Average Pore size (nm)
CZA-1*	64.3791	5.7272
CZA-1**	46.1706	6.4308
CZA-2*	29.8622	4.5763
CZA-2**	14.5596	6.5879
CZA-3*	65.9300	3.0800
CZA-3**	52.9054	6.1071
CZA-4*	80.2610	3.8380
CZA-4**	52.2456	6.3761
CZA-5*	10.4408	5.3414
CZA-5**	7.6765	5.4728
Hifuel R-120*	77.2820	1.9426
Hifuel R-120**	54.6669	2.4720

In **Table *7.2***, * sign represent the measurements before the MSR reaction, and ** sign represents the measurements after the MSR reaction. The highest surface area was observed for catalysts of CZA-3 and CZA-4.

IUPAC classified the adsorption isotherms into six types (Type I to VI), along with four hysteresis pattern types (H1 to H4). The different hysteresis patterns H1 to H4 are characteristic of different mesoporous shapes. The IUPAC classification of adsorption isotherms is shown in **Figure *7.8*** (Alothman, 2012).

The shape of the isotherm and its hysteresis pattern provide useful information about the physisorption mechanism, the solid and gas interactions, and can be used to qualitatively predict the types of pores present in the adsorbent. Typical N_2 isotherm shapes exhibited by microporous (type I), non-porous or macroporous (types II, III and VI), or mesoporous (types IV and V).

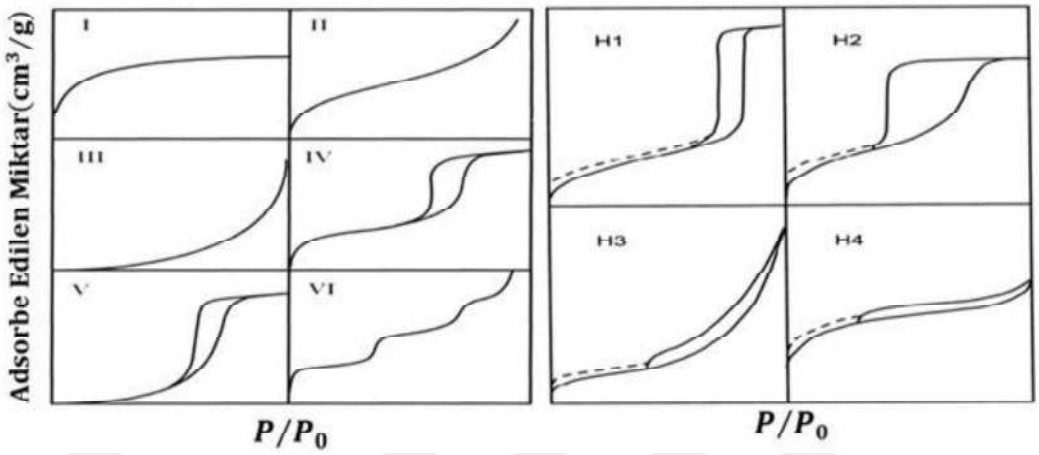

Figure 7.8. *IUPAC adsorption-desorption isotherms (Alothman, 2012)*

Figure ***7.8*** shows the N_2 adsorption/desorption isotherms accompanied by the corresponding to surface area. All the samples showed IV type isotherm with type H3 hysteresis loop. The IV type isotherm is assigned to mesoporous structures and the type H3 hysteresis is characteristic for slit-shaped pores (Sadeghinia et al., 2020). Adsorption/desorption isotherms for the synthesized catalyst and Hifuel R-120 are shown in between **Figure** ***7.9*** and **Figure** ***7.20***.

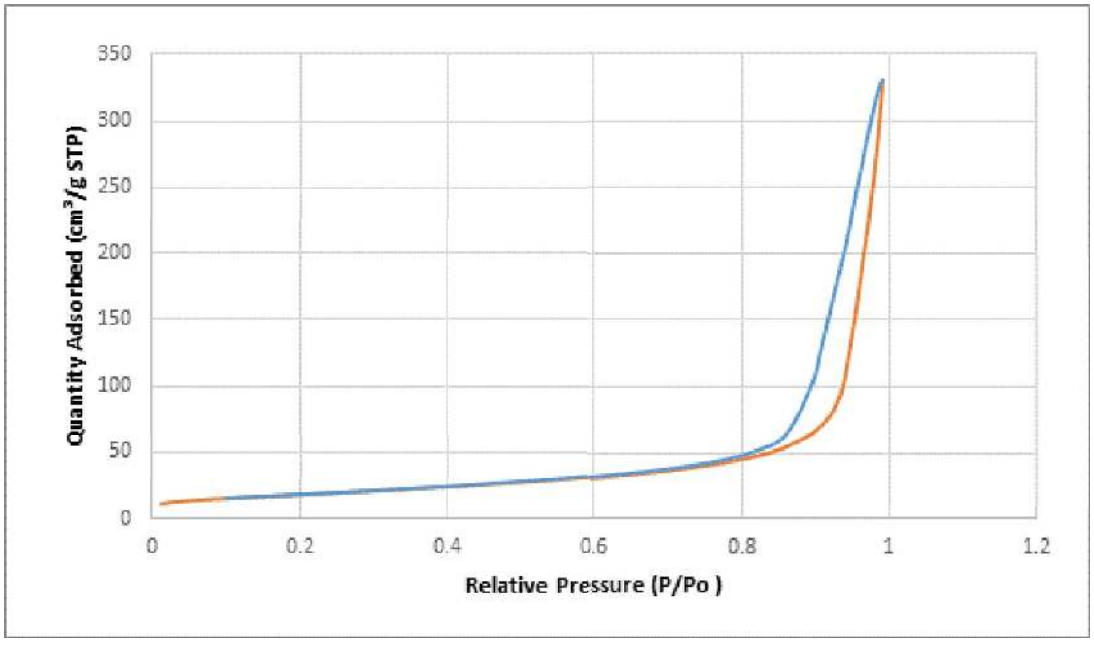

Figure 7.9. *N_2 adsorption/desorption isotherms for CZA-1 before the reaction*

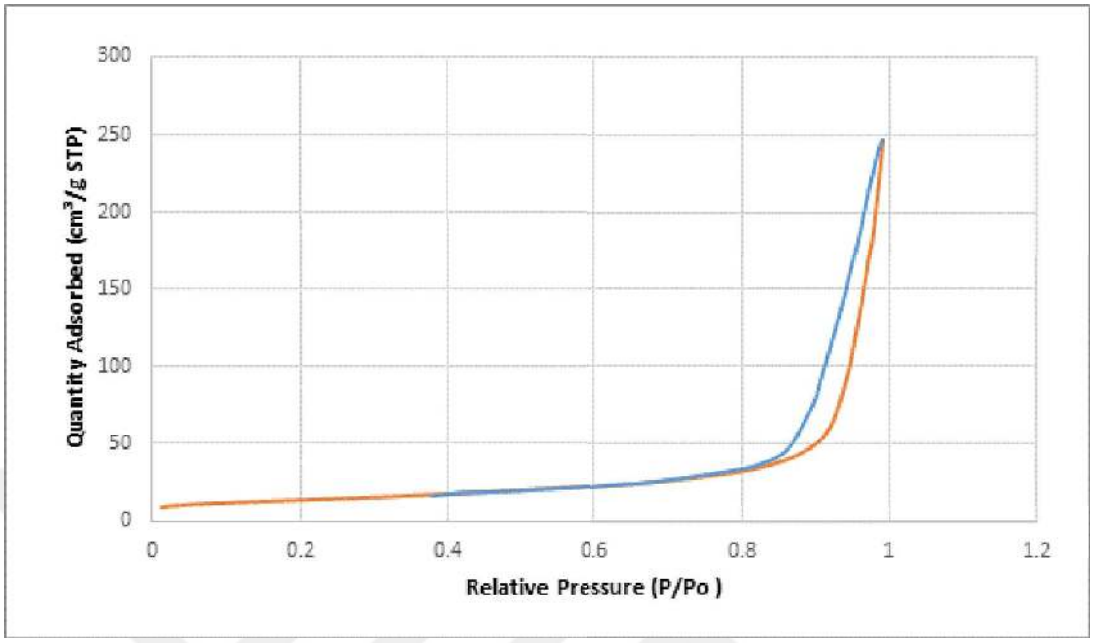

Figure 7.10. *N_2 adsorption/desorption isotherms for CZA-1 after the reaction*

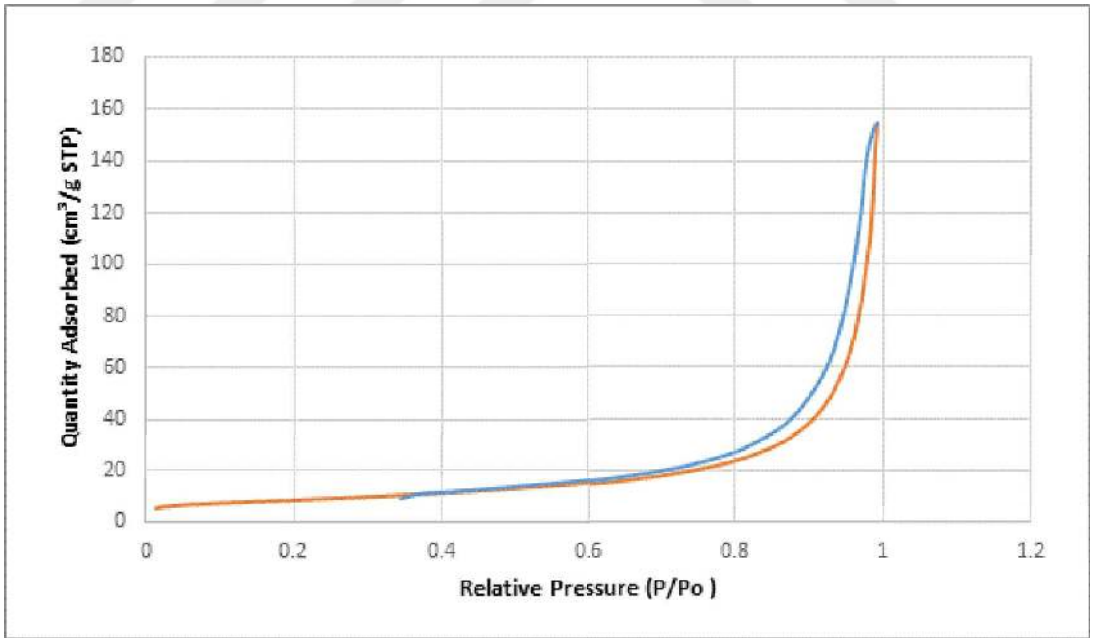

Figure 7.11. *N_2 adsorption/desorption isotherms for CZA-2 before the reaction*

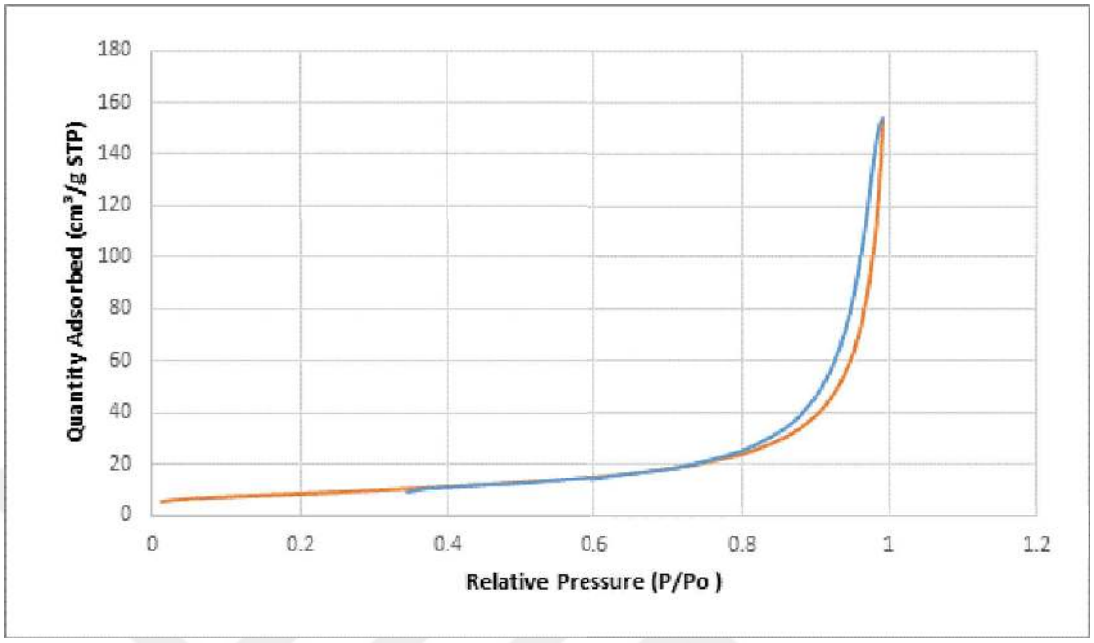

Figure 7.12. *N_2 adsorption/desorption isotherms for CZA-2 after the reaction*

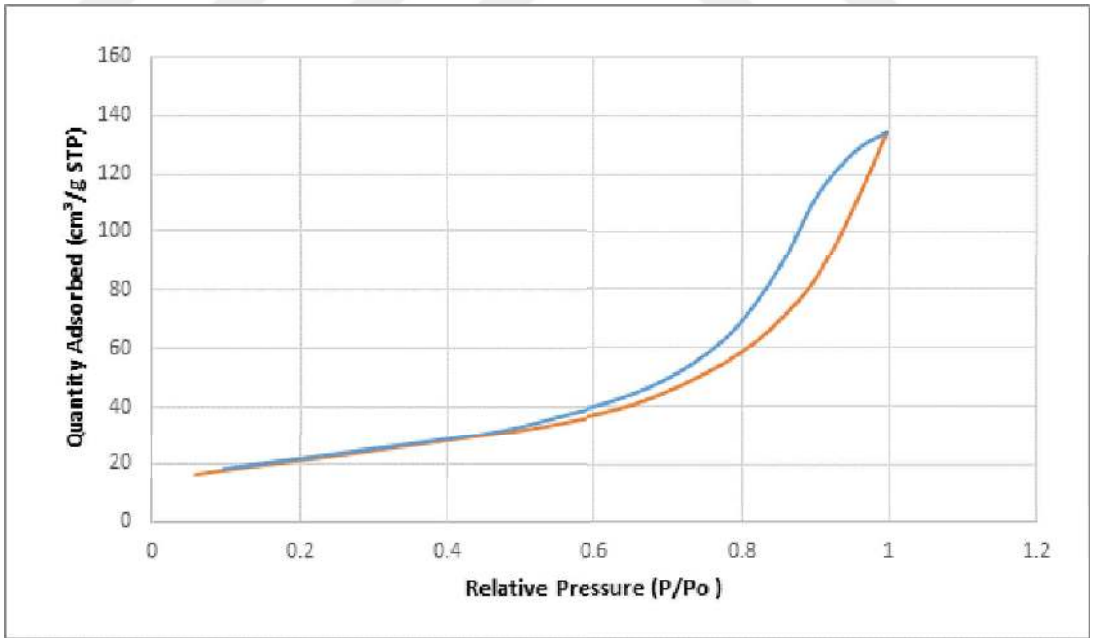

Figure 7.13. *N_2 adsorption/desorption isotherms for CZA-3 before the reaction*

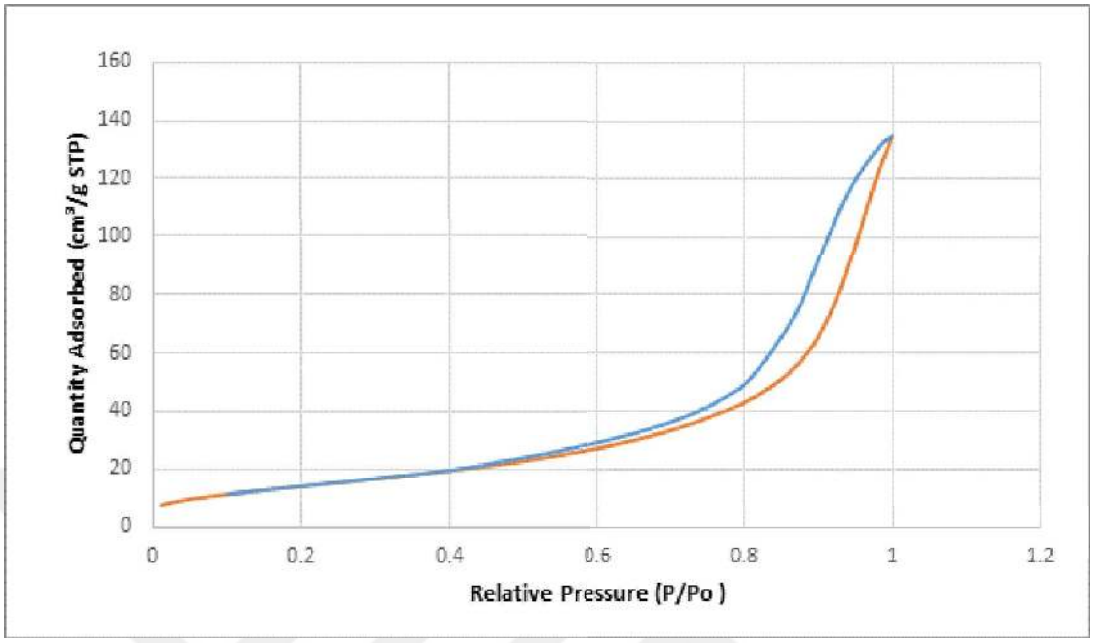

Figure 7.14. *N_2 adsorption/desorption isotherms for CZA-3 after the reaction*

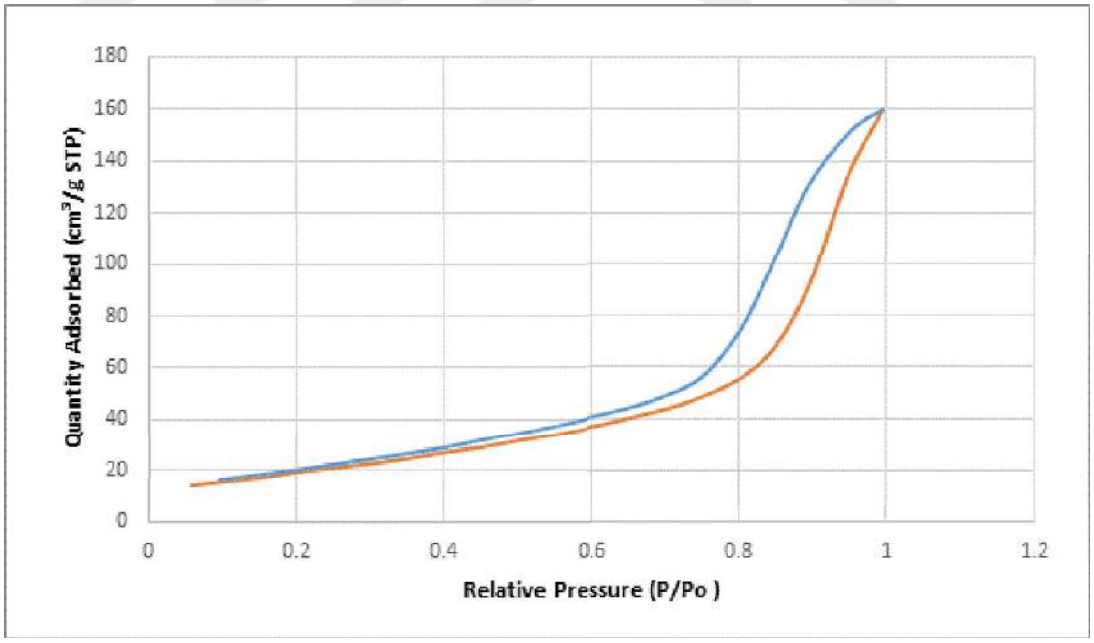

Figure 7.15. *N_2 adsorption/desorption isotherms for CZA-4 before the reaction*

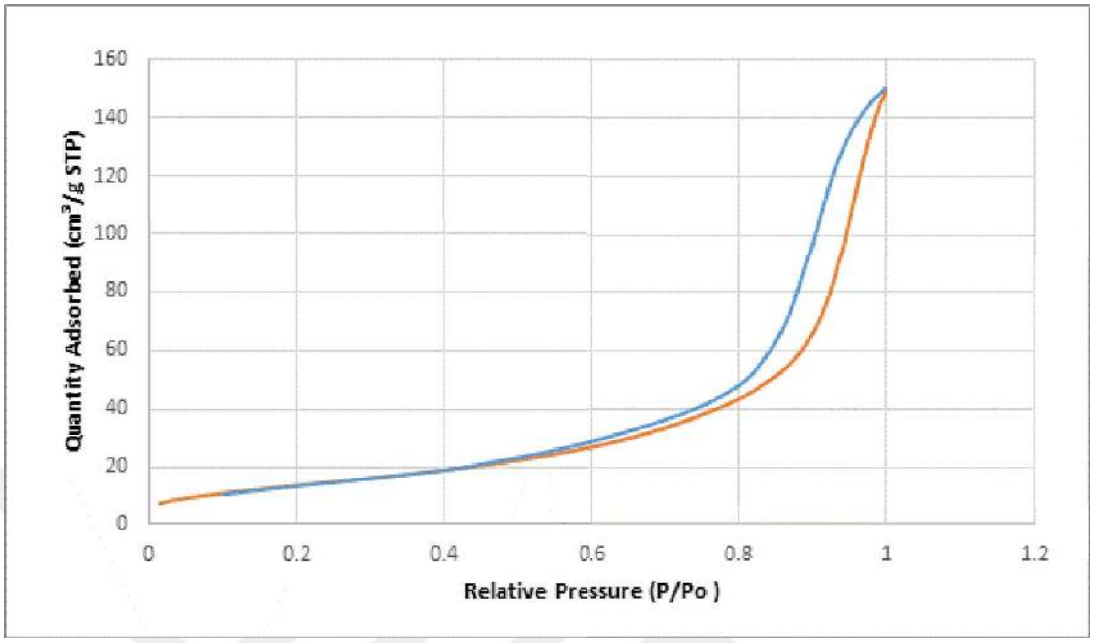

Figure 7.16. *N_2 adsorption/desorption isotherms for CZA-4 after the reaction*

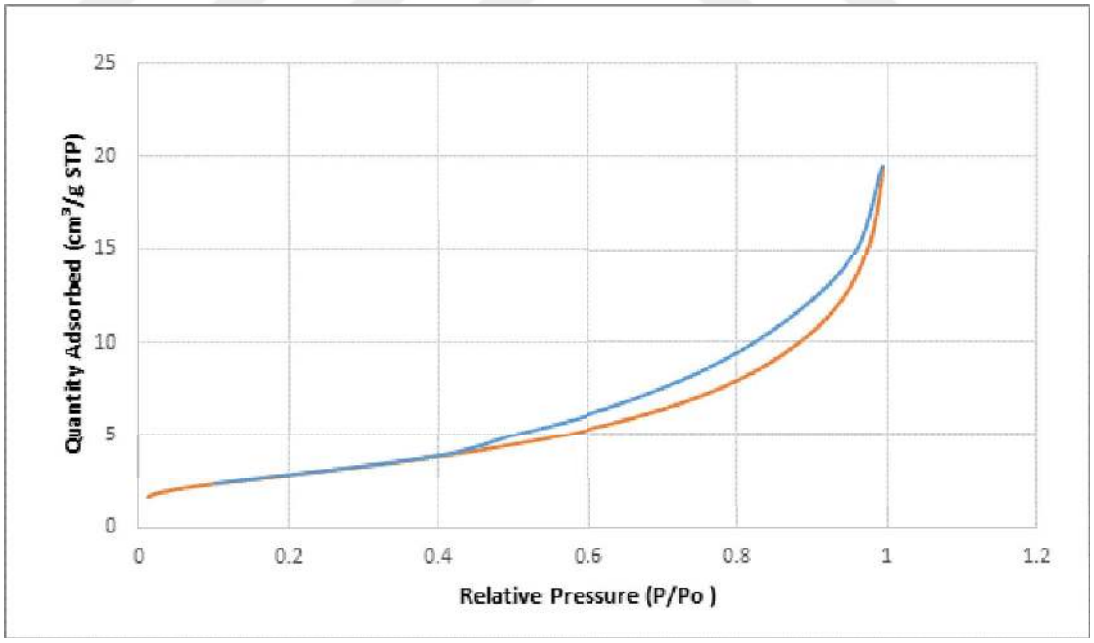

Figure 7.17. *N_2 adsorption/desorption isotherms for CZA-5 before the reaction*

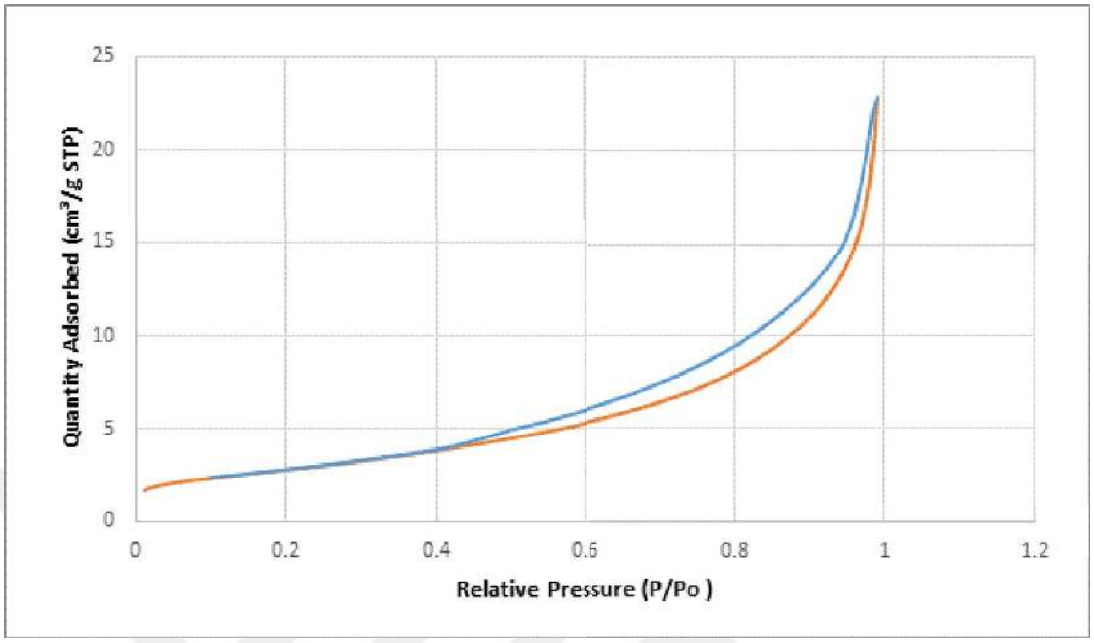

Figure 7.18. *N_2 adsorption/desorption isotherms for CZA-5 after the reaction*

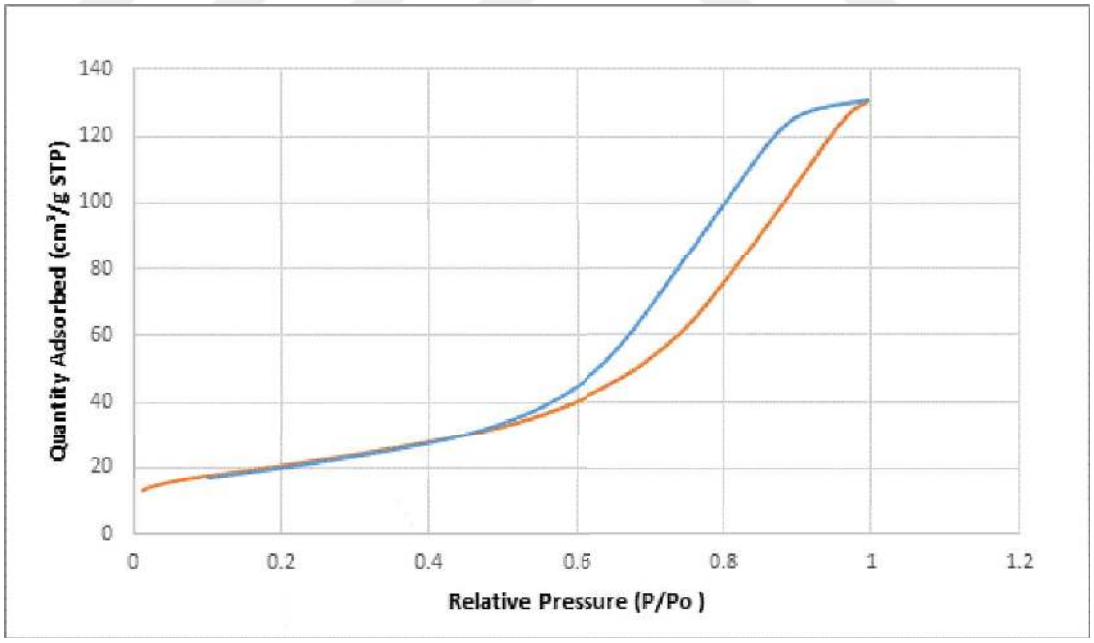

Figure 7.19. *N_2 adsorption/desorption isotherms for Hifuel R-120 before the reaction*

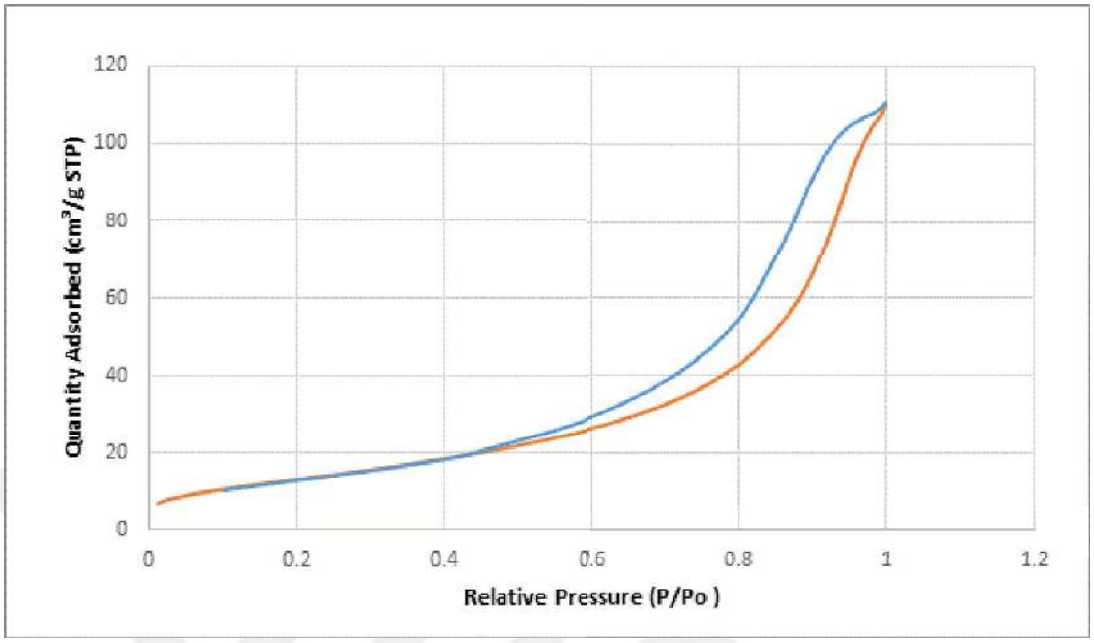

Figure 7.20. *N_2 adsorption/desorption isotherms for Hifuel R-120 after the reaction*

7.1.3 Scanning Electron Microscopy (SEM) results

SEM images of CZA-1 catalyst are shown in **Figure *7.21***. Homogeneous distribution of the CuO particles was achieved for this catalyst. Smaller copper oxide and zinc oxide particles in SEM image can be seen.

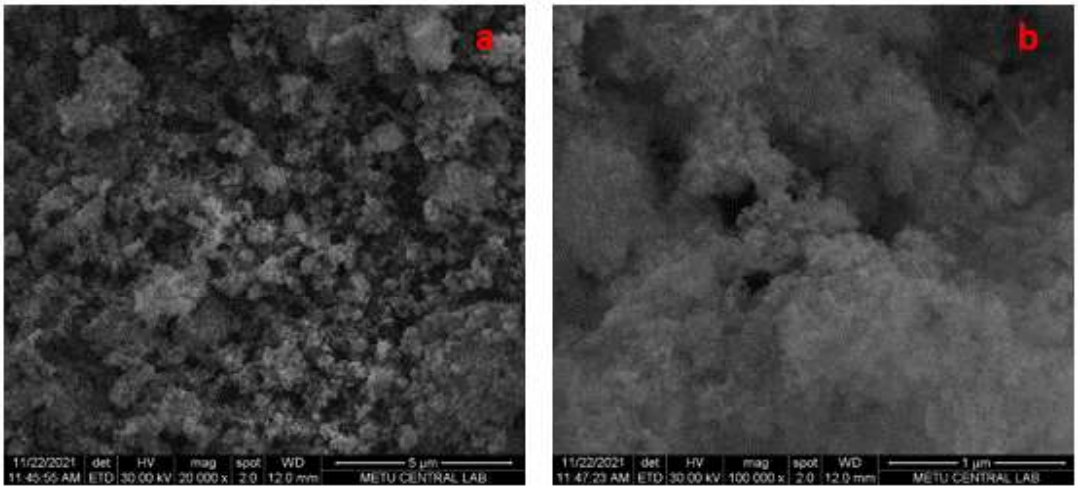

Figure 7.21. *SEM images of the CZA-1 at a) 20000X and b) 100000X magnifications*

SEM images of CZA-2 catalyst are shown in **Figure *7.22***. Small copper oxide and zinc oxide particles can be seen. In view of the SEM images, copper oxide had a good dispersion in the catalyst. However, while binder usage supports porosity and surface area of the catalyst, it may cause agglomerations at some points giving a larger particle size.

EDX result of **Figure *7.23*** shows that the copper amount in the catalyst was 47 % and the zinc amount in the catalyst was 36 % by weight.

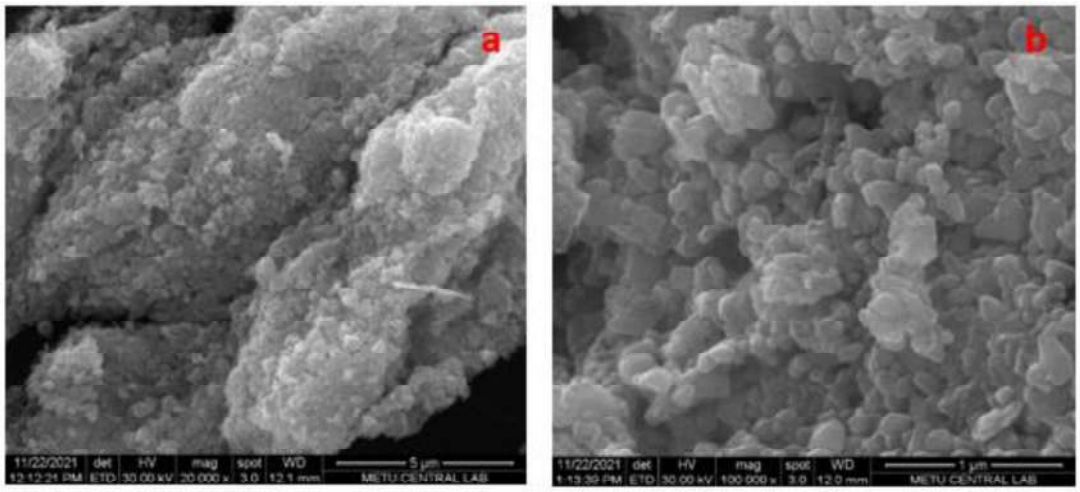

Figure 7.22. *SEM images of the CZA-2 at a) 20000X and b) 100000X magnifications*

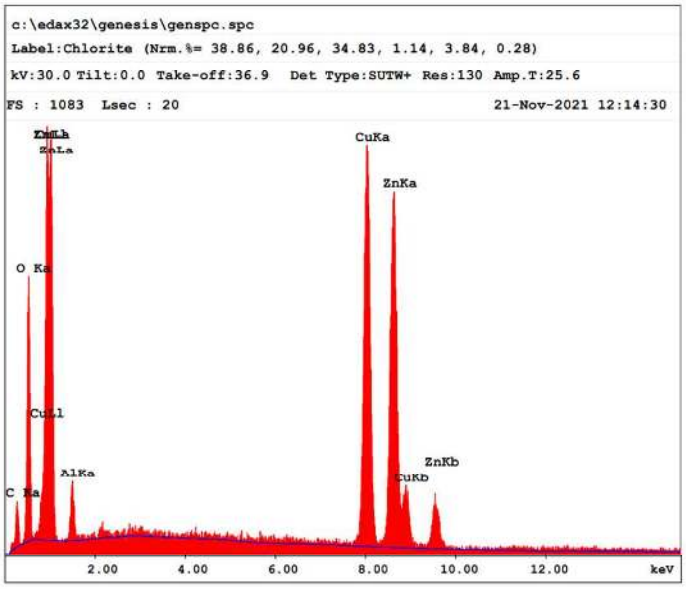

Figure 7.23. *EDX spectrum of CZA-2*

SEM images of catalyst CZA-4 are shown in **Figure *7.24***. Small copper oxide and zinc oxide particles can be seen in SEM image. Homogeneous distribution of the CuO particles was achieved for this catalyst. Copper oxide was successfully loaded into the catalyst. In view of the SEM images, copper oxide was well dispersed in the catalyst and ZnO is incorporated to the copper oxide particles to prevent agglomeration and sintering of copper particles. It was proved that co-precipitation method decreased the copper oxide crystal sizes and well dispersion of copper crystals was achieved with this method.

EDX result in **Figure *7.25*** shows that the copper amount in the catalyst was 46 % and the zinc amount in the catalyst was 25 % by weight.

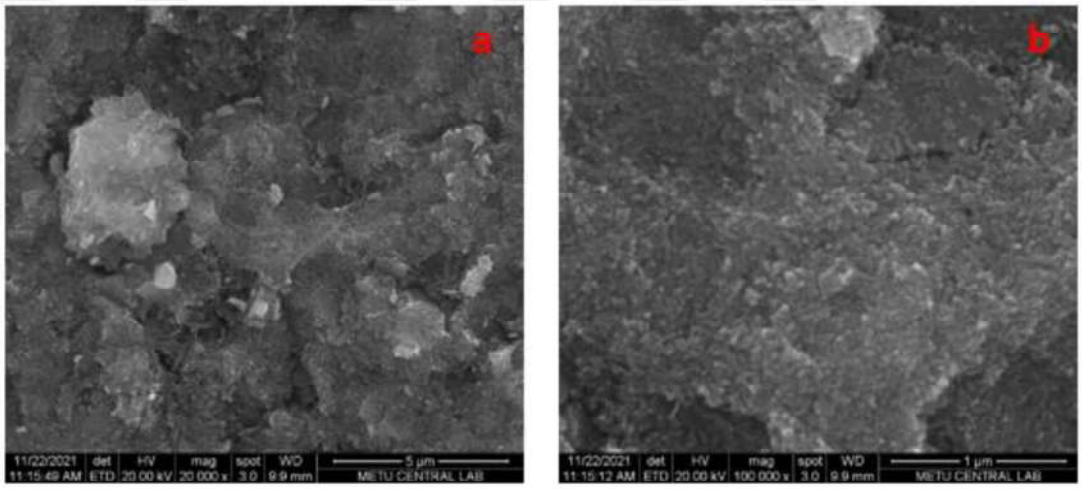

Figure 7.24. *SEM images of the CZA-4 at a) 20000X and b) 100000X magnifications*

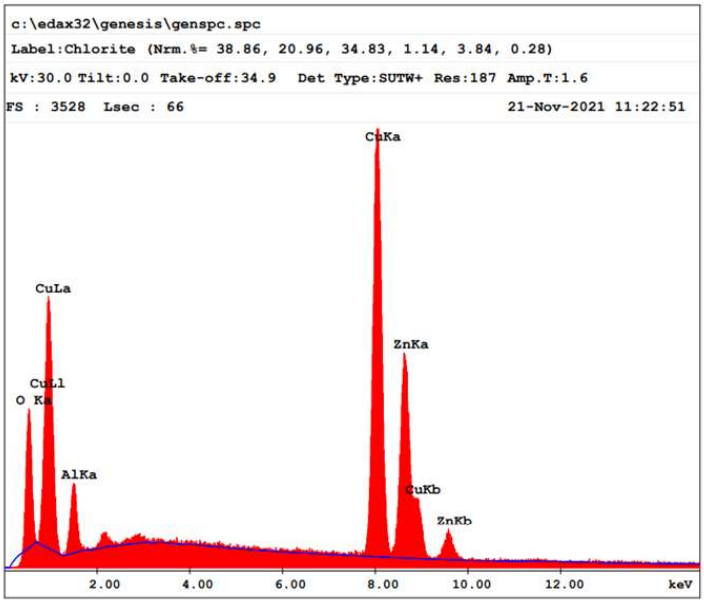

Figure 7.25. *EDX spectrum of CZA-4*

SEM images of CZA-3 catalyst are shown in **Figure *7.26***. Similarly, small copper oxide and zinc oxide particles in SEM image can be seen and homogeneous distribution of the CuO particles was also achieved well. EDX result of the **Figure *7.27*** shows that the copper amount in the catalyst was 51 % and the zinc amount in the catalyst was 25 % by weight.

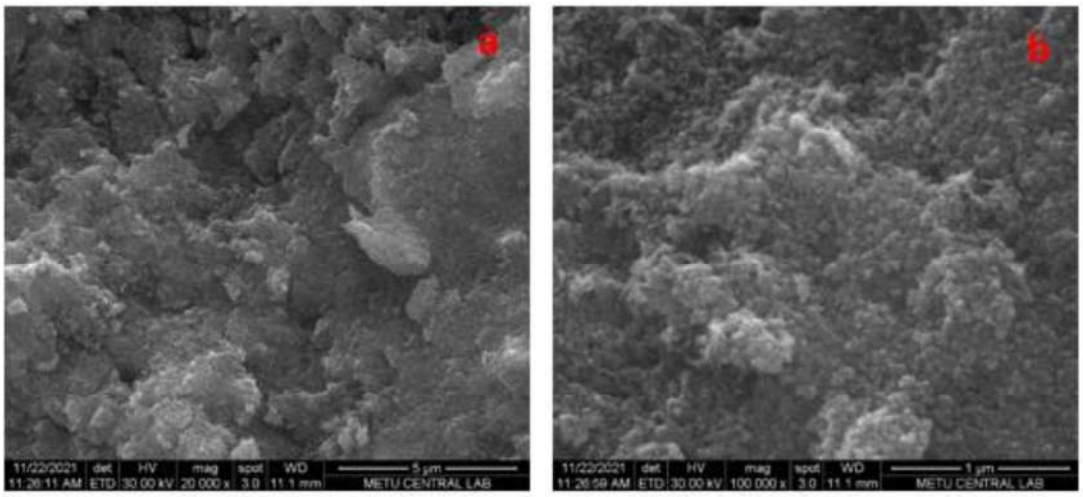

Figure 7.26. *SEM images of the CZA-3 at a) 20000X and b) 100000X magnifications*

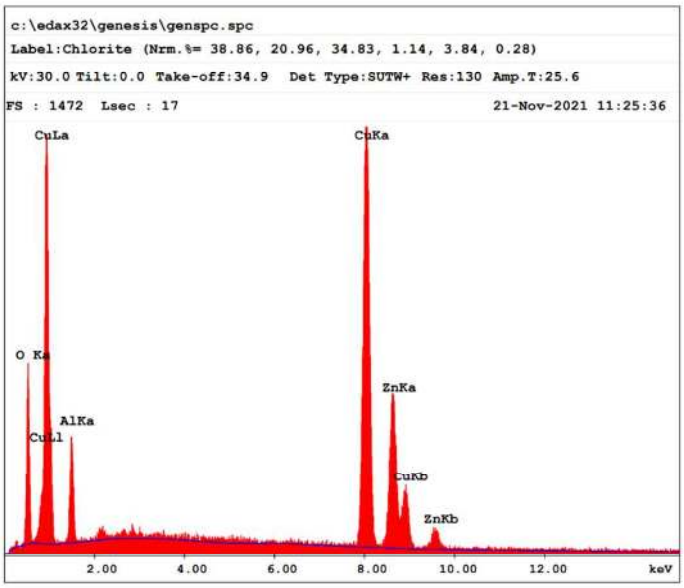

Figure 7.27. *EDX spectrum of CZA-3*

SEM images of CZA-5 catalyst are represented in **Figure *7.28***. Ball milling method of oxide forms method does not show well dispersion and homogeneous structure. Some agglomerations can be seen from the SEM image. Also, it has a bigger particle size. EDX result of **Figure *7.29*** shows that the copper amount in the catalyst was 51 % and the zinc amount in the catalyst was 30 % by weight.

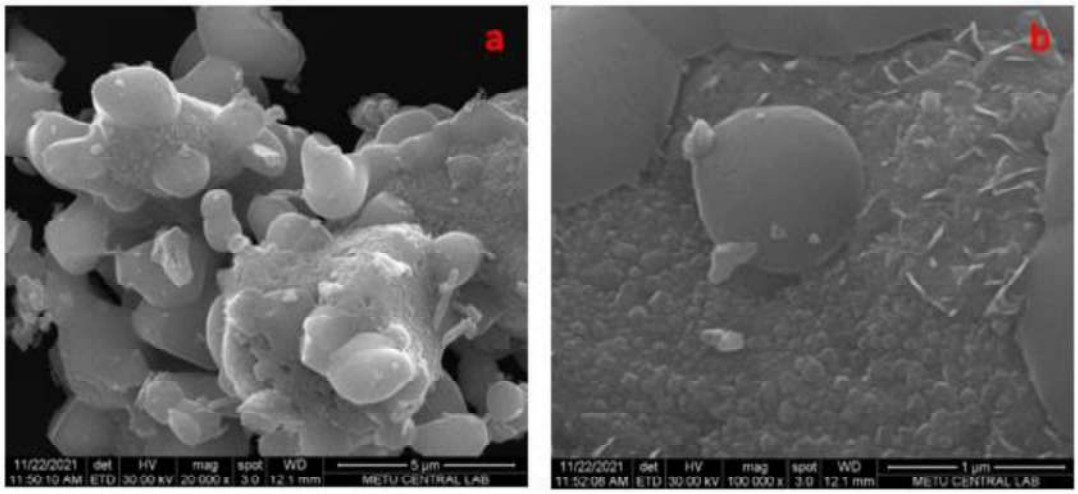

Figure 7.28. *SEM images of the CZA-5 at a) 20000X and b) 100000X magnifications*

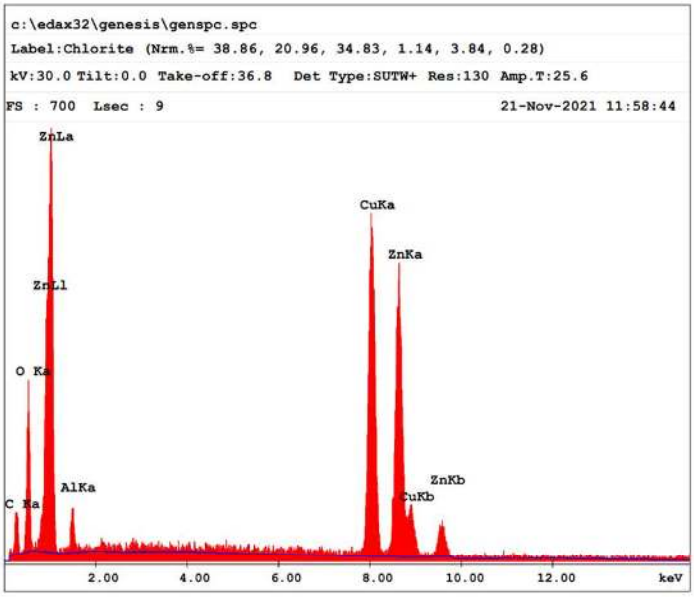

Figure 7.29. *EDX spectrum of CZA-5*

Regarding having a same preparation method as a precipitation, SEM images of commercial catalyst Hifuel R-120 are shown in **Figure *7.30*** for the comparison. It has a similar morphology, size, and dispersion with CZA-3 and CZA-4 catalysts.

EDX result of **Figure *7.31*** shows that the copper amount in the catalyst was 49 % and the zinc amount in the catalyst was 18 % by weight.

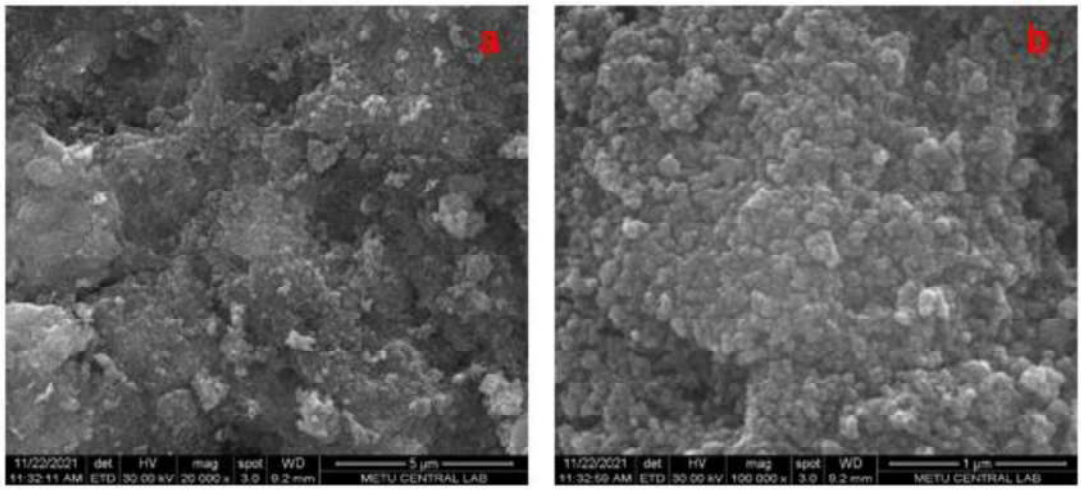

Figure 7.30. *SEM images of commercial catalyst Hifuel R-120 at a) 20000X and b) 100000X magnifications*

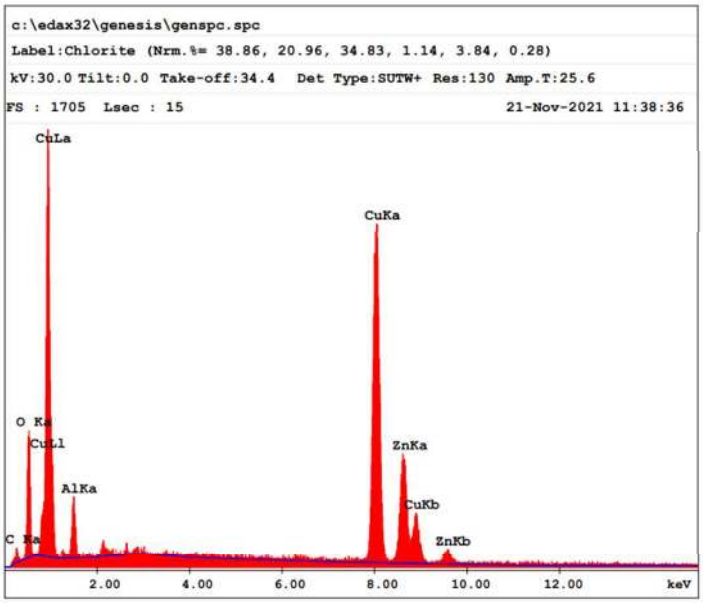

Figure 7.31. *EDX spectrum of commercial catalyst Hifuel R-120*

According to metal loading calculation, expected results for all synthesized catalysts' metal compositions results in terms of weight percentage were compared to EDX results. In addition, Hifuel R-120 EDX and ICP results are included in

Table ***7.3***. There is agreement in expected and actual values for all synthesized catalyst as well as Hifuel R-120. It is also consisted with desired oxide compositions $55\%\ CuO$, $33\%\ ZnO$ $12\%\ Al_2O_3$. It shows that, successive precipitation and metal loading at desired amounts are achieved.

Table 7.3. *Metal compositions of synthesized catalysts*

		EDX Results						
Element	**Expected Wt % for sythesized catalyst**	**Actual Wt % CZA-1**	**Actual Wt % CZA-2**	**Actual Wt % CZA-3**	**Actual Wt % CZA-4**	**Actual Wt % CZA-5**	**Actual Wt % Hifuel R-120**	**ICP Result Wt% Hifuel R-120**
Al	8.27	7.60	8.65	9.98	8.77	9.34	12.19	11.60
Cu	57.21	56.59	52.20	58.43	56.68	53.93	55.18	54.40
Zn	34.52	35.81	39.15	31.59	34.54	36.73	32.63	34.00

7.2. Catalytic Activity Results

7.2.1 Activity results of synthesized catalyst in MSR

Performance of $Cu/ZnO/Al_2O_3$ catalysts prepared by different procedures were evaluated in MSR reaction. Catalytic activity was evaluated in terms of methanol conversion. These calculations are given in Appendix B and Appendix C. Conversion results are shown in

Table 7.4. The best catalytic activity was obtained with the catalyst of CZA-3 and CZA-4 synthesized by sequentially precipitation method. Amorphous georgeite and crystalline malachite structures obtained by sequentially co-precipitation show superior catalytic performance with high methanol conversion above 90% percentage and low CO formation comparing other prepared catalyst samples. For the comparison, performance of commercial catalyst Hifuel R-120 in MSR was also evaluated under the same experimental conditions. After the end of the six hours experiment methanol conversion was calculated as 85.79%. The hydrogen-rich reformer outlet gas composition ($\sim 75\%$ H_2, $\sim 25\%$ CO_2) for each catalyst was calculated.

Table 7.4. *Conversion results of synthesized catalysts and Hifuel R-120*

Catalyst Sample ID	Preparation method	Phases	Conversion (%)
CZA-1	Co-Precipitation	Zincian malachite/ aurichalcite	74.36
CZA-2	Co-Precipitation	Zincian malachite/ aurichalcite	56.00
CZA-3	Sequentially co-Precipitation	Zincian georgeite	94.55
CZA-4	Sequentially co-Precipitation	Zincian malachite/ aurichalcite	94.99
CZA-5	Ball milling	-	68.5
Hifuel R-120			85.79

The system reached to a steady state at reaction time of 25-30 minutes. Therefore, gas sampling was started at the end of the first hour and repeated at the end of each hour during the six-hour experiment period. Gas chromatograph results showed that the reformer outlet average gas compositions were similar and about $75.28 \pm 0.3\%$ H_2,

$24.7 \pm 0.4\%$ CO_2, and almost 0% CO and CH_4 regarding to all the synthesized catalyst. Average product distribution is given in **Figure *7.32***.

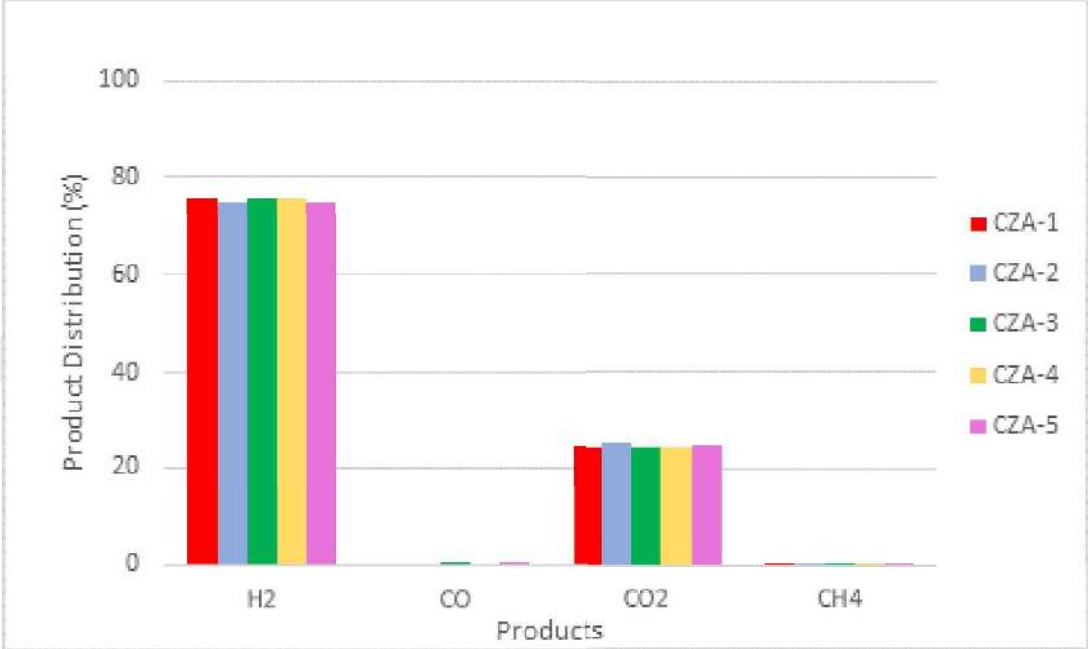

Figure 7.32. *Distribution of average mole percentage of products for all synthesized catalysts (T=280°C H_2O/CH_3OH=1.5)*

Hydrogen yield obtained with the synthesized catalysts is shown in **Figure *7.33***. Amorphous georgeite CZA-3 and crystalline malachite CZA-4 prepared by sequentially co-precipitation method have 96.31% and 96.63% hydrogen yield, respectively. Hydrogen yield of catalyst CZA-1 prepared by conventional co-precipitation method was 74.90%. The catalyst CZA-2 synthesized conventional co-precipitation method and shaped with extrusion as well as using binder shows 55.86% hydrogen yield. The catalyst CZA-5 synthesized with ball milling method gave 68.48% hydrogen yield.

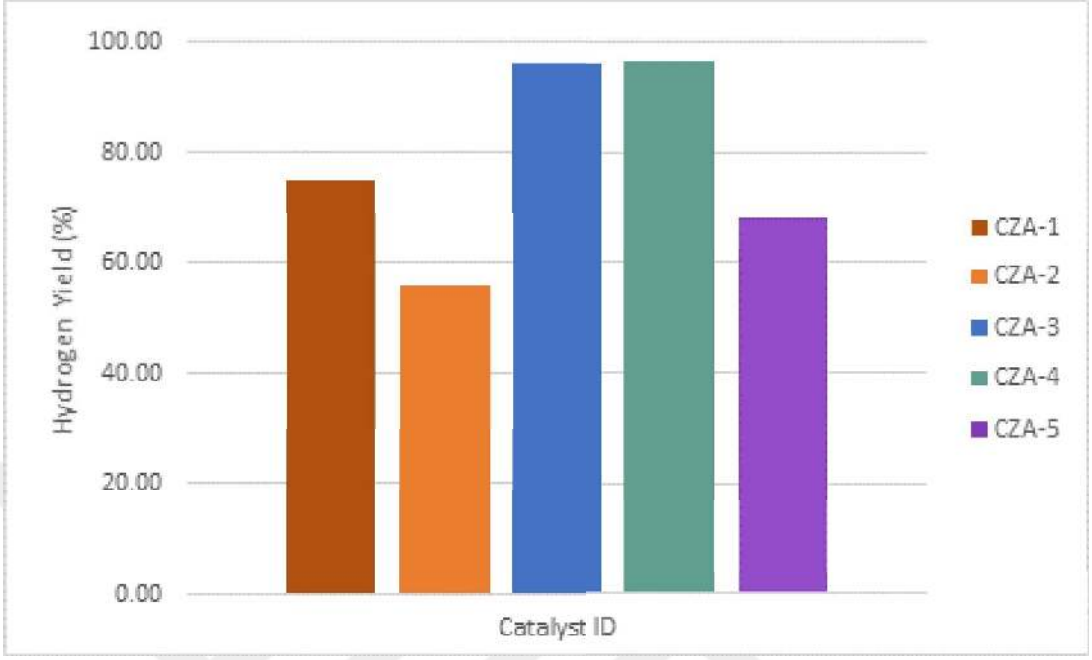

Figure 7.33. *Percentage of hydrogen yield for synthesized catalysts (T=280°C H_2O/CH_3OH=1.5)*

Average product distribution, methanol conversion and hydrogen yield are given in **Table *7.5*** according to each synthesized catalyst. Methanol conversion and hydrogen yield calculations were given in detail in the Appendix C. As it can be seen from **Table *7.5***, highest methanol conversion and highest hydrogen yield were achieved by the catalysts CZA-3 and CZA-4. However, other synthesized catalysts CZA-1 and also CZA-5 show good catalytic performance regarding conversion and hydrogen yield values.

Table 7.5. *Hydrogen production average results for synthesized catalysts*

Catalyst ID	Average Gas Composition (%)		Methanol Conversion (%)	Hydrogen Yield (%)
	yH2	yCO2		
CZA-1	75.54	24.46	74.36	74.90
CZA-2	74.81	25.19	56.00	55.86
CZA-3	75.60	24.41	94.55	96.31
CZA-4	75.50	24.50	94.99	96.63
CZA-5	74.97	25.03	68.51	68.48

Furthermore, product distributions in molar percentage were plotted according to 1-hour time intervals throughout the experiment period in **Figure *7.34*** to observe continuous hydrogen production throughout the the experiment duration. In this figure, left and right y-axes represent H_2 and CO_2 molar percentages respectively.

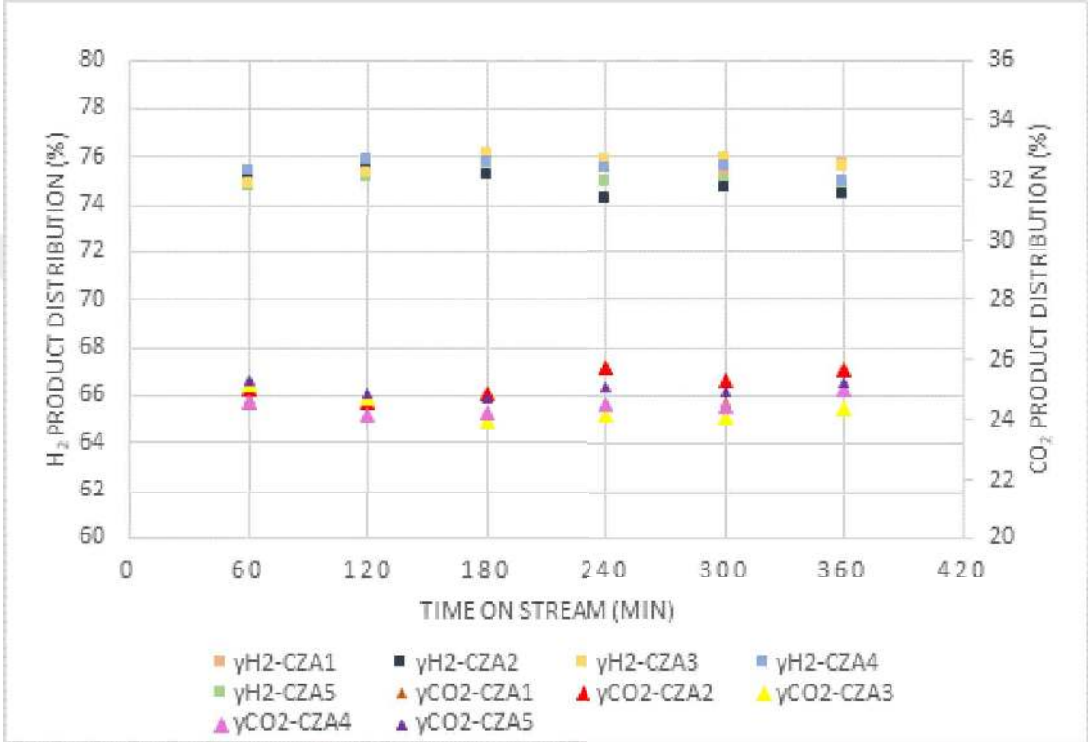

Figure 7.34. *Product distribution in a mole percentage in the experiment period for synthesized catalysts (T=280°C H_2O/CH_3OH=1.5)*

7.2.2. Reproducibility

For repeatability, one more experiment was performed for each catalyst under the same conditions at different time. Average outlet gas composition was $75.15 \pm 0.3\%$ H_2, $24.7 \pm 0.3\%$ CO_2, and 0% CO Methanol conversion and hydrogen yield calculations gave similar results comparing first experiment set. Products distributions also showed similarity and were given in **Figure *7.35***. The results of both experiment sets were consistent with each other. Hence, it was concluded that experiments were reproducible.

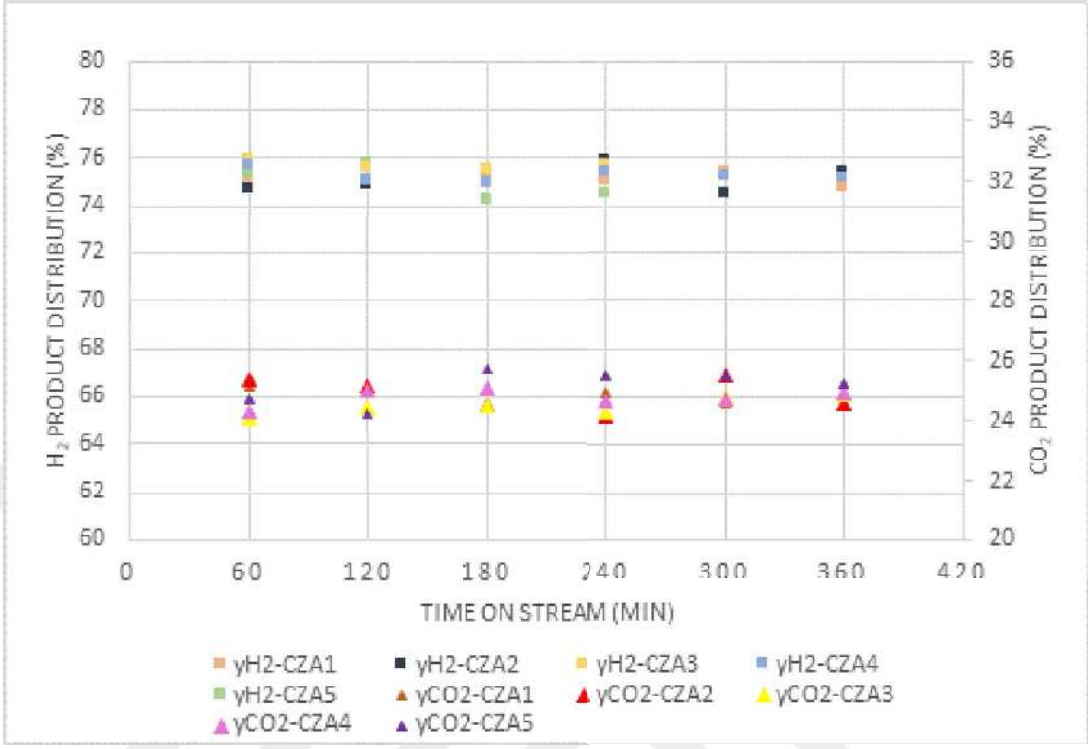

Figure 7.35. *Product distribution in a mole percentage in the reproducible experiment period for synthesized catalysts (T=280°C H_2O/CH_3OH=1.5)*

7.2.3. Long-term stability test

To test the long-term stability of one of the best catalysts synthesized, CZA-3, under the same reaction conditions of atmospheric pressure and reaction temperature of 280℃ as well as H_2O/CH_3OH molar ratio of 1.5, the MSR experiment with a 72-hour duration was studied. Activity tests result was examined in terms of methanol conversion. For the reliability and comparison, commercial Hifuel R-120 catalyst was also studied under the same reaction conditions with a 72-hour experiment. **Figure *7.36*** represents the comparison of CZA-3 and Hifuel R-120 catalysts activity results in terms of methanol conversion. In both experiments formation of the same amounts of products of hydrogen and carbon dioxide (no carbon monoxide) was observed. From the **Figure *7.36*** it was concluded that within the 24 and 44-hours catalyst showed stability and no significant change in methanol conversion. These conversion values were close to conversion of Hifuel R-120 and stability behavior. At the end of 60 hours conversion dropped to 85%. This decrease can be related to the deactivation of copper and coke formation. After 60 hours methanol conversion was maintained at around 85% and keep it throughout the rest of the experiment. At the end of the experiment, it recorded as 84.81%. As a result, CZA-3 throughout the long-term stability test, keeps the activity stabile showing approximately 95% methanol conversion in the first 16 hours then with the 5% activity drop the catalyst maintained its stability at around 90% for 24 hours and after the 60 hours it shows again stability which is 85% in terms of methanol conversion. On the other hand, Hifuel R-120 shows similar methanol conversion path during the same experiment duration. Methanol conversion value was dropped from 91.2% to the 81.8% at the end of the experiment. The activity loss due to the deactivation of catalyst and coke formation can be handled with regeneration cycles. These regeneration cycles help catalyst to gain properties again so that long term activity and stability can be enhanced.

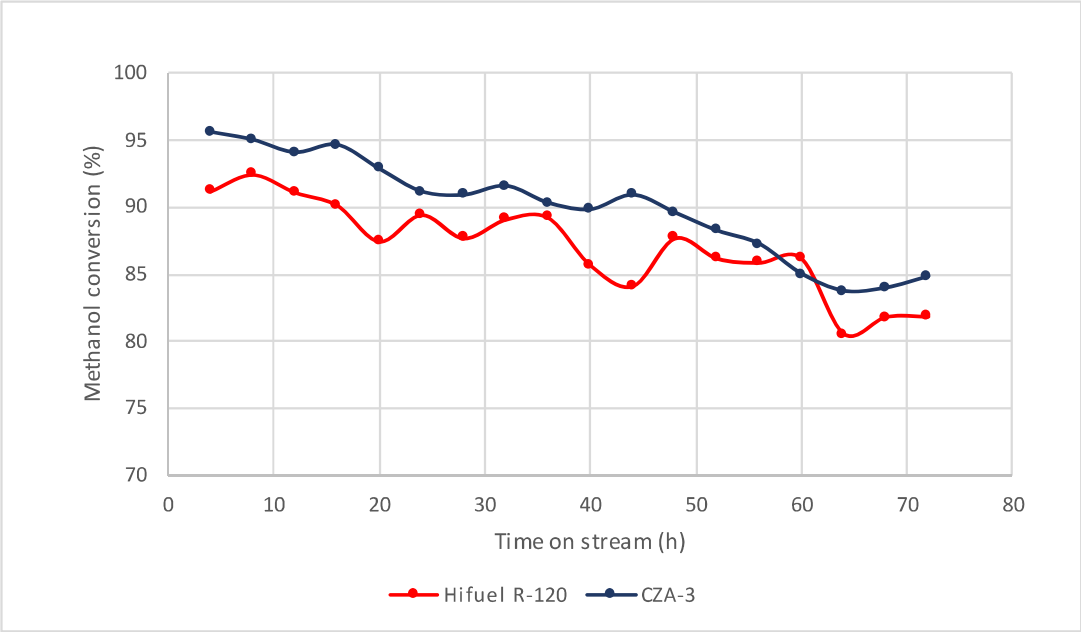

Figure 7.36. *Long- term stability comparison of Hifuel R-120 and CZA-3 catalysts (T=280°C H_2O/CH_3OH=1.5)*

7.2.4. Regeneration

Firstly, the catalytic performance was tested in stop-start experiments via sythesized catalyst CZA-3. Five experiments, each lasting 6 hours, were repeated for five consecutive days. The performance results of these five cycles are shown in **Figure** ***7.37*** in terms of methanol conversion. Methanol conversion was dropped from 95.09% to the 70.9% at the end of the fifth cycle.

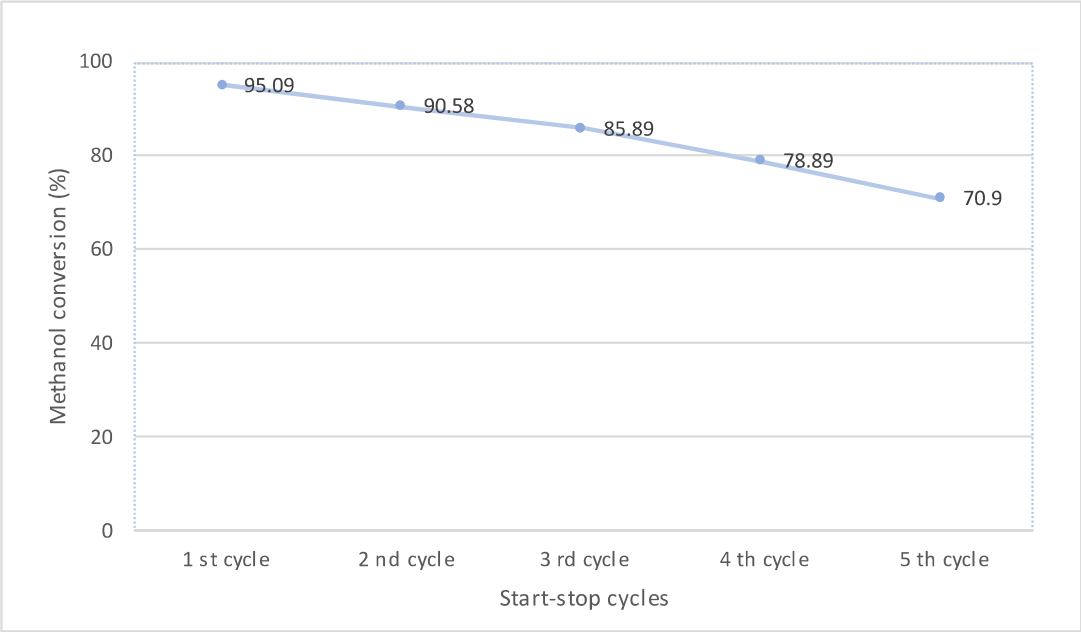

Figure 7.37. *Effect of stop-start operation on methanol conversion as a function of test cycle over CZA-3 catalyst (T=280°C H_2O/CH_3OH=1.5)*

Secondly, regeneration effect was investigated over CZA-3 catalyst. The catalyst was regenerated before each cyclic experiment and subjected to a 6 hour activity test again. The regeneration of the used catalyst was done by exposing the catalyst to oxygen flow for 3 hours and then it was left cool down. Before to be used in cyclic experiments, it was also reduced with hydrogen. The methanol conversion results of at the end of five cyclic experiments are shown in the **Figure *7.38***. When the catalyst was tested in a stop-start operation, its performance decreased from 95.09% to 90.58% in terms of methanol conversion at the end of the second cycle. However, when the catalyst activity was re-tested after being regenerated at the end of the first cycle, the methanol conversion was calculated as 92.58% after the second cycle. Furthermore, at the end of fifth cycle including regeneration process, methanol conversion value was recorded as 88.84% while it was observed 70.9% at the end the fifth cycle of stop-start operation. Therefore, it can be concluded that the negative effects of stop-start operations and activity losses can be eliminated by regeneration which can be repeated at proper time intervals regarding desired operating durations and catalyst performance can be enhanced. There are several studies related to different regeneration conditions to improve catalyst performance improvement have been invetigated in the literature (Sierra et al., 2010).

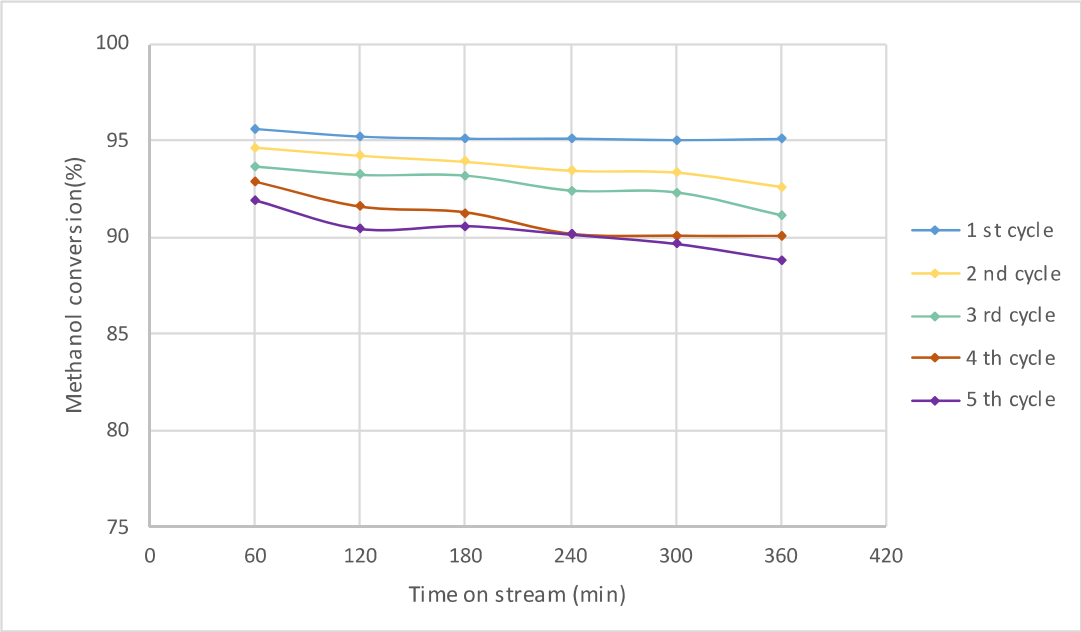

Figure 7.38. *Methanol conversion results of CZA-3 catalyst at different regeneration cycles (T=280°C H_2O/CH_3OH=1.5)*

7.2.5. The effect of reaction temperature on hydrogen production from MSR

The effect of reaction temperature was investigated on the hydrogen production from the MSR in a temperature range of 260 ℃ – 290 ℃ by using CZA-3 catalyst. Hydrogen composition and methanol conversion results were given in **Figure *7.39***. As can be seen from **Figure *7.39***, the hydrogen composition in the product distribution slightly increased from 74.8% to 75.78% with an increase in the temperature from 260 ℃ – 280 ℃. However, it showed 75.18% hydrogen composition and CO formation at ppm level was observed only at a temperature of 290 ℃. Since methanol decomposition reaction as well as reverse water gas shift reaction occurs at high temperatures, it led to CO formation albeit at ppm level. In addition, the methanol conversion rose from 64.51% to 90.47% with an increase in the temperature from 260 ℃ – 280 ℃. As a result, the highest hydrogen yield and methanol conversion were achieved with increasing the reaction temperature to 280 ℃.

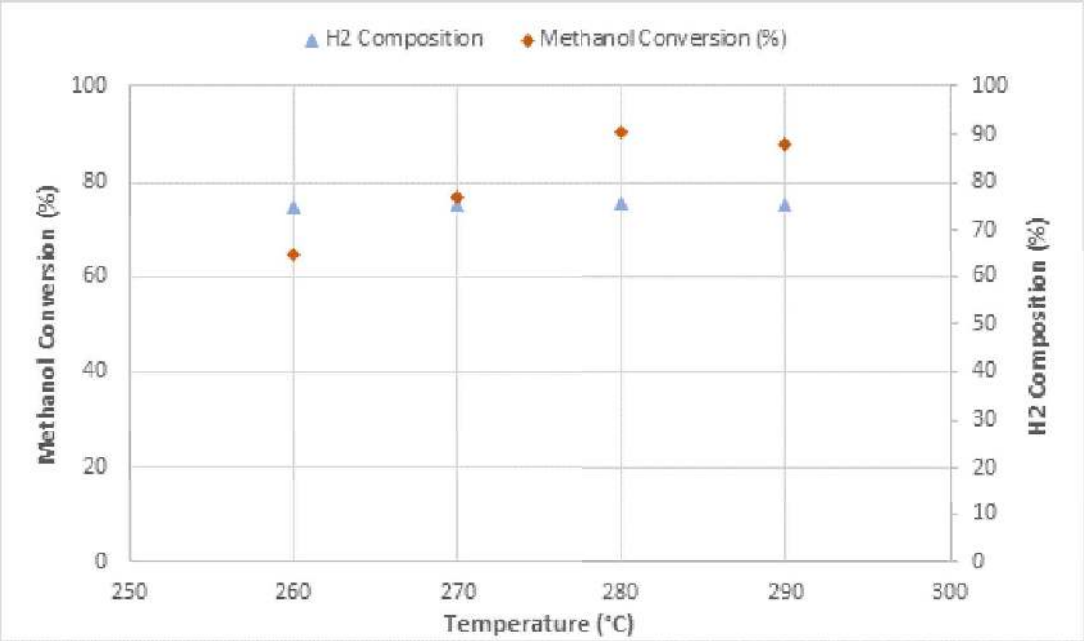

Figure 7.39. *Effect of reaction temperature on hydrogen composition and methanol conversion in MSR*

7.2.6. The effect of GHSV on hydrogen production from MSR

Gas hour space velocity (GHSV) defined as volumetric flow rate of reactants divided by volume of catalyst. It gives the contact time and has a significant effect on catalyst performance. In order to investigate the effect of GHSV on the catalytic performance for MSR, experiments were conducted by varying GHSV value in the range of 3000–20000 h^{-1}. The catalyst CZA-3 was used for the 6 hour experiments at a temperature of 280 ℃ and under atmospheric pressure with a steam methanol ratio of 1.5. Catalyst amount was kept the same and the reactant feed was changed to provide different GHSV values. The related calculation was given in Appendix C. The results obtained are shown in **Figure *7.40***. As it can be seen that the conversion curve of methanol significantly decreased with increasing GHSV. Therefore, it can be concluded that the catalytic performance can be enhanced by decreasing GHSV. Because, decreasing the GHSV value, the higher residence time obtained and this leads to higher methanol conversion.

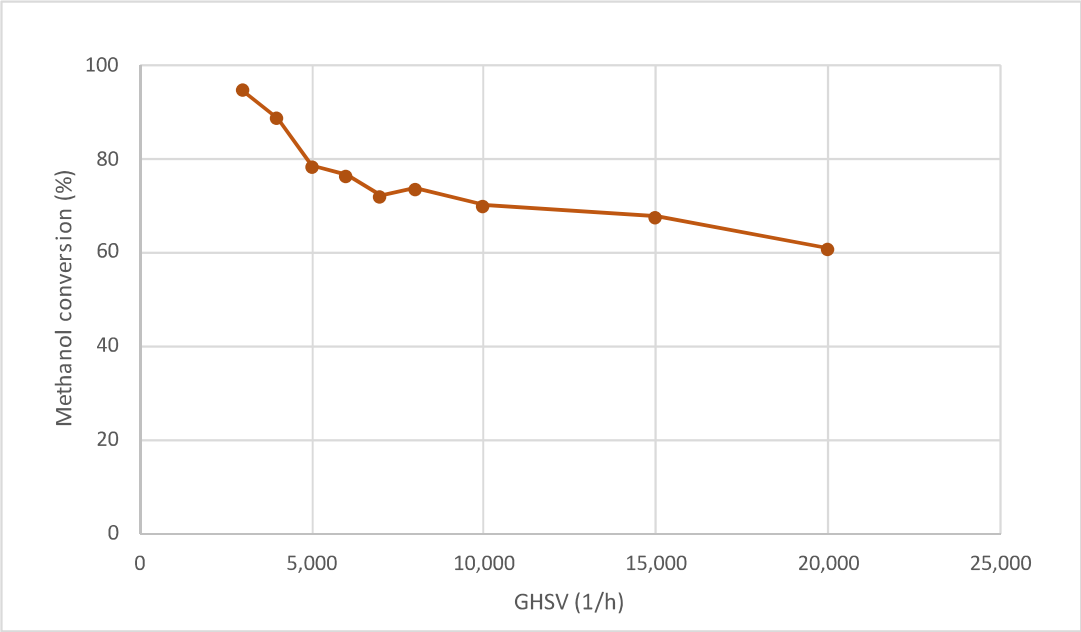

Figure 7.40. *Effect of GHSV on methanol conversion (CZA-3 at T=280°C with H_2O/CH_3OH=1.5)*

8. CONCLUSION

In this study, hydrogen production from MSR was studied over synthesized copper-based $Cu/ZnO/Al_2O_3$and a commercial Hifuel R-120 catalysts. Activity of Hifuel R-120 catalyst was tested under the same conditions that synthesized catalysts were tested. A group of catalysts were prepared by the co-precipitation method from Cu, Zn, and Al nitrate solution, while one catalyst sample was prepared by ball milling method in such a way of mechanical mixing of metal oxides. Co-precipitation method was followed in two different routes as a conventional and sequentially co precipitation. With the goal of producing various precursor structures in sequentially co precipitation, two different catalyst samples were produced by changing the pH, temperature, and ageing parameters. One catalyst was synthesized to test effectiveness of the ball milling method based on the principle of mechanical mixing of oxides for obtaining uniform metal oxide dispersion with crystalline refining as a promising and alternative method since it has cost advance and short-term preparation period compared to multi-step impregnation and precipitation methods. All catalyst samples were shaped in a pellet form except that CZA-2 which is prepared by conventional co-precipitation was shaped with extruder. PVA and CMC binders were used as a pore forming agent and also to facilitate the extraction process.

$Cu, ZnO\ and\ Al_2O_3$successfully loaded into the catalyst structure by both two co-precipitation routes (conventional and sequentially co-precipitation). The relationship between the technique of preparation, the structure, and the activity were examined. Additionally, numerous activity tests were carried out in order to investigate the influence of various parameters, such as GHSV, reaction temperature, stop-start operating condition, regeneration, short term and long-term stability and activity test.

According to SEM results, in the catalysts synthesized by co-precipitation, copper was well distributed on the catalyst surface thanks to proper incorporation of zinc oxide species into precursor. EDX results shows agreement between expected and achieved metal compositions in all successfully synthesized catalysts. Presence of both copper and zinc oxide was identified in XRD with the corresponding diffraction peaks clearly. Furthermore, ordered mesoporous structures were observed in the XRD patterns. All synthesized catalysts showed IV type isotherm with type H3 hysteresis loop, which is assigned to mesoporous structures and the type. CZA-3 and CZA-4 have the highest BET

surface areas of 65.93 $^{m^2}/_{g}$ and 80.26 $^{m^2}/_{g}$, respectively. Pore diameters are 3.0800 nm and 3.8380 nm respectively.

CZA-1 prepared by conventional co-precipitation with 74.36% methanol conversion showed lower performance compared to catalyst of CZA-3 and CZA-4 which was prepared by sequentially co-precipitation. The improvement in activity and stability were achieved by modification in co-precipitation method. The catalysts CZA-3 and CZA-4 show the best activity in MSR at 280℃, which led to 94.55% and 95.99% methanol conversion respectively. At this temperature, the hydrogen yield reached to 96.31% and 96.63% respectively. The high activity of the catalysts CZA-3 and CZA-4 prepared by the sequentially co-precipitation method is due to the high surface area, high dispersion of Cu metal particles and higher accessibility of these active sites to reactants of methanol and steam, small copper crystallite size and successfully established amorphous and crystalline structure which favor activity in MSR. CZA-3 (amorphous zincian georgeite) was synthesized successfully via a sequentially co-precipitation route under strictly controlled pH, precipitation temperature, efficient washing steps and calcination temperature. The activity in MSR was similar to those of CZA-4 (crystalline zincian malachite) and the commercial Hifuel R-120. We have shown that zincian georgeite can be readily prepared by co-precipitation. However, the co-precipitated zincian georgeite derived catalyst still displayed as good as performance in MSR in comparison to a zincian malachite and commercial Hifuel R-120. The zincian georgeite and zincian malachite showed similar structural and physical characteristics. It was seen that CZA-3 and CZA-4 were a stable and regenerable catalyst. Reproducibility experiments showed consistency. The catalyst CZA-3 exhibited a good stability at 280℃ for 72 hours of time on stream. The methanol conversion was maintained constant at about $95 - 91\%$ in the first 44 hours period of stability test. After activity loss, it decreased to 85% at the end of the 60 hours and maintained performance stable at this level during the rest of 12 hours of the test period. All synthesized catalysts yielded similar product distribution of hydrogen and carbon dioxide in terms of molar percentages. There was no CO production during the experiments. The highest hydrogen yield and methanol conversion were achieved with increasing the reaction temperature. The hydrogen composition in the product distribution slightly increased from 74.8% to 75.78% with an increase in the temperature with respect to $260℃ - 280℃$. In addition,

the methanol conversion rose from 64.51% to 90.47% with an increase in the temperature. CO formation was observed only at a temperature of 290℃. The conversion was increased with the decreasing of GHSV. The higher residence time leads to higher methanol conversion.

It was able to show that the preparation method plays an important role to achieve catalysts with enhanced properties. The key point is that synthesizing of catalyst with superior properties in terms of activity and stability is rely on the relationship between synthesis method, structure, and catalytic properties.

9. FUTURE WORK

Followings will be studied as future work:

- Further studies related to different regeneration conditions to improve catalyst performance can be investigated.
- Ball milling conditions can be studied more to enhance catalyst structure and activity.
- Extrusion process is needed to be improved to give proper strength and surface area.

REFERENCES

Agrell, J., Birgersson, H., Boutonnet, M., Melián-Cabrera, I., Navarro, R. M., & Fierro, J. L. G. (2003). Production of hydrogen from methanol over Cu/ZnO catalysts promoted by ZrO2 and Al2O3. *Journal of Catalysis*, *219*(2), 389–403. https://doi.org/10.1016/S0021-9517(03)00221-5

Alothman, Z. A. (2012). A review: Fundamental aspects of silicate mesoporous materials. *Materials*, *5*(12), 2874–2902. https://doi.org/10.3390/ma5122874

Asadullah, M., Ito, S. I., Kunimori, K., Yamada, M., & Tomishige, K. (2002). Energy efficient production of hydrogen and syngas from biomass: Development of low-temperature catalytic process for cellulose gasification. *Environmental Science and Technology*, *36*(20), 4476–4481. https://doi.org/10.1021/es020575r

Azizan, M. T., Aqsha, A., Ameen, M., Syuhada, A., Klaus, H., Abidin, S. Z., & Sher, F. (2020). Catalytic reforming of oxygenated hydrocarbons for the hydrogen production: an outlook. *Biomass Conversion and Biorefinery*. https://doi.org/10.1007/s13399-020-01081-6

Bermudez, J. M., & Hannula, I. (2021). *Hydrogen*. https://www.iea.org/reports/hydrogen

Bhandari, R., Trudewind, C. A., & Zapp, P. (2014). Life cycle assessment of hydrogen production via electrolysis – a review. *Journal of Cleaner Production*, *85*, 151–163. https://doi.org/10.1016/J.JCLEPRO.2013.07.048

Chin, Y., Wang, Y., Dagle, R. A., & Li, X. S. (2003). *Methanol steam reforming over Pd / ZnO : Catalyst preparation and pretreatment studies*. *83*, 193–201. https://doi.org/10.1016/S0378-3820(03)00067-5

Chorkendorff, I., & Niemantsverdriet, J. W. (2003). *Concepts of Modern Catalysis and Kinetics*. Wiley-VCH Verlag GmbH & Co. KGaA. https://onlinelibrary.wiley.com/doi/book/10.1002/3527602658

Choudhury, H. A., Chakma, S., & Moholkar, V. S. (2015). Biomass Gasification Integrated Fischer-Tropsch Synthesis: Perspectives, Opportunities and Challenges. In *Recent Advances in Thermochemical Conversion of Biomass*. https://doi.org/10.1016/B978-0-444-63289-0.00014-4

Conant, T., Karim, A. M., Lebarbier, V., Wang, Y., Girgsdies, F., Schlögl, R., & Datye, A. (2008). Stability of bimetallic Pd-Zn catalysts for the steam reforming of methanol. *Journal of Catalysis*, *257*(1), 64–70. https://doi.org/10.1016/j.jcat.2008.04.018

Demirbas, M. F. (2006). Hydrogen from various biomass species via pyrolysis and steam gasification processes. *Energy Sources, Part A: Recovery, Utilization and Environmental Effects*, *28*(3), 245–252. https://doi.org/10.1080/009083190890003

Dincer, I., & Acar, C. (2015). Review and evaluation of hydrogen production methods for better sustainability. *International Journal of Hydrogen Energy*, *40*(34), 11094–11111. https://doi.org/10.1016/J.IJHYDENE.2014.12.035

Ewan, B. C. R., & Allen, R. W. K. (2005). A figure of merit assessment of the routes to hydrogen. *International Journal of Hydrogen Energy*, *30*(8), 809–819. https://doi.org/10.1016/J.IJHYDENE.2005.02.003

Holladay, J. D., Hu, J., King, D. L., & Wang, Y. (2009). An overview of hydrogen production technologies. In *Catalysis Today* (Vol. 139, Issue 4, pp. 244–260). Elsevier. https://doi.org/10.1016/j.cattod.2008.08.039

Huang, L., Kramer, G. J., Wieldraaijer, W., Brands, D. S., Poels, E. K., Castricum, H. L., & Bakker, H. (1997). Methanol synthesis over Cu/ZnO catalysts prepared by ball milling. In *Catalysis Letters* (Vol. 48, Issues 1–2, pp. 55–59). https://doi.org/10.1023/a:1019014701674

IEA. (2019). *The Future of Hydrogen*. https://www.iea.org/reports/the-future-of-hydrogen

IGBN Makertihartha, S., & Gunawan, M. L. (2009). Synthesis and activity test of Cu/ZnO/Al2O3 for the methanol steam reforming as a fuel cell's hydrogen supplier. *ITB Journal of Engineering Science*, *41 B*(1), 37–49. https://doi.org/10.5614/itbj.eng.sci.2009.41.1.3

Iulianelli, A., Ribeirinha, P., Mendes, A., & Basile, A. (2014). Methanol steam reforming for hydrogen generation via conventional and membrane reactors: A review. *Renewable and Sustainable Energy Reviews*, *29*, 355–368. https://doi.org/10.1016/j.rser.2013.08.032

Iwasa, N., Mayanagi, T., Ogawa, N., Sakata, K., & Takezawa, N. (1998). New catalytic functions of Pd–Zn, Pd–Ga, Pd–In, Pt–Zn, Pt–Ga.pdf. *Catalysis Letters*, *54*, 119–123.

Jeong, H., Kim, K. I., Kim, T. H., Ko, C. H., Park, H. C., & Song, I. K. (2006). Hydrogen production by steam reforming of methanol in a micro-channel reactor coated with Cu/ZnO/ZrO2/Al2O3 catalyst. *Journal of Power Sources*, *159*(2), 1296–1299. https://doi.org/10.1016/j.jpowsour.2005.11.095

Jin, C. L., Wu, Z. M., Wang, S. W., Cai, Z. Q., Chen, T., Farahani, M. R., & Li, D. X. (2017). Economic assessment of biomass gasification and pyrolysis: A review. *Energy Sources, Part B: Economics, Planning and Policy*, *12*(11), 1030–1035. https://doi.org/10.1080/15567249.2017.1358309

Kalamaras, C. M., & Efstathiou, A. M. (2013). *Hydrogen Production Technologies : Current State and Future Developments*. *2013*.

Laboratory, P. N. N. (2021). *Basic Hydrogen Properties | Hydrogen Tools*. https://h2tools.org/hyarc/hydrogen-data/basic-hydrogen-properties%0Ahttp://files/190/basic-hydrogen-properties.html

Lakeman, J. B. (2003). *The Role of Fuel Cells in the Supply of Silent Power for Operations in Littoral Waters POWER SOURCES FOR PRESENT AND FUTURE UNDERWATER*. *April*, 7–10.

Li, Y. F., Dong, X. F., & Lin, W. M. (2004). Effects of ZrO2-promoter on catalytic performance of CuZnAlO catalysts for production of hydrogen by steam reforming of methanol. *International Journal of Hydrogen Energy*, *29*(15), 1617–1621. https://doi.org/10.1016/j.ijhydene.2004.03.001

Methanol Steam Reforming Over Silica Aerogel Supported (Issue June). (2018).

Prasetyaningsih, Y., Hendriyana, & Susanto, H. (2016). Influence of impregnation and coprecipitation method in preparation of Cu/ZnO catalyst for methanol synthesis. *Journal of Engineering and Technological Sciences*, *48*(4), 442–450. https://doi.org/10.5614/j.eng.technol.sci.2016.48.4.6

PubChem Compound Summary for CID 887, Methanol. (2022). National Center for Biotechnology Information. https://pubchem.ncbi.nlm.nih.gov/compound/Methanol

Ren, S., Fan, X., Shang, Z., Shoemaker, W. R., Ma, L., Wu, T., Li, S., Klinghoffer, N. B., Yu, M., & Liang, X. (2019). Enhanced catalytic performance of Zr modified CuO/ZnO/Al2O3 catalyst for methanol and DME synthesis via CO2 hydrogenation. *Journal of CO2 Utilization*, *36*(C), 82–95. https://doi.org/10.1016/J.JCOU.2019.11.013

Rosen, M. A. (2010). Advances in hydrogen production by thermochemical water decomposition: A review. *Energy*, *35*(2), 1068–1076. https://doi.org/10.1016/J.ENERGY.2009.06.018

Rothenberg, G. (2008). *Catalysis: Concepts and Green Applications*. WILEY-VCH Verlag GmbH & Co. KGaA. http://www.adarothenberg.com

Royal society of Chemistry (RSC). (2017). *Hydrogen - Element information, properties and uses | Periodic Table*. Period Table. http://www.rsc.org/periodic-table/element/1/hydrogen

Ryan O'Hayre, Suk-Won Cha, Whitney Colella, F. B. P. (2016). *Fuel Cell Fundamentals* (3rd Edition). https://www.wiley.com/en-us/Fuel+Cell+Fundamentals%2C+3rd+Edition-p-9781119113805

Sá, S., Silva, H., Brandão, L., Sousa, J. M., & Mendes, A. (2010). Catalysts for methanol steam reforming-A review. *Applied Catalysis B: Environmental*, *99*(1–2), 43–57. https://doi.org/10.1016/j.apcatb.2010.06.015

Sadeghinia, M., Rezaei, M., Nemati Kharat, A., Namayandeh Jorabchi, M., Nematollahi, B., & Zareiekordshouli, F. (2020). Effect of In2O3 on the structural properties and catalytic performance of the CuO/ZnO/Al2O3 catalyst in CO2 and CO hydrogenation to methanol. *Molecular Catalysis*, *484*(December 2019), 110776. https://doi.org/10.1016/j.mcat.2020.110776

Safari, F., & Dincer, I. (2020). A review and comparative evaluation of thermochemical water splitting cycles for hydrogen production. *Energy Conversion and Management*, *205*, 112182. https://doi.org/10.1016/J.ENCONMAN.2019.112182

Sengodan, S., Lan, R., Humphreys, J., Du, D., Xu, W., Wang, H., & Tao, S. (2018). Advances in reforming and partial oxidation of hydrocarbons for hydrogen

production and fuel cell applications. *Renewable and Sustainable Energy Reviews*, *82*(July 2016), 761–780. https://doi.org/10.1016/j.rser.2017.09.071

Shen, J. P., & Song, C. (2002). Influence of preparation method on performance of Cu/Zn-based catalysts for low-temperature steam reforming and oxidative steam reforming of methanol for H2 production for fuel cells. *Catalysis Today*, *77*(1–2), 89–98. https://doi.org/10.1016/S0920-5861(02)00235-3

Shishido, T., Yamamoto, Y., Morioka, H., Takaki, K., & Takehira, K. (2004). Active Cu/ZnO and Cu/ZnO/Al2O3 catalysts prepared by homogeneous precipitation method in steam reforming of methanol. *Applied Catalysis A: General*, *263*(2), 249–253. https://doi.org/10.1016/j.apcata.2003.12.018

Sierra, I., Ereña, J., Aguayo, A. T., Arandes, J. M., & Bilbao, J. (2010). Regeneration of CuO-ZnO-Al2O3/γ-Al2O3 catalyst in the direct synthesis of dimethyl ether. *Applied Catalysis B: Environmental*, *94*(1–2), 108–116. https://doi.org/10.1016/J.APCATB.2009.10.026

Smith, Paul J., Kondrat, S. A., Chater, P. A., Yeo, B. R., Shaw, G. M., Lu, L., Bartley, J. K., Taylor, S. H., Spencer, M. S., Kiely, C. J., Kelly, G. J., Park, C. W., & Hutchings, G. J. (2017). A new class of Cu/ZnO catalysts derived from zincian georgeite precursors prepared by co-precipitation. *Chemical Science*, *8*(3), 2436–2447. https://doi.org/10.1039/c6sc04130b

Smith, Paul John. (2015). *Georgeite : A rare gem for catalysis*. *February*.

Tellez-cruz, M. M., Escorihuela, J., & Solorza-feria, O. (2021). *Proton Exchange Membrane Fuel Cells (PEMFCs): Advances and Challenges*. 1–54.

Walter, K. M., Serrer, M. A., Kleist, W., & Grunwaldt, J. D. (2019). Continuous production of higher alcohols from synthesis gas and ethanol using Cs-modified CuO/ZnO/Al2O3 catalysts. *Applied Catalysis A: General*, *585*, 117150. https://doi.org/10.1016/J.APCATA.2019.117150

Wang, Y., Zhang, J., & Xu, H. (2006). Interaction between Pd and ZnO during Reduction of Pd/ZnO Catalyst for Steam Reforming of Methanol to Hydrogen. *Chinese Journal of Catalysis*, *27*(3), 217–222. https://doi.org/10.1016/S1872-2067(06)60015-6

World Nuclear Association. (2021). *Hydrogen Production and Uses - World Nuclear Association*. World-Nuclear.Org. https://www.world-nuclear.org/information-library/energy-and-the-environment/hydrogen-production-and-uses.aspx

Yao, C. Z., Wang, L. C., Liu, Y. M., Wu, G. S., Cao, Y., Dai, W. L., He, H. Y., & Fan, K. N. (2006). Effect of preparation method on the hydrogen production from methanol steam reforming over binary Cu/ZrO2 catalysts. *Applied Catalysis A: General*, *297*(2), 151–158. https://doi.org/10.1016/j.apcata.2005.09.002

Zhang, X. R., Wang, L. C., Yao, C. Z., Cao, Y., Dai, W. L., He, H. Y., & Fan, K. N. (2005). A highly efficient Cu/ZnO/Al2O3 catalyst via gel-coprecipitation of oxalate precursors for low-temperature steam reforming of methanol. *Catalysis Letters*, *102*(3–4), 183–190. https://doi.org/10.1007/s10562-005-5853-7

Zhang, Y. (2020). Preparation of heterogeneous catalysts based on CWAO technology. *Journal of Physics: Conference Series*, *1549*, 32052. https://doi.org/10.1088/1742-6596/1549/3/032052

APPENDICIES

Appendix A: Calculation of Metal Loading Amount to Catalyst

In catalyst preparation chapter catalyst samples were prepared according to calculations given in this section.

In total five samples of $Cu/ZnO/Al_2O_3$ catalysts (30 gram of each one) are prepared. One of them is prepared from directly mixing of metal oxides of CuO, ZnO and Al_2O_3 having the mass fraction and amount calculated below. The remaining four samples are prepared by co-precipitation method.

Mass fraction percentages of $CuO/ZnO/Al_2O_3$ are selected as follows:

$$m_{CuO}\ \% = 55\ \%$$

$$m_{ZnO}\ \% = 33\ \%$$

$$m_{Al_2O_3}\ \% = 12\ \%$$

where, m_{CuO} %, m_{ZnO} % and $m_{Al_2O_3}$ % represent mass fraction percentage of CuO, ZnO and Al_2O_3 respectively. Therefore, all the catalysts are prepared with respect to this ratio. Required mass of nitrate salts and Na_2CO_3 are calculated to ensure that all the catalysts have the same mass fraction.

To prepare 30 gram of catalyst which has given mass fraction percentages, required CuO, ZnO and Al_2O_3 amount can be calculated as below.

$$m_{catalyst\ sample} = 30\ (g)$$

$$m_{CuO} = \frac{m_{catalyst\ sample} * m_{CuO}\ \%}{m_{CuO}\ \% + m_{ZnO}\ \% + m_{Al_2O_3}\ \%} = \frac{30 * 55\ \%}{55\ \% + 33\ \% + 12\ \%} = 16.5\ g$$

$$m_{ZnO} = \frac{m_{catalyst\ sample} * m_{ZnO}\ \%}{m_{CuO}\ \% + m_{ZnO}\ \% + m_{Al_2O_3}\ \%} = \frac{30 * 33\ \%}{55\ \% + 33\ \% + 12\ \%} = 9.9\ g$$

$$m_{Al_2O_3} = \frac{m_{catalyst\ sample} * m_{Al_2O_3}\ \%}{m_{CuO}\ \% + m_{ZnO}\ \% + m_{Al_2O_3}\ \%} = \frac{30 * 12\ \%}{55\ \% + 33\ \% + 12\ \%} = 3.6\ g$$

where, m_{CuO}, m_{ZnO} and $m_{Al_2O_3}$ represent mass of CuO, ZnO and Al_2O_3 in terms of (g) respectively. Additionally, $m_{catalyst\ sample}$ refers to the total mass of the catalyst in terms of (g).

Required moles of CuO, ZnO and Al_2O_3 was calculated as division of mass of oxides by molecular weight of oxides where n_{CuO}, n_{ZnO}, $n_{Al_2O_3}$ represent moles of CuO, ZnO and Al_2O_3 respectively. MW_{CuO}, MW_{ZnO}, and $MW_{Al_2O_3}$represent the molecular weight of CuO, ZnO and Al_2O_3 respectively.

$$MW_{CuO} = 79.5454 \text{ g/mol}$$

$$MW_{ZnO} = 81.38 \text{ g/mol}$$

$$MW_{Al_2O_3} = 101.96 \text{ g/mol}$$

$$n_{CuO} = \frac{m_{CuO}}{MW_{CuO}} = \frac{16.5}{79.5454} = 0.207\ mol$$

$$n_{ZnO} = \frac{m_{ZnO}}{MW_{ZnO}} = \frac{9.9}{81.38} = 0.122\ mol$$

$$n_{Al_2O_3} = \frac{m_{Al_2O_3}}{MW_{Al_2O_3}} = \frac{3.6}{101.96} = 0.035\ mol$$

The amount of oxides are obtained from nitrate salts where $m_{Cu(NO_3)_2}$, $m_{Zn(NO_3)_2}$, $m_{Al(NO_3)_3}$represent mass of $Cu(NO_3)_2$, $Zn(NO_3)_2$, and $Al(NO_3)_3$ respectively. Therefore, required amount of nitrate salts were calculated via equations below where $n_{Cu(NO_3)_2}$, $n_{Zn(NO_3)_2}$, $n_{Al(NO_3)_3}$ represent the moles of $Cu(NO_3)_2$, $Zn(NO_3)_2$, and $Al(NO_3)_3$ respectively.

$$n_{Cu(NO_3)_2} = n_{CuO} = 0.207\ mol$$

$$n_{Zn(NO_3)_2} = n_{ZnO} = 0.122\ mol$$

$$n_{Al(NO_3)_3} = n_{Al_2O_3} * 2 = 0.035 * 2 = 0.070\ mol$$

$$MW_{Cu(NO_3)_2} = \text{Moleculer weight of } Cu(NO_3)_2 = 241.6 \text{ g/mol}$$

$$MW_{Zn(NO_3)_2} = \text{Moleculer weight of } Zn(NO_3)_2 = 261.44 \text{ g/mol}$$

$MW_{Al(NO_3)_3}$ = Moleculer weight of $Al(NO_3)_3 = 395$ g/mol in a form of $Al(NO_3)_3.9H_2O$

$$m_{Cu(NO_3)_2} = \frac{MW_{Cu(NO_3)_2} * n_{Cu(NO_3)_2}}{0.995} = \frac{241.6 * 0.207}{0.995} = 50.366\ g$$

$$m_{Zn(NO_3)_2} = \frac{MW_{Zn(NO_3)_2} * n_{Zn(NO_3)_2}}{0.985} = \frac{261.44 * 0.122}{0.985} = 32.289\ g$$

$$m_{Al(NO_3)_3} = MW_{Al(NO_3)_3} * n_{Al(NO_3)_3} = 395 * 0.070 = 27.882\ g$$

Precipitation is performed by mixing 1 molar Na_2CO_3 solutions with 1 molar nitrate solutions prepared according to mass amounts calculated above.

Molarity is defined as moles of solute (nitrate salts) divided by the volume of solution where $v_{Cu(NO_3)_2}$, $v_{Zn(NO_3)_2}$, and $v_{Al(NO_3)_3}$ represent the volume of $Cu(NO_3)_2$, $Zn(NO_3)_2$, and $Al(NO_3)_3$ respectively.

To obtain 1 Molar nitrate solution for each nitrate salts for precipitation, calculations are followed as;

$$v_{Cu(NO_3)_2} = \text{Volume of } Cu(NO_3)_2 \text{ solution}$$

$$v_{Zn(NO_3)_2} = \text{Volume of } Zn(NO_3)_2 \text{ solution}$$

$$v_{Al(NO_3)_3} = \text{Volume of } Al(NO_3)_3 \text{ solution}$$

$$M = Molarity$$

$$v_{Cu(NO_3)_2} = \frac{n_{Cu(NO_3)_2}}{M} = \frac{0.207}{1} * 1000 = 207\ ml$$

$$v_{Zn(NO_3)_2} = \frac{n_{Zn(NO_3)_2}}{M} = \frac{0.122}{1} * 1000 = 122\ ml$$

$$v_{Al(NO_3)_3} = \frac{n_{Al(NO_3)_3}}{M} = \frac{0.070}{1} * 1000 = 70\ ml$$

According to equations below required Na_2CO_3 moles for precipitation of Cu(NO3)2 Zn(NO3)2 and Al(NO3)3 are found as 0.207 (mol), 0.122 (mol) and 0.105 (mol) with respectively.

$$n_{Na_2CO_3\_1} = mol\ of\ Na_2CO_3\ required\ for\ precipitation\ of\ Cu(NO_3)_2$$

$$n_{Na_2CO_3\_1} = 0.207\ mol$$

$$n_{Na_2CO_3\_2} = mol\ of\ Na_2CO_3\ required\ for\ precipitation\ of\ Zn(NO_3)_2$$

$$n_{Na_2CO_3\_2} = 0.122\ mol$$

$$n_{Na_2CO_3\_3} = mol\ of\ Na_2CO_3\ required\ for\ precipitation\ of\ Al(NO_3)_3$$

$$n_{Na_2CO_3\_3} = 0.105\ mol$$

Multiplying mole values by molecular weight of Na_2CO_3 (105.99 gram/mol), required mass of Na_2CO_3 for each precipitation is calculated as 21.985 grams, 12.894 gram and 11.222 gram.

To obtain 1 Molar Na_2CO_3 solution for each precipitation, required solution volumes are prepared by adding distilled water.

$v_{Na_2CO_3\_1}$

$=$ Volume of $of\ Na_2CO_3\ solution\ required\ for\ precipitation\ of\ Cu(NO_3)_2$

$v_{Na_2CO_3\_2}$

$=$ Volume of $Na_2CO_3\ solution\ required\ for\ precipitation\ of\ Zn(NO_3)_2$

$v_{Na_2CO_3\_3}$

$=$ Volume of $Na_2CO_3\ solution\ required\ for\ precipitation\ of\ Al(NO_3)_3$

$$v_{Na_2CO_3\_1} = \frac{n_{Na_2CO_3\_1}}{M} = \frac{0.207}{1} * 1000 = 207\ ml$$

$$v_{Na_2CO_3\_2} = \frac{n_{Na_2CO_3\_2}}{M} = \frac{0.122}{1} * 1000 = 122\ ml$$

$$v_{Na_2CO_3\_3} = \frac{n_{Na_2CO_3\_3}}{M} = \frac{0.105}{1} * 1000 = 105\ ml$$

Appendix B: Methanol – Water Density Calibration

To evaluate the catalyst performance, conversion calculations are performed based on methanol. For this purpose, the amount of unconverted methanol in the methanol – water mixture, which is collected in the condenser as a result of the reaction, was calculated.

The mass percentage of methanol in the collected methanol – water mixture was obtained from the measured density of mixture.

First, a calibration curve was drawn for the methanol and water that we used in our process. This calibration curve is given in **Figure B.*1***.

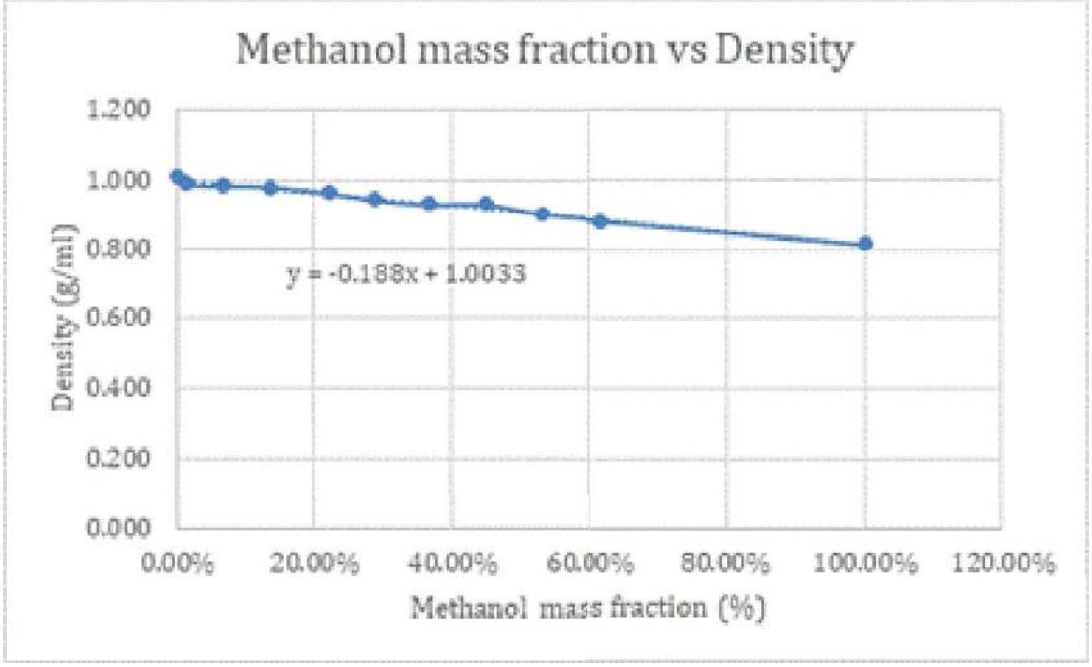

Figure B.1. *Graph of methanol – water calibration curve*

In **Figure B.*1***, the x-axis of the curve represents the mass percentage of methanol, and the y-axis represents the density of the methanol – water mixture. The mass percentage of methanol in the waste is calculated by using the density of methanol – water mixture which is collected at certain time intervals during the experiment.

From the graph, the mass percentage of methanol corresponding to the measured density was found and then unconverted mole of methanol was calculated. In this process pycnometer was used for the density measurements.

mass %	V_methanol (ml)	m_methanol (g)	d_methanol (g/ml)	V_water (ml)	V_total (ml)	volume withdrawn (ml)	m_mixture (g)	d_mixture (g/ml)
0.00%	0	0		60	60	20	20.228	1.011
1.29%	1	0.772	0.772	59	60	10	9.926	0.993
6.85%	5	4.043	0.809	55	60	10	9.844	0.984
13.50%	10	7.802	0.780	50	60	10	9.823	0.982
22.03%	15	12.715	0.848	45	60	10	9.649	0.965
28.74%	20	16.13	0.807	40	60	10	9.450	0.945
36.75%	25	20.34	0.814	35	60	10	9.309	0.931
44.76%	30	24.313	0.810	30	60	10	9.313	0.931
53.04%	35	28.238	0.807	25	60	10	9.016	0.902
61.79%	40	32.34	0.809	20	60	10	8.843	0.884
100.00%	60	48.86	0.814	0	60	10	8.143	0.814

Figure B.2. *Methanol – water calibration curve data*

In **Figure B.*2***, the measured data in this process is shown.

Appendix C: Methanol Conversion Calculations

Catalytic activity of the catalysts in MSR is evaluated based on methanol conversion. Following nomenclature is used during the conversion calculations:

$v_{feed}\ (ml)$: $Volume\ of\ the\ methanol - water\ mixture\ feed$

$\rho_{feed}\ \left(\frac{g}{ml}\right)$: $Density\ of\ the\ methanol - water\ mixture\ feed$

$v_{condensed}\ (ml)$: $Volume\ of\ the\ condensed\ methanol - water\ mixture$

$\rho_{condensed}\ \left(\frac{g}{ml}\right)$: $Density\ of\ the\ condensed\ methanol - water\ mixture$

$m_{methanol\ feed}\ \%$: $Mass\ fraction\ of\ methanol\ in\ feed$

$m_{methanol\ condensed}\ \%$: $Mass\ fraction\ of\ the\ methanol\ in\ condensed$

$MW_{methanol}$: $Moleculer\ weight\ of\ methanol$

$n_{methanol\ condensed}$: $mol\ of\ condensed\ methanol$

$n_{methanol\ feed}$: $mol\ of\ methanol\ feed$

$n_{methanol\ comsumed}$: $mol\ of\ methanol\ comsumed\ in\ the\ reaction$

The equation of density with respect to methanol mass fraction (%) graph is expressed in equation below:

$$\rho_{condensed} = -0.188 * (m_{methanol\ condensed}\ \%) + 1.0033$$

Therefore, mass fraction of the methanol in condensed can be found as follows;

$$m_{methanol\ condensed}\ \% = \frac{\rho_{condensed} - 1.0033}{-0.188}$$

By using this result, mol of condensed methanol and methanol feed can be calculated as;

$$n_{methanol\ condensed} = \frac{\rho_{condensed} * v_{condensed} *\ \ m_{methanol\ condensed}\ \%}{MW_{methanol}}$$

$$n_{methanol\ feed} = \frac{\rho_{feed} * v_{feed} *\ \ m_{methanol\ feed}\ \%}{MW_{methanol}}$$

Finally, mol of methanol consumed in the reaction can be derived as follows:

$$n_{methanol\ comsumed} = n_{methanol\ feed} - n_{methanol\ condensed}$$

Then the conversion percentage of the methanol can be written as:

$$Conversion\ \% = \frac{n_{methanol\ comsumed}}{n_{methanol\ feed}} * 100$$

Now these calculation steps are applied to all synthesized catalysts as well as commercial Hifuel R-120 catalyst.

1) <u>Hifuel R-120</u>

Firstly, the commercial Hifuel R-120 catalyst is investigated. The measured values of this catalyst are given as follows:

$\rho_{condensed} = 0.955475\ g/ml$

$v_{condensed} = 74\ ml$

$v_{feed} = 256\ ml$

$\rho_{feed} = 0.9004\ g/ml$

$m_{methanol\ feed}\ \% = 54.70\ \%$

Conversion calculation for the commercial catalyst Hifuel R-120 can be conducted as follows:

$$m_{methanol\ condensed}\ \% = \frac{0.955475 - 1.0033}{-0.188} = 25.44\ \%$$

$$n_{methanol\ condensed} = \frac{0.955475 * 74 * \ 25.44\ \%}{32.04} = 0.56\ mol$$

$$n_{methanol\ feed} = \frac{0.9004 * 256 * \ 54.70\ \%}{32.04} = 3.94\ mol$$

$$n_{methanol\ comsumed} = \ 3.94 - 0.56 = 3.38\ mol$$

$$Conversion\ \% = \frac{3.38}{3.94} * 100 = 85.79\ \%$$

2) <u>CZA-1</u>

Secondly, CZA-1 catalyst is investigated. The measured values of the corresponding catalyst are given as follows:

$\rho_{condensed} = 0.945300\ g/ml$

$v_{condensed} = 215\ ml$

$v_{feed} = 496.43\ ml$

$\rho_{feed} = 0.9004\ g/ml$

$m_{methanol\ feed}\ \% = 54.70\ \%$

Conversion calculation for the catalyst CZA-1:

$$m_{methanol\ condensed}\ \% = \frac{0.945300\ - 1.0033}{-0.188} = 30.85\ \%$$

$$n_{methanol\ condensed} = \frac{0.945300\ * 215 * \ 30.85\ \%}{32.04} = 1.96\ mol$$

$$n_{methanol\ feed} = \frac{0.9004 * 496.43 * \ 54.70\ \%}{32.04} = 7.64\ mol$$

$$n_{methanol\ comsumed} = \ 7.64 - 1.96 = 5.68\ mol$$

$$Conversion\ \% = \frac{5.68}{7.64} * 100 = 74.36\ \%$$

3) <u>CZA-2</u>

Thirdly, CZA-2 catalyst is investigated. The measured values of the corresponding catalyst are given as follows:

$\rho_{condensed} = 0.929050\ g/ml$

$v_{condensed} = 265.5\ ml$

$v_{feed} = 449.50\ ml$

$\rho_{feed} = 0.9004\ g/ml$

$m_{methanol\ feed}\ \% = 54.70\ \%$

Conversion calculation for the catalyst CZA-2:

$$m_{methanol\ condensed}\ \% = \frac{0.929050 - 1.0033}{-0.188} = 39.49\ \%$$

$$n_{methanol\ condensed} = \frac{0.929050 * 265.5 * \ 39.49\ \%}{32.04} = 3.04\ mol$$

$$n_{methanol\ feed} = \frac{0.9004 * 449.50 * \ 54.70\ \%}{32.04} = 6.91\ mol$$

$$n_{methanol\ comsumed} = \ 6.91 - 3.04 = 3.87\ mol$$

$$Conversion\ \% = \frac{3.87}{6.91} * 100 = 56\ \%$$

4) <u>CZA-3</u>

In this part CZA-3 catalyst is investigated. The measured values of the corresponding catalyst are given as follows:

$\rho_{condensed} = 0.98285$ g/ml

$v_{condensed} = 60.5\ ml$

$v_{feed} = 239\ ml$

$\rho_{feed} = 0.9004\ g/ml$

$m_{methanol\ feed}\ \% = 54.70\ \%$

Conversion calculation for the catalyst CZA-3 can be given as follows:

$$m_{methanol\ condensed}\ \% = \frac{0.98285 - 1.0033}{-0.188} = 10.88\ \%$$

$$n_{methanol\ condensed} = \frac{0.98285 * 60.5 * \ 10.88\ \%}{32.04} = 0.20\ mol$$

$$n_{methanol\ feed} = \frac{0.9004 * 239 * \ 54.70\ \%}{32.04} = 3.67\ mol$$

$$n_{methanol\ comsumed} = \ 3.67 - 0.20 = 3.47\ mol$$

$$Conversion\ \% = \frac{3.47}{3.67} * 100 = 94.55\ \%$$

5) <u>CZA-4</u>

Let's investigate the CZA-4 catalyst. The measured values of the corresponding catalyst are given as follows:

$\rho_{condensed} = 0.98307\ g/ml$

$v_{condensed} = 59\ ml$

$v_{feed} = 247\ ml$

$\rho_{feed} = 0.9004\ g/ml$

$m_{methanol\ feed}\ \% = 54.70\ \%$

Conversion calculation for the catalyst CZA-4 can be given as follows:

$$m_{methanol\ condensed}\ \% = \frac{0.98307\ - 1.0033}{-0.188} = 10.60\ \%$$

$$n_{methanol\ condensed} = \frac{0.98307\ * 59 * \ 10.60\ \%}{32.04} = 0.19\ mol$$

$$n_{methanol\ feed} = \frac{0.9004 * 247 * \ 54.70\ \%}{32.04} = 3.79\ mol$$

$$n_{methanol\ comsumed} = \ 3.79 - 0.19 = 3.60\ mol$$

$$Conversion\ \% = \frac{3.60}{3.79} * 100 = 94.99\ \%$$

6) CZA-5

Finally, CZA-5 catalyst is investigated. The measured values of the corresponding catalyst are given as follows:

$\rho_{condensed} = 0.91917 \text{g/ml}$

$v_{condensed} = 176.5\ ml$

$v_{feed} = 468.93\ ml$

$\rho_{feed} = 0.9004\ g/ml$

$m_{methanol\ feed}\ \% = 54.70\ \%$

Conversion calculation for the catalyst CZA-5 can be given as follows:

$$m_{methanol\ condensed}\ \% = \frac{0.91917 - 1.0033}{-0.188} = 44.75\ \%$$

$$n_{methanol\ condensed} = \frac{0.91917 * 176.5 * \ 44.75\ \%}{32.04} = 2.27\ mol$$

$$n_{methanol\ feed} = \frac{0.9004 * 468.93 * \ 54.70\ \%}{32.04} = 7.21\ mol$$

$$n_{methanol\ comsumed} = 7.21 - 2.27 = 4.94\ mol$$

$$Conversion\ \% = \frac{4.94}{7.21} * 100 = 68.51\ \%$$

Gas Hour Space Velocity (GHSV) Calculation

All synthesized catalysts' performances in MSR are studied at the same GHSV values. Since each catalysts have different densities, different volumetric flow rates of methanol-water feed which is represented by $Q_{avg_{feed}}$ are studied for each catalyst to keep the the GHSV values constant. T_{feed} and P_{feed} represent temperature of methanol-water feed and pressure of methanol-water feed respectively.

$$T_{feed} = 300\ ℃$$

$$P_{feed} = 88\ kPa$$

$$Q_{avg_{feed}} = 0.8\ ml/min$$

GHSV can be expressed as volumetric flow rate of reactants divided by volume of catalyst.

$$\text{GHSV} = \frac{Q_{gas\ feed}}{v_{catalyst}}$$

where $Q_{gas\ feed}$ and $v_{catalyst}$ represent volumetric flow rate of methanol-water gas feed and volume of catalyst respectively. To obtain $Q_{gas\ feed}$, firstly $\acute{n}_{feed}$ which refers to mole of methanol-water feed is calculated via summation of mole of methanol feed and mole of water feed represented by $\acute{n}_{methanol\ feed}$ and $\acute{n}_{water\ feed}$ respectively. Calculations are done as follows:

$$\acute{n}_{methanol\ feed} = \frac{Q_{avg_{feed}} * \rho_{feed} * m_{methanol\ feed}\ \%}{MW_{methanol}} = \frac{0.8 * 0.9004 * 54.70\ \%}{32.04}$$
$$= 0.012\ mol/min$$

$$\acute{n}_{water\ feed} = \frac{Q_{avg_{feed}} * \rho_{feed} * m_{water\ feed}\ \%}{MW_{water}} = \frac{0.8 * 0.9004 * 45.3\ \%}{18.02}$$
$$= 0.018\ mol/min$$

$$\acute{n}_{feed} = 0.012 + 0.018 = 0.030\ mol/min$$

Then, $Q_{gas\ feed}$ is calculated by following equation.

$$Q_{gas\ feed} = \frac{\acute{n}_{feed} * 8.314 * (273.15 + T_{feed})}{P_{feed}} = \frac{0.030 * 8.314 * (273.15 + 300)}{88}$$
$$= 1.65\ L/min$$

Secondly, volume of catalyst is calculated by following equation below. Height of catalyst which is represented by $h_{catalyst}$ is measured as 3.5 cm. *D* represents the diameter of the reactor that we used in experiments, and it is 2.5 cm.

$$v_{catalyst} = \frac{D^2 * \pi * h_{catalyst}}{4} = \frac{(D/100)^2 * \pi * (h_{catalyst}/100)}{4} * 10^6$$

$$= \frac{\left(\frac{2.5}{100}\right)^2 * \pi * \left(\frac{3.5}{100}\right)}{4} * 10^6 = 17.18\, ml$$

Finally, GHSV is calculated as:

$$\text{GHSV} = \frac{1.65 * 60}{17.18/1000} = \frac{1.65 * 60}{17.18/1000} = 5757\ 1/h$$